UNIVERSIDAD DE CONCEPCION
ESCUELA DE GRADUADOS
CONCEPCION-CHILE

ANÁLISIS NUMÉRICO DE MODELOS DE TRANSPORTE Y DEGRADACIÓN DE CONTAMINANTES EN MEDIOS ACUÁTICOS

Tesis para optar al grado de
Doctor en Ciencias Aplicadas con mención en Ingeniería Matemática

Edwin Marcelo Enrique Behrens Rincón

FACULTAD DE CIENCIAS FISICAS Y MATEMATICAS
DEPARTAMENTO DE INGENIERIA MATEMATICA

2006

Contents

Chapter 1

Introducción

Los cursos de agua, además de ser un recurso esencial para la vida del hombre, son utilizados para eliminar desechos. Con la creciente población y número de fábricas que arrojan hoy en día sus desechos en ellos, una gran cantidad de ríos han sido contaminados. Al arrojar residuos, éstos son transportados, obedeciendo este fenómeno principalmente a tres factores: difusión, advección y reacción.

Debido a que la capacidad de los ríos está siendo agotada, es necesario tener herramientas de predicción ante eventuales escenarios de caudales y descarga de contaminantes. Entre estas herramientas se encuentran los modelos matemáticos, y en la medida que seamos capaces de resolver de forma adecuada las ecuaciones provenientes del modelo, las predicciones serán mejores.

En el modelo considerado, donde denotaremos por u la concentración de contaminantes en el río, la difusión o dilución se modela con el término de segundo orden $-\varepsilon\Delta u$. La advección, que es el transporte del contaminante debido a la velocidad, se modela por $\boldsymbol{a}\cdot\nabla u$ y para la reacción (degradación) del polutante, se considera el término bu.

Los parámetros físicos de difusión y reacción (ε y b), se determinan experimentalmente, mientras que el campo de velocidades $\boldsymbol{a}$ se obtiene al resolver las ecuaciones de Navier-Stokes.

Finalmente, denotaremos al río por Ω. Para la descarga puntual de contaminantes consideraremos una fuente tipo delta soportada en el punto x_0 en el interior de Ω, que es donde se vierte la substancia.

Para modelar lo que ocurre en la frontera Γ del dominio Ω, dividiremos ésta en dos partes disjuntas, que denominaremos Γ_D, que es donde la concentración es conocida (que supondremos nula) y generalmente se ubica aguas arriba del río, y Γ_N, que corresponde a la orilla y aguas abajo, donde supondremos una condición sobre la derivada normal para tener en cuenta, por ejemplo, que la concentración no varía en dirección perpendicular a la frontera.

En esta tesis estudiaremos solamente el problema estacionario, en el cual la solución no depende del tiempo. Consideraremos tanto términos fuente suaves como tipo delta de Dirac, las que genéricamente denotaremos por f. De esta forma, la ecuación que describe el fenómeno de transporte es la siguiente:

$$\begin{aligned} -\varepsilon\Delta u + \boldsymbol{a}\cdot\nabla u + bu &= f \quad \text{en } \Omega,\\ u &= 0 \quad \text{en } \Gamma_D,\\ \frac{\partial u}{\partial \boldsymbol{n}} &= 0 \quad \text{en } \Gamma_N, \end{aligned} \tag{1.1}$$

donde $\boldsymbol{n}$ es el vector unitario normal exterior a Γ.

Considerando espacios adecuados W_1 para la solución u y W_2 para las funciones test, escribimos (1.1) en forma distribucional, por lo que ahora el problema es: Hallar $u \in W_1$ tal que satisface

$$B(u,v) = \langle f, v\rangle, \qquad \forall v \in W_2, \tag{1.2}$$

con $\frac{1}{p}+\frac{1}{q}=1$ y la forma bilineal $B(u,v) := \displaystyle\int_\Omega (\nabla u\cdot\nabla v + \boldsymbol{a}\cdot\nabla u v + buv)$.

Ahora consideremos una triangulación $\mathcal{T}_h$ de Ω, y sea $V_h \subset W_2 \subset W_1$ un espacio de elementos finitos asociado a la triangulación. Una aproximación u_h de u está dada por

$$B(u_h, v_h) = \langle f, v_h\rangle, \qquad \forall v_h \in V_h. \tag{1.3}$$

Incluso en el caso de términos fuente regulares, cuando la advección es dominante y dependiendo de las condiciones de frontera, la solución de (1.1) frecuentemente presenta capas límite tanto interiores como de borde.

Es sabido que el esquema numérico (1.3) en estas circuntancias introduce oscilaciones no físicas en la solución cuando el orden de los polinomios de V_h usado en la aproximación es bajo y la malla no es lo suficientemente fina como para resolver la capa límite. Para ejemplificar este comportamiento, en la figura (1.1) se muestra la solución exacta de un problema de este tipo que presenta una capa límite de frontera y su aproximación numérica dada por (1.3).

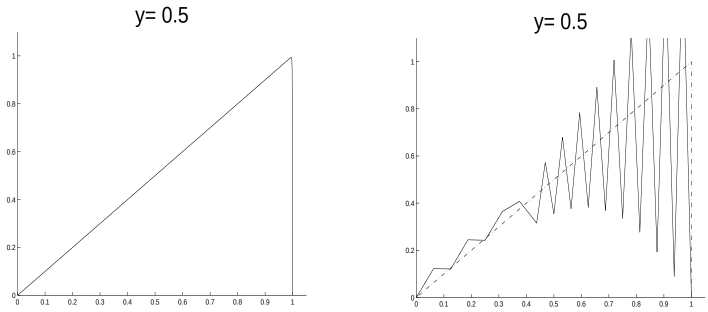

Figure 1.1: Oscilaciones de la solución numérica. Solución exacta y aproximada.

Para mejorar la calidad de la solución, en esta tesis utilizaremos dos técnicas: estabilización del método numérico y adaptividad de la malla.

Por una parte, la técnica de estabilización consiste en sumar a la formulación variacional (1.3) algo de difusión numérica para reducir las oscilaciones de la aproximación. La estabilización utilizada en este trabajo es la propuesta en [19]. Debido a la cantidad de difusión numérica adicionada, la capa límite de la solución no queda bien resuelta. La Figura (1.2) muestra la solución numérica obtenida en este caso, y en línea punteada la solución exacta. Se aprecia que incluso con mallas tan finas como la tercera la capa límite no es resuelta de manera adecuada.

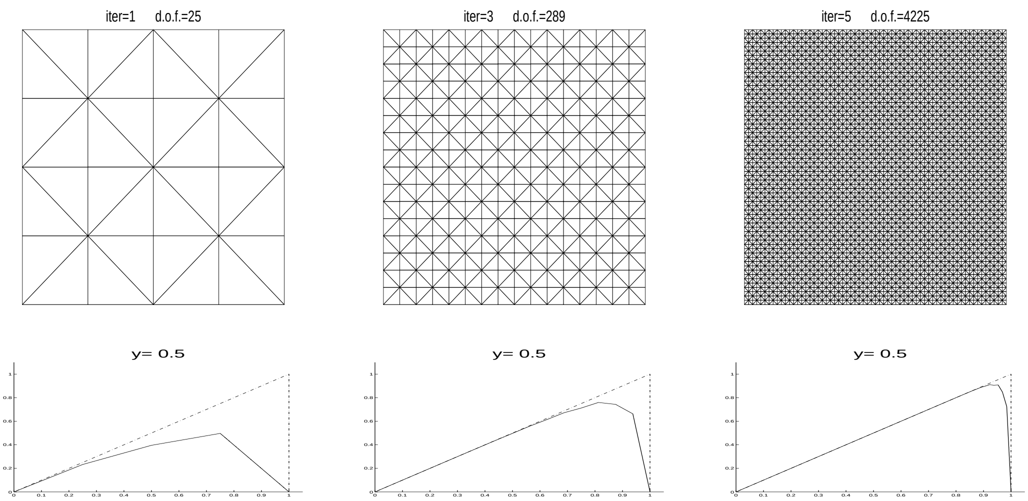

Figure 1.2: Mallas y solución numérica estabilizada.

Otra alternativa para mejorar la solución numérica, es calcular la aproximación en una malla capaz de resolver la capa límite. Los métodos adaptivos se basan en estimadores a posteriori, que dan información cuantitativa del error que se comete en cada elemento de la triangulación, la que permite hacer modificaciones en la malla tendientes a corregir la solución numérica. La figura (1.3) muestra algunas soluciones y mallas obtenidas por medio de un proceso adaptivo aplicado a la solución de (1.3) sin estabilización.

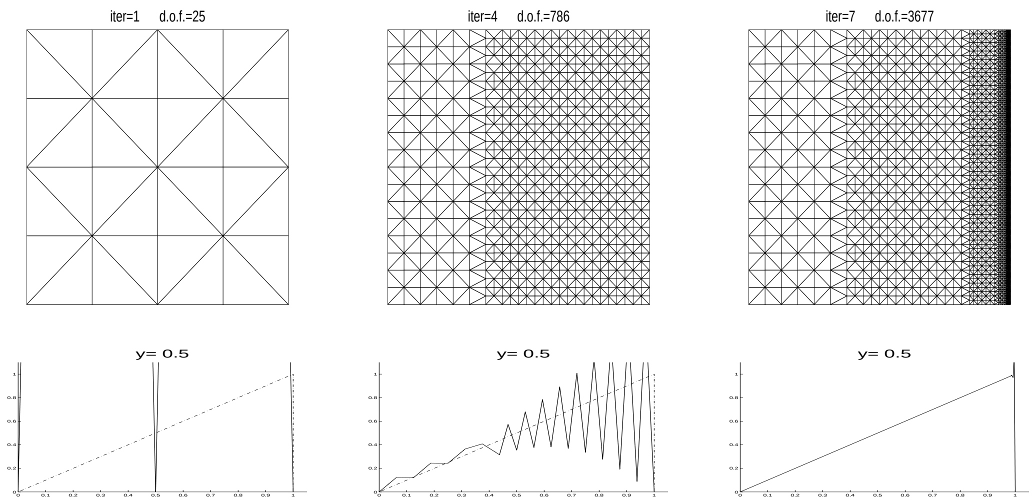

Figure 1.3: Mallas adaptadas y solución numérica.

De la Figura 1.3 se aprecia que en mallas tan finas y adaptadas como la última, todavía existen oscilaciones en la solución numérica.

Dado que ambos métodos permiten mejorar la aproximación, es natural usar ambas técnicas a la vez para calcular la solución numérica.

Uno de los temas de esta tesis consiste en desarrollar un estimador a posteriori del error de tipo residual para el método numérico estabilizado propuesto por [19], similar al desarrollado en [32], donde se considera términos fuente suaves. Los resultados de esta investigación dieron origen a la publicación [4]. Los resultados que se obtienen basados en este esquema adaptivo se muestran en la Figura (1.4), de donde se aprecia que la capa límite está bien resuelta y sin oscilaciones.

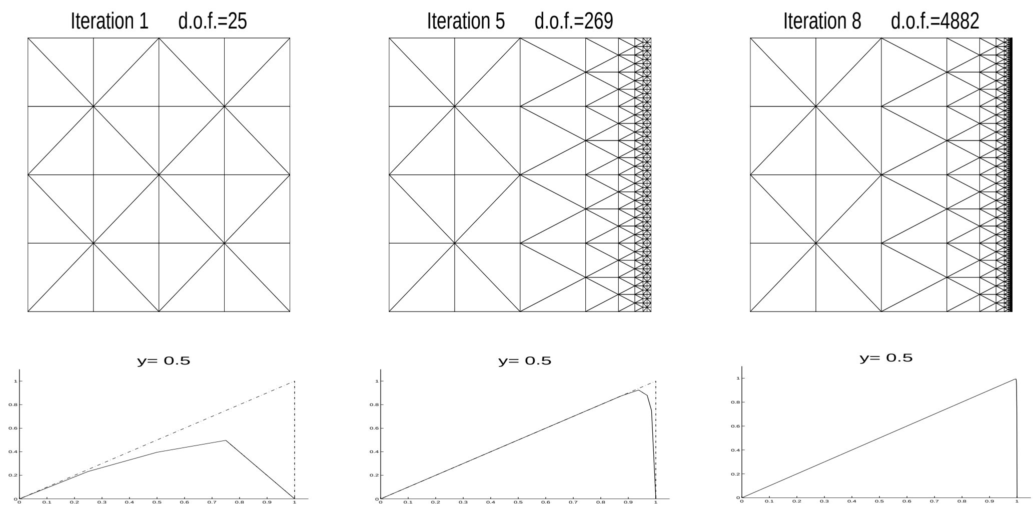

Figure 1.4: Mallas adaptadas y solución numérica estabilizada.

Cabe repetir que el comportamiento numérico anteriormente descrito es independiente del término fuente presente en el modelo. Resuelto el problema para fuentes suaves, corresponde analizar la ecuación en presencia de fuentes delta.

Comenzaremos con un caso simplificado, en el que no existe velocidad ni reacción, y la difusión es unitaria, es decir la ecuación

$$\begin{aligned} -\Delta u &= \delta_{x_0} \quad \text{en } \Omega, \\ u &= 0 \quad\ \ \text{en } \Gamma, \end{aligned} \tag{1.4}$$

donde se ha considerado toda la frontera de tipo Dirichlet.

Estimadores a priori para esta clase de problemas han sido demostrados en [29] y [12]. Sin embargo, análisis de error a posteriori no se ha realizado todavía.

Es fácil darse cuenta que para obtener una buena aproximación de la solución debemos utilizar mallas correctamente refinadas alrededor de x_0. En esta tesis se introducen y analizan estimadores a posteriori de tipo residual para esta ecuación. Los resultados aquí obtenidos se encuentran descritos en el reporte técnico [5].

Estos indicadores se usan para guiar un procedimiento adaptivo, con buenos resultados, como se muestra en la figura (1.5).

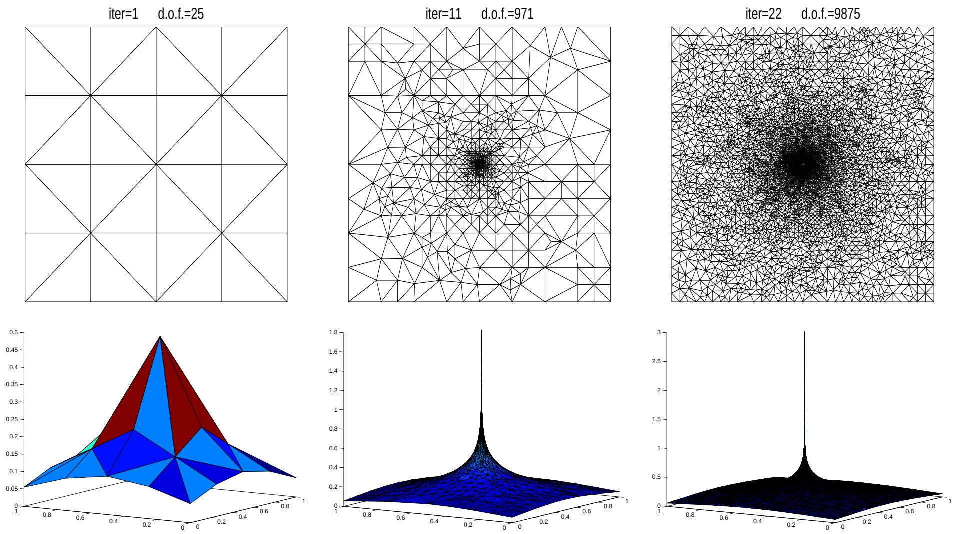

Figure 1.5: Mallas y solución aproximada del problema (1.4).

Por último abordamos la ecuación de transporte (1.1) con fuentes delta de Dirac, que corresponde a modelar la descarga puntual de contaminantes. Debido a que la advección es dominante, la solución de esta ecuación tiene una fuerte capa límite interior en x_0 alineada con la velocidad del fluido. Por esto la solución numérica debe ser calculada en una malla bien adaptada. Para esto se introduce un esquema de elementos finitos adaptivo basado en el método estabilizado de [19], combinado con un estimador a posteriori, el cual es una variante del desarrollado en [4] en el caso de fuentes en $L^2(\Omega)$. Los resultados aquí obtenidos están detallados en el reporte técnico [3].

La figura (1.6) muestra una malla y la solución obtenida al utilizar dicho esquema adaptivo.

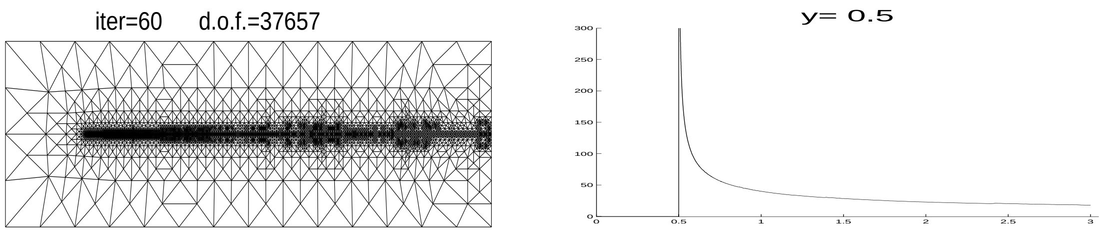

Figure 1.6: Ecuación de transporte con fuente delta. Malla adaptada y corte.

Como se aprecia, la capa límite interior está bien resuelta y no presenta oscilaciones.

Esta tesis está organizada en 5 capítulos.

Después de la presente introducción, en el segundo capítulo introducimos un esquema de elementos finitos adaptivo para la ecuación de transporte, considerando fuentes en $L^2(\Omega)$. Este esquema se basa en un método estabilizado de elementos finitos combinado con un estimador de error de tipo residual similar al presentado en [32]. En este capítulo se demuestra la equivalencia del error y este estimador. Los resultados obtenidos están detallados en el artículo [4].

En el capítulo 3 se trata nuevamente la ecuación de advección-reacción-difusión con fuentes en $L^2(\Omega)$. Se presentan estimadores a posteriori del error basados en la solución de problemas locales y se demuestra la equivalencia entre estos estimadores y el de tipo residual anteriormente analizado. Las constantes de equivalencia, dependiendo del problema local elegido, eventualmente involucran el parámetro ε. Los resultados obtenidos están descritos en el reporte técnico [6].

El capítulo 4 estudia la ecuación de Laplace con una fuente delta soportada en un punto interior x_0. Se muestra que la solución de este problema pertenece a $W^{1,p}(\Omega)$, $1 \leq p < 2$, y por lo tanto a $L^r(\Omega)$, $r < \infty$. Por esta razón, se introducen algunos estimadores a posteriori del error de tipo residual equivalentes al error tanto en norma $W^{1,p}(\Omega)$ como $L^r(\Omega)$. Estos resultados están detallados en el reporte técnico [5].

Por último, en el capítulo 5 se resuelve la ecuación de transporte con fuentes delta, mediante un esquema adaptivo estabilizado, en el que se desarrollan estimadores a posteriori equivalentes al error, aunque con constantes eventualmente dependientes del parámetro ε. Estos estimadores permiten obtener mallas correctamente refinadas. Los resultados acá obtenidos están detallados en el reporte técnico [3].

En todos los capítulos se incluyen ejemplos numéricos, que muestran el buen comportamiento de los estimadores desarrollados.

Chapter 2

An adaptive stabilized finite element scheme for the advection-reaction-diffusion equation

An adaptive finite element scheme for the advection-reaction-diffusion equation is introduced and analyzed in this chapter. This scheme is based on a stabilized finite element method combined with a residual error estimator. The estimator is proved to be reliable and efficient. More precisely, global upper and local lower error estimates with constants depending at most on the local mesh Peclet number are proved. The effectiveness of this approach is illustrated by several numerical experiments.

2.1 Introduction

This chapter deals with the advection-diffusion-reaction equation. This kind of problems arise in many applications, for instance, when linearizing the Navier-Stokes problem, to model pollutant transport and degradation in aquatic media, etc. In particular, our work is motivated by the need of an efficient scheme to be used in a water quality model for the Bío Bío River in Chile.

Specially interesting is the case when advective or reactive terms are dominant. In this case, the solution of the equation frequently has exponential or parabolic boundary layers (for details see [24]). The standard Galerkin approximation usually fails in this situation because this method introduces nonphysical oscillations. A possible remedy is to add to the variational formulation some numerical diffusion terms to stabilize the finite element solution. Some examples of this approach are the streamline upwind Petrov-

Galerkin method (SUPG) (see [11]), the Galerkin least squares approximation (GLS) (see [18]), the Douglas-Wang method (see [16]), the 'unusual' stabilized finite element method (USFEM) (see [19]), and the residual-free bubbles approximation (RFB) (see [10]). The drawback with most of these methods is that the solution layers are not very well resolved, because of the numerical diffusion added to the discretization.

In spite of the abundant literature on adaptivity (see, for instance [31]), there are not so many references dealing with *a posteriori* techniques for this equation. The reason of this is that most of the standard error estimators involve equivalence constants depending on negative powers of the diffusion parameter, which lead to very poor results in the advective or reactive dominated cases. An error estimator which is robust in the sense of leading to global upper and local lower bounds depending at most on the local mesh Peclet number has been developed by Verfürth (see [33] and [32]). Using these results Sangalli has analyzed a residual *a posteriori* error estimate for the residual-free bubbles scheme (see [25]). On the other hand, Knopp *et al.* have developed some *a posteriori* error estimates using a stabilized scheme combined with a shock-capturing technique to control the local oscillations in the crosswind direction (see [22]). Finally, Wang has introduced an error estimate for the advection-diffusion equation based on the solution of local problems on each element of the triangulation (see [35]).

In this paper we introduce and analyze from theoretical and experimental points of view an adaptive scheme to efficiently solve the advection-reaction-diffusion equation. This scheme is based on the stabilized finite element method introduced in [19] combined with an error estimator similar to the one developed in [32]. We prove global upper and local lower error estimates in the energy norm, with constants which only depend on the shape-regularity of the mesh, the polynomial degree of the finite element approximating space and the local mesh Peclet number. We perform several numerical experiments to show the effectiveness of our approach to capture boundary and inner layers very sharply and without significant oscillations. The experiments also show that the scheme attains optimal order of convergence.

The paper is organized as follows. In Section 2.2 we recall the advection-diffusion-reaction problem under consideration and the stabilized scheme. In Section 2.3 we define an *a posteriori* error estimator and prove its equivalence with the energy norm of the finite element approximation error. Finally, in Section 2.4, we introduce the adaptive scheme and report the results of the numerical tests.

2.2 A stabilized method for a model problem

Our model problem is the advection-reaction-diffusion equation

$$\begin{cases} -\varepsilon\Delta u + \boldsymbol{a}\cdot\nabla u + bu &= f \quad \text{in } \Omega, \\ u &= 0 \quad \text{on } \Gamma_{\mathrm{D}}, \\ \varepsilon\dfrac{\partial u}{\partial \boldsymbol{n}} &= g \quad \text{on } \Gamma_{\mathrm{N}}, \end{cases} \tag{2.1}$$

where $\Omega\subset\mathbb{R}^2$ is a bounded polygonal domain with a Lipschitz boundary $\Gamma = \bar{\Gamma}_{\mathrm{D}}\cup\bar{\Gamma}_{\mathrm{N}}$, with $\Gamma_{\mathrm{D}}\cap\Gamma_{\mathrm{N}}=\emptyset$. We denote by $\boldsymbol{n}$ the outer unit normal vector to Γ.

We are interested in the advection-reaction dominated case and assume that:

(A1) $\varepsilon\in\mathbb{R}:\ 0<\varepsilon\ll 1$;

(A2) $\boldsymbol{a}\in \mathrm{W}^{1,\infty}(\Omega)^2,\ \ b\in \mathrm{L}^\infty(\Omega),\quad \|\boldsymbol{a}\|_{\infty,\Omega}+\|b\|_{\infty,\Omega}=\mathcal{O}(1)$;

(A3) $\operatorname{div}\boldsymbol{a}=0,\ \ b\geq 1$;

(A4) $\Gamma_{\mathrm{D}}\supset\{\boldsymbol{x}\in\Gamma:\ \boldsymbol{a}(\boldsymbol{x})\cdot\boldsymbol{n}(\boldsymbol{x})<0\}$;

(A5) $f\in \mathrm{L}^2(\Omega),\ \ g\in \mathrm{L}^2(\Gamma_{\mathrm{N}})$.

We use standard notation for Sobolev and Lebesgue spaces and norms. Moreover, let $\mathrm{H}^1_{\Gamma_{\mathrm{D}}}(\Omega) := \left\{\varphi\in \mathrm{H}^1(\Omega):\ \varphi|_{\Gamma_{\mathrm{D}}}=0\right\}$ and B be the bilinear form defined on $\mathrm{H}^1(\Omega)$ by

$$B(v,w) := \int_\Omega (\varepsilon\nabla v\cdot\nabla w + \boldsymbol{a}\cdot\nabla v\ w + bvw)\,. \tag{2.2}$$

Then, the standard variational formulation of problem (2.1) is the following: Find $u\in \mathrm{H}^1_{\Gamma_{\mathrm{D}}}(\Omega)$ such that

$$B(u,v) = \int_\Omega fv + \int_{\Gamma_{\mathrm{N}}} gv \quad \forall v\in \mathrm{H}^1_{\Gamma_{\mathrm{D}}}(\Omega). \tag{2.3}$$

We consider the (energy) norm $|||u||| := \left(\varepsilon\|\nabla u\|^2_{0,\Omega}+\|u\|^2_{0,\Omega}\right)^{\frac12}$ defined on $\mathrm{H}^1(\Omega)$. Assumptions (A1)–(A4) and integration by parts imply that

$$B(v,v)\geq |||v|||^2 \quad \forall v\in \mathrm{H}^1_{\Gamma_{\mathrm{D}}}(\Omega) \tag{2.4}$$

and

$$B(v,w)\leq \left(1+\|b\|_{\infty,\Omega}+\varepsilon^{-\frac12}\|\boldsymbol{a}\|_{\infty,\Omega}\right)|||v|||\,|||w|||\,.$$

Hence, as a consequence of Lax-Milgram's Lemma, problem (2.3) has a unique solution.

Let $\{\mathcal{T}_h\}_{h>0}$, be a family of shape-regular partitions of Ω into triangles. Let $V_h := \left\{\varphi \in \mathrm{H}^1_{\Gamma_\mathrm{D}}(\Omega) :\ \varphi|_T \in \mathcal{P}_k\ \forall T \in \mathcal{T}_h\right\}$, where, for $k \in \mathbb{N}$, $\mathcal{P}_k$ denotes the space of polynomials of degree at most k. It is well known that the standard Galerkin method with this finite element space yields poor approximation when $\varepsilon \ll |\boldsymbol{a}|$ or $\varepsilon \ll b$. For this reason we consider the following stabilized formulation introduced in [19]: Find $u_h \in V_h$ such that

$$B_\tau(u_h, v_h) = F_\tau(v_h) \quad \forall v_h \in V_h, \tag{2.5}$$

where, for $v_h, w_h \in V_h$,

$$\begin{aligned} B_\tau(v_h, w_h) &:= B(v_h, w_h) \\ &- \sum_{T\in\mathcal{T}_h} \int_T \tau_T \left(-\varepsilon\Delta v_h + \boldsymbol{a}\cdot\nabla v_h + b v_h\right)\left(-\varepsilon\Delta w_h - \boldsymbol{a}\cdot\nabla w_h + b w_h\right) \end{aligned} \tag{2.6}$$

and

$$F_\tau(v_h) := \int_\Omega f v_h + \int_{\Gamma_\mathrm{N}} g v_h - \sum_{T\in\mathcal{T}_h} \int_T \tau_T f(-\varepsilon\Delta v_h - \boldsymbol{a}\cdot\nabla v_h + b v_h). \tag{2.7}$$

In the expressions above we use a stabilization parameter τ_T defined as follows:

$$\tau_T(\boldsymbol{x}) := \frac{h_T^2}{b(\boldsymbol{x}) h_T^2 \max\{1, \mathrm{Pe}_T^{\mathrm{R}}(\boldsymbol{x})\} + (2\varepsilon/m_k)\max\{1, \mathrm{Pe}_T^{\mathrm{A}}(\boldsymbol{x})\}}, \tag{2.8}$$

where $\mathrm{Pe}_T^{\mathrm{R}}(\boldsymbol{x})$ and $\mathrm{Pe}_T^{\mathrm{A}}(\boldsymbol{x})$ are respectively defined by

$$\mathrm{Pe}_T^{\mathrm{R}}(\boldsymbol{x}) := \frac{2\varepsilon}{m_k b(\boldsymbol{x}) h_T^2} \qquad \text{and} \qquad \mathrm{Pe}_T^{\mathrm{A}}(\boldsymbol{x}) := \frac{m_k\,|\boldsymbol{a}(\boldsymbol{x})|\,h_T}{\varepsilon}, \tag{2.9}$$

where

$$m_k := \min\{1/3, C_k\},$$

with C_k being a positive constant satisfying

$$C_k \sum_{T\in\mathcal{T}_h} h_T^2\,\|\Delta v_h\|_{0,T}^2 \le \|\nabla v_h\|_{0,\Omega}^2 \quad \forall v_h \in V_h,$$

which only depends on the polynomial degree k and the shape-regularity of the mesh.

Finally h_T is a measure of the element size. Under the presence of advection ($\boldsymbol{a} \neq \boldsymbol{0}$), it is reported in [19] that an element parameter h_T which yields very good numerical results is the largest streamline distance in the element, as shown in Fig. 2.1. As can be seen in this figure, to compute h_T, we take the velocity constant on the element: $\boldsymbol{a}_T := \boldsymbol{a}(\boldsymbol{x}_T)$, with $\boldsymbol{x}_T$ being the barycenter of T. If $\boldsymbol{a}_T = \boldsymbol{0}$, we take h_T equal to the diameter of T.

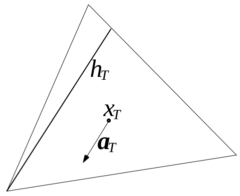

Figure 2.1: Element parameter h_T.

The following lemma shows that the bilinear form B_τ is positive definite and, consequently, the stabilized discrete problem (2.5) is well posed. This has been proved in Lemma 1 of [19] under the assumptions that the coefficients of the advection-diffusion-reaction equation (2.1) are constant and the boundary conditions are purely Dirichlet. It is straightforward to extend the same arguments to our case to prove the following result.

LEMMA 2.2.1 *Under assumptions (A1)–(A4),*

$$B_\tau(v_h, v_h) \geq \sum_{T\in\mathcal{T}_h} \left[\int_T \varepsilon\beta_T \left|\nabla v_h\right|^2 + \int_T \tau_T \left(\boldsymbol{a}\cdot\nabla v_h\right)^2 + \int_T b\beta_T \left|v_h\right|^2 \right],$$

for all $v_h \in V_h$, *with* $\beta_T := \dfrac{\varepsilon}{m_k b h_T^2 + 2\varepsilon} > 0$, $T \in \mathcal{T}_h$.

The convergence and stabilization properties of this scheme have also been investigated in [19], where numerical experiments proving the effectiveness of this approach have been reported. However, these experiments also show that the method does not allow a sharp resolution of inner layers when quasi-uniform meshes are used. In the following section we introduce an error indicator which will allow us to create in an automatic fashion meshes correctly refined around inner and boundary layers of the solution.

2.3 A posteriori error estimator.

In this section we define a residual error estimator, similar to one analyzed in [32] in the context of advection-reaction-diffusion.

Let $\mathcal{E}_h$ denote the set of all edges in $\mathcal{T}_h$ and, for $E \in \mathcal{E}_h$, let h_E be the length of E. For each mesh $\mathcal{T}_h$, let $f_h \in V_h$ and $g_h \in \{v_h|_{\Gamma_N} : \ v_h \in V_h\}$ be arbitrary but fixed approximations of f and g, respectively. We define the approximate volumetric and edge residuals by

$$R_T^h(u_h) := f_h + \varepsilon\Delta u_h - \boldsymbol{a}\cdot\nabla u_h - b u_h, \qquad T \in \mathcal{T}_h, \tag{2.10}$$

$$
R^h_{E}(u_h) := \begin{cases} -\left[\!\!\left[\varepsilon \dfrac{\partial u_h}{\partial \boldsymbol{n}_{E}}\right]\!\!\right]_E, & \text{if } E \in \mathcal{E}_h : \ E \not\subseteq \Gamma, \\ g_h - \varepsilon \dfrac{\partial u_h}{\partial \boldsymbol{n}}, & \text{if } E \in \mathcal{E}_h : \ E \subset \Gamma_{\mathrm{N}}, \\ 0, & \text{if } E \in \mathcal{E}_h : \ E \subset \Gamma_{\mathrm{D}}. \end{cases} \tag{2.11}
$$

These residuals are used to define an estimator of the local error in energy norm, $|||u - u_h|||^2_T := \varepsilon \left\|\nabla(u - u_h)\right\|^2_{0,T} + \left\|u - u_h\right\|^2_{0,T}$, as follows

$$
\eta^2_T := \alpha^2_{T} \left\|R^h_{T}(u_h)\right\|^2_{0,T} + \frac{1}{2} \sum_{E\subset\partial T\cap\Omega} \varepsilon^{-\frac{1}{2}} \alpha_E \left\|R^h_{E}(u_h)\right\|^2_{0,E} + \sum_{E\subset\partial T\cap\Gamma_{\mathrm{N}}} \varepsilon^{-\frac{1}{2}} \alpha_E \left\|R^h_{E}(u_h)\right\|^2_{0,E}, \tag{2.12}
$$

with

$$
\alpha_S := \min\left\{h_S \varepsilon^{-\frac{1}{2}}, 1\right\}, \qquad S \in \mathcal{T}_h \cup \mathcal{E}_h. \tag{2.13}
$$

Let us recall that h_T is not the diameter of T, but the largest streamline distance in the element (see Fig. 2.1). However, h_T is equivalent to the diameter of T with equivalence constants only depending on the element shape ratio.

The efficiency and reliability of a similar estimator applied to a standard SUPG method has been proved in [32]. In what follows we show that analogous results hold for our estimator applied to the stabilized method described in the previous section. To this aim we first prove the following technical lemmas.

Lemma 2.3.1 *Given $T \in \mathcal{T}_h$, let τ_T be defined by (2.8). Then the following bounds hold $\forall \boldsymbol{x} \in T$:*

$$
\varepsilon\tau_T(\boldsymbol{x}) \le \frac{1}{6} h^2_{T}, \qquad |\boldsymbol{a}(\boldsymbol{x})|\, \tau_T(\boldsymbol{x}) \le \frac{1}{2} h_{T}, \qquad b(\boldsymbol{x})\tau_T(\boldsymbol{x}) \le 1.
$$

Furthermore,

$$
b(\boldsymbol{x})\tau_T(\boldsymbol{x}) \le C\alpha_{T}, \qquad \textit{with } C := \max\left\{1, \left(\|b\|_{\infty,\Omega}/6\right)^{\frac{1}{2}}\right\}.
$$

Proof. For the first estimate, we use (2.8) and (2.9) to obtain

$$
\varepsilon\tau_T(\boldsymbol{x}) \le \frac{\varepsilon h^2_T}{b(\boldsymbol{x}) h^2_T \max\{1, \mathrm{Pe}^{\mathrm{R}}_T(\boldsymbol{x})\}} \le \frac{\varepsilon h^2_T}{b(\boldsymbol{x}) h^2_T \mathrm{Pe}^{\mathrm{R}}_T(\boldsymbol{x})} \le \frac{m_k}{2} h^2_T \le \frac{1}{6} h^2_T.
$$

For the second one, if $\boldsymbol{a}(\boldsymbol{x}) = \boldsymbol{0}$ there is nothing to prove; otherwise, by using (2.8) and (2.9) we have

$$
|\boldsymbol{a}(\boldsymbol{x})|\, \tau_T(\boldsymbol{x}) \le \frac{|\boldsymbol{a}(\boldsymbol{x})|\, m_k h^2_T}{2\varepsilon \max\{1, \mathrm{Pe}^{\mathrm{A}}_T(\boldsymbol{x})\}} \le \frac{|\boldsymbol{a}(\boldsymbol{x})|\, m_k h^2_T}{2\varepsilon \mathrm{Pe}^{\mathrm{A}}_T(\boldsymbol{x})} \le \frac{1}{2} h_T.
$$

For the third bound, from (2.8),

$$b(\boldsymbol{x})\tau_T(\boldsymbol{x}) \leq \frac{1}{\max\{1, \mathrm{Pe}_T^{\mathrm{R}}(\boldsymbol{x})\}} \leq 1.$$

Moreover, from the first estimate of this lemma, $b(\boldsymbol{x})\tau_T(\boldsymbol{x}) \leq b(\boldsymbol{x})h_T^2/(6\varepsilon)$, too. Hence, taking the geometric mean of this and the third estimate we have

$$b(\boldsymbol{x})\tau_T(\boldsymbol{x}) \leq \left(\frac{\|b\|_{\infty,\Omega}}{6}\right)^{\frac{1}{2}} h_T\varepsilon^{-\frac{1}{2}}.$$

From this and the third estimate again, we conclude the last inequality. □

Here and thereafter, C denotes a generic positive constant, not necessarily the same at each occurrence, but always independent of the mesh-size and the small parameter ε.

LEMMA 2.3.2 *The following estimates hold for all $w_h \in V_h$:*

$$\|\nabla w_h\|_{0,T} \leq Ch_T^{-1}\alpha_T\, |||w_h|||_T \qquad \textit{and} \qquad \|\Delta w_h\|_{0,T} \leq Ch_T^{-2}\alpha_T\, |||w_h|||_T\,.$$

PROOF. The definition of the energy norm $|||\cdot|||$ implies

$$\|\nabla w_h\|_{0,T} \leq \varepsilon^{-\frac{1}{2}}\, |||w_h|||_T\,, \tag{2.14}$$

whereas, from a standard scaling argument,

$$\|\nabla w_h\|_{0,T} \leq Ch_T^{-1}\, \|w_h\|_{0,T} \leq Ch_T^{-1}\, |||w_h|||_T\,,$$

with the constant C only depending on the shape ratio of the element T and the polynomial degree k in the definition of the finite element space V_h. Then, from these two inequalities, we obtain the first estimate.

On the other hand, another scaling argument and (2.14) yield

$$\|\Delta w_h\|_{0,T} \leq Ch_T^{-1}\, \|\nabla w_h\|_{0,T} \leq Ch_T^{-1}\varepsilon^{-\frac{1}{2}}\, |||w_h|||_T\,,$$

whereas, using scaling arguments again, we have

$$\|\Delta w_h\|_{0,T} \leq Ch_T^{-2}\, |||w_h|||_T\,.$$

Finally, we obtain the second estimate from these last two inequalities. □

In what follows we will show that the energy norm of the error can be bounded by means of the estimators η_T. To do this, first we write from (2.4)

$$|||u-u_h||| \leq \sup_{v\in \mathrm{H}^1_{\Gamma_{\mathrm{D}}}(\Omega)\setminus\{0\}} \frac{B(u-u_h,v)}{|||v|||}.$$

Second, let $I_h : L^2(\Omega) \longrightarrow V_h$ be the Clément interpolation operator (see [14]). Several estimates in energy norm for this operator have been proved in Lemma 3.2 of [32]. In particular, it has been shown that for all $T \in \mathcal{T}_h$ and $v \in \mathrm{H}^1(\widetilde{\omega}_T)$, with $\widetilde{\omega}_T := \bigcup\{\bar{T}' \in \mathcal{T}_h : \bar{T}' \cap \bar{T} \neq \emptyset\}$, there holds

$$|||I_h v|||_T \leq C\, |||v|||_{\widetilde{\omega}_T}\,. \tag{2.15}$$

Now, consider an arbitrary $v \in \mathrm{H}^1_{\Gamma_\mathrm{D}}(\Omega)$ with $|||v||| = 1$. Obviously, we have

$$B(u-u_h, v) = B(u-u_h, v-I_h v) + B(u-u_h, I_h v). \tag{2.16}$$

To estimate this terms we introduce the exact volumetric and edge residuals $R_T(u_h)$ and $R_E(u_h)$, which are defined as in (2.10) and (2.11), but with f_h and g_h substituted by f and g, respectively. For the first term in the right hand side above, we have the following estimate,

$$B(u-u_h, v-I_h v) \leq C \left[\sum_{T\in\mathcal{T}_h} \alpha_T^2 \left\|R_T(u_h)\right\|_{0,T}^2 + \sum_{E\in\mathcal{E}_h} \varepsilon^{-\frac{1}{2}}\alpha_E \left\|R_E(u_h)\right\|_{0,E}^2\right]^{\frac{1}{2}}, \tag{2.17}$$

which has been proved in [32] (see equation (4.5)) with h_T being the diameter of T. However the same arguments are valid in our case.

For the second term in the right hand side of (2.16) we have the following estimate.

Lemma 2.3.3 *For all $v \in \mathrm{H}^1_{\Gamma_\mathrm{D}}(\Omega)$ with $|||v||| = 1$,*

$$B(u-u_h, I_h v) \leq C \left[\sum_{T\in\mathcal{T}_h} \alpha_T^2 \left\|R_T(u_h)\right\|_{0,T}^2\right]^{\frac{1}{2}}.$$

Proof. For all $w_h \in V_h$, from (2.2), (2.3), (2.5), (2.6), and (2.7), we have

$$B(u-u_h, w_h) = -\sum_{T\in\mathcal{T}_h} \int_T \tau_T R_T(u_h)(-\varepsilon\Delta w_h - a\cdot\nabla w_h + b w_h).$$

Next, from Lemmas 2.3.1 and 2.3.2, straightforward computations lead to

$$\int_T \tau_T R_T(u_h)(-\varepsilon\Delta w_h - a\cdot\nabla w_h + b w_h) \leq C\alpha_T \left\|R_T(u_h)\right\|_{0,T} |||w_h|||_T\,.$$

Finally, we replace w_h by $I_h v$ and use (2.15) to obtain

$$B(u-u_h, I_h v) \leq C \sum_{T\in\mathcal{T}_h} \alpha_T \left\|R_T(u_h)\right\|_{0,T} |||v|||_{\widetilde{\omega}_T}\,.$$

Thus, the lemma follows from the regularity of the mesh. □

Now we are able to state the main theoretical result of this paper.

Theorem 2.3.1 *Let u and u_h be the solutions of problems (2.3) and (2.5), respectively. Let f_h and g_h be arbitrary approximations of f and g by elements of V_h and traces on Γ_{N} of elements of V_h, respectively. Let η_T be defined by (2.10)–(2.13). Then, there holds*

$$\begin{aligned} |||u-u_h||| \;\; &\leq \;\; C\left[\left(\sum_{T\in\mathcal{T}_h}\eta_T^2\right)^{\frac{1}{2}}\right.\\ &\qquad\left. + \left(\sum_{T\in\mathcal{T}_h}\alpha_T^2\,\|f-f_h\|_{0,T}^2 + \sum_{E\subset\Gamma_{\mathrm{N}}}\varepsilon^{-\frac{1}{2}}\alpha_E\,\|g-g_h\|_{0,E}^2\right)^{\frac{1}{2}}\right] \end{aligned}$$

and

$$\begin{aligned} \eta_T \;\; &\leq C \;\; \left(1+\|b\|_{\infty,\omega_T}+\varepsilon^{-\frac{1}{2}}\,\|\boldsymbol{a}\|_{\infty,\omega_T}\,\alpha_T\right)|||u-u_h|||_{\omega_T}\\ &\qquad + \alpha_T\,\|f-f_h\|_{0,\omega_T} + \left(\sum_{E\subset\partial T\cap\Gamma_{\mathrm{N}}}\varepsilon^{-\frac{1}{2}}\alpha_E\,\|g-g_h\|_{0,E}^2\right)^{\frac{1}{2}} \qquad \forall T\in\mathcal{T}_h, \end{aligned}$$

where $\omega_T := \bigcup\{\bar{T}'\in\mathcal{T}_h:\ \bar{T}'\cap\bar{T}\supset E\in\mathcal{E}_h\}$.

Proof. The first estimate is a consequence of (2.16), (2.17), Lemma 2.3.3, and the definition of the estimator η_T. The second estimate can be proved by following similar techniques to those used in Proposition 4.1 of [32]. □

2.4 Numerical experiments

In this section we report three series of numerical experiments with the unusual stabilized method described in Section 2.2 and an h-adaptive mesh-refinement strategy based on the error estimator analyzed in Section 2.3. In all the experiments we have used piecewise linear finite elements (i.e., polynomial degree $k=1$) and we have taken as geometric domain the unit square $\Omega := (0,1)\times(0,1)$, although with different boundary conditions. We have considered varying values of the coefficients ε, $\boldsymbol{a}$, and b of the advection-reaction-diffusion equation (2.1).

The adaptive procedure consists in solving problem (2.5) on a sequence of meshes up to finally attain a solution with an estimated error within a prescribed tolerance. To attain this purpose, we initiate the process with a quasi-uniform mesh and, at each step, a new mesh better adapted to the solution of problem (2.3) must be created. This is done by computing the local error estimators η_T for all T in the “old” mesh $\mathcal{T}_h$, and refining those elements T with $\eta_T \geq \mu \max\{\eta_T : T \in \mathcal{T}_h\}$, where $\mu \in (0,1)$ is a prescribed parameter. In all our experiments we have chosen $\mu = \frac{1}{2}$.

We have used a `Matlab` code adapted by us from [2] and the mesh generator `Triangle`. This generator allows us to create successively refined meshes based on a hybrid Delaunay refinement algorithm (see [30]).

2.4.1 A reaction-diffusion problem

The first test consists in solving a purely reaction-diffusion problem. We have chosen the following data: $\boldsymbol{a} = \mathbf{0}$, $b = 1$, $f = 1$, the boundary conditions shown in Fig. 2.2, and various values of the parameter ε. We report the results obtained for $\varepsilon = 10^{-2}$ and $\varepsilon = 10^{-4}$.

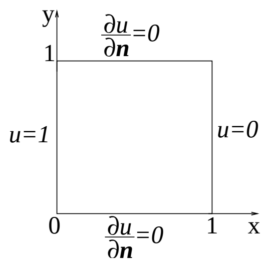

Figure 2.2: Boundary conditions for the reaction-diffusion problem.

The exact solution of this problem is analytically known:

$$u(x,y) = 1 - \frac{\sinh(\varepsilon^{-1/2}x)}{\sinh(\varepsilon^{-1/2})};$$

thus, we have been able to compute the exact errors of our finite element approximations.

Fig. 2.3 shows some of the successively refined meshes created in the adaptive process for $\varepsilon = 10^{-2}$. This figure also shows the level sets and the horizontal cuts at $y = 0.5$ of the corresponding computed solution. The iteration number and the number of degrees of freedom (d.o.f.) of each mesh are also reported in this figure.

Fig. 2.4 shows the error curves of the whole process for the exact and estimated errors. This figure also includes a line with slope $-\frac{1}{2}$, which corresponds to the theoretically optimal order of convergence for piecewise linear elements.

Fig. 2.5 and 2.6 show analogous results for the same problem with the parameter $\varepsilon = 10^{-4}$.

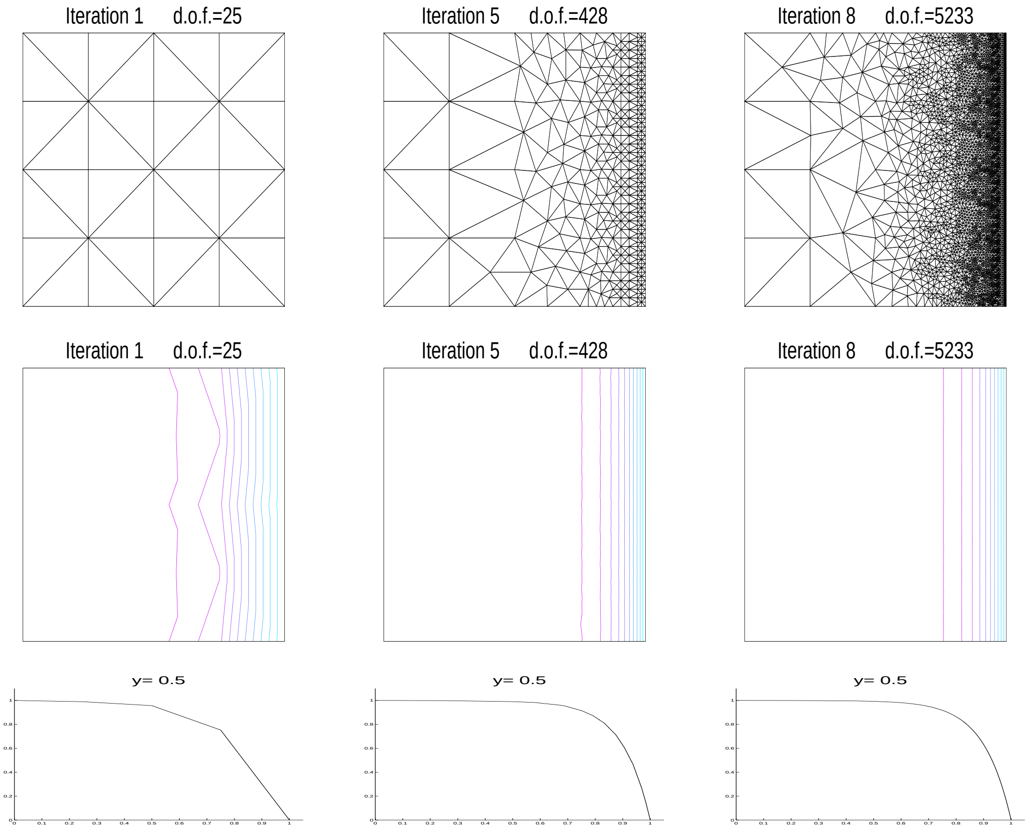

Figure 2.3: Reaction-diffusion problem: $\varepsilon = 10^{-2}$. Meshes, level sets, and horizontal cuts of the approximate solutions.

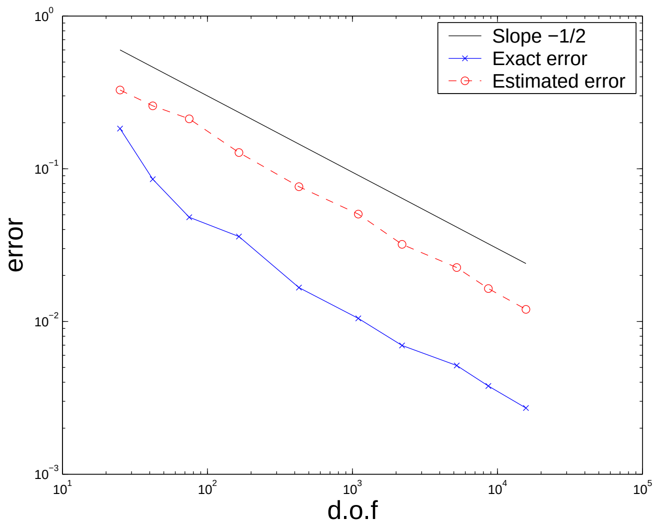

Figure 2.4: Reaction-diffusion problem: $\varepsilon = 10^{-2}$. Estimated and exact error curves.

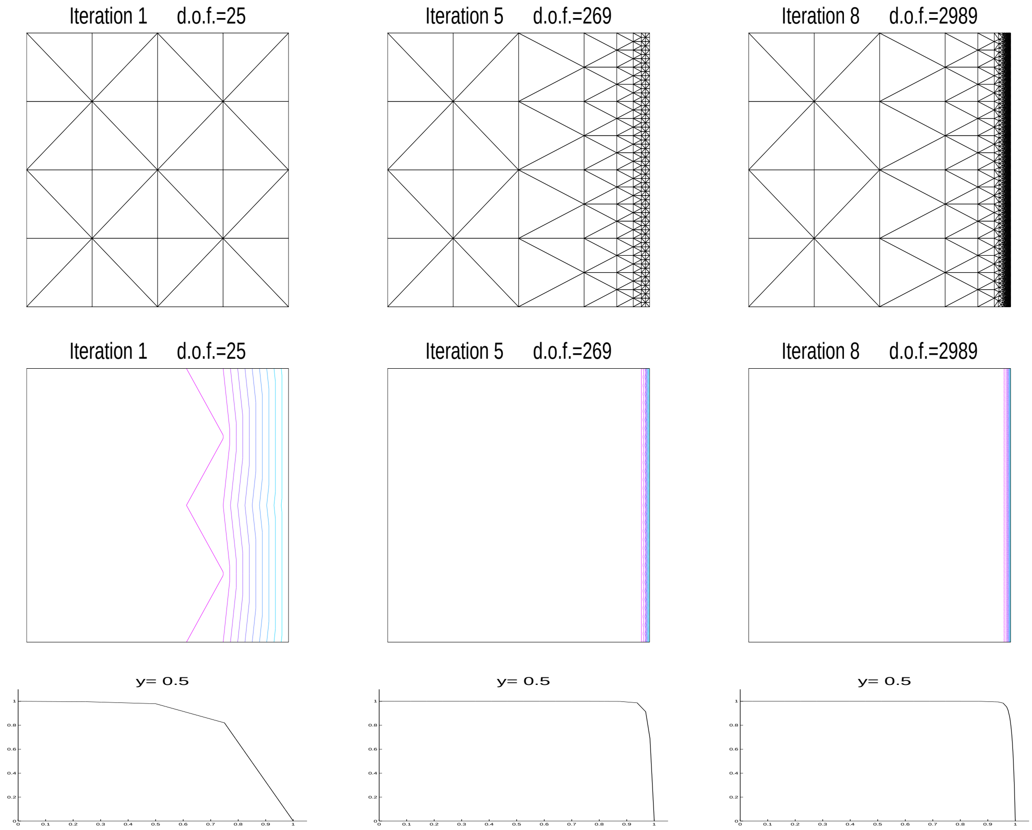

Figure 2.5: Reaction-diffusion problem: $\varepsilon = 10^{-4}$. Meshes, level sets, and horizontal cuts of the approximate solutions.

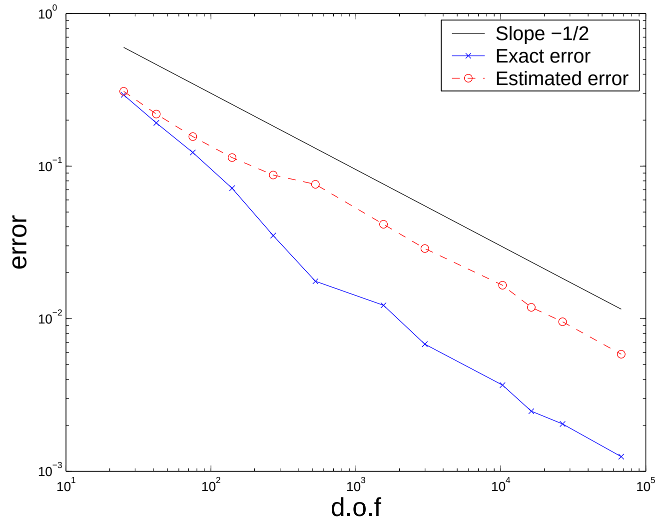

Figure 2.6: Reaction-diffusion problem: $\varepsilon = 10^{-4}$. Estimated and exact error curves.

It can be seen from Fig. 2.3 and 2.5 that the adaptive process leads to meshes correctly refined in the boundary layer zone. Notice that in the second case ($\varepsilon = 10^{-4}$) in which the boundary layer is much narrower, the adaptive scheme detects this and creates much more concentrated meshes. In both cases we are able to capture the boundary layers very sharply and without any significant oscillation.

On the other hand, the error curves show that, independently of how small the parameter ε is, the adaptive process yields optimal order convergence. This happens in spite of the fact that the effectivity indices are very poor. Indeed, it can be observed in Fig. 2.4 and 2.6 that the exact error is severely overestimated. Anyway, the exact and estimated error curves have approximately the same optimal slope $-\frac{1}{2}$.

2.4.2 An advection-diffusion problem

The second test consists in solving a purely advection-diffusion problem. We have chosen the following data: $\boldsymbol{a} = (1, 0)$, $b = 0$, $f = 1$, the boundary conditions shown in Fig. 2.7, and various values of the parameter ε. Let us remark that this problem is not covered by our theoretical results, since the chosen value of b violates assumption (A3). We report again the results obtained for $\varepsilon = 10^{-2}$ and $\varepsilon = 10^{-4}$.

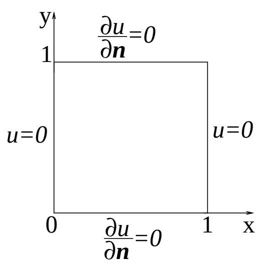

Figure 2.7: Boundary conditions for the advection-diffusion problem.

The exact solution of this problem is also analytically known:

$$u(x, y) = x - \frac{e^{-\frac{1-x}{\varepsilon}} - e^{-\frac{1}{\varepsilon}}}{1 - e^{-\frac{1}{\varepsilon}}}; \tag{2.18}$$

thus, we have been able to compute the exact errors, too.

Fig. 2.8 shows some of the successively refined meshes created in the adaptive process for $\varepsilon = 10^{-2}$, as well as the level sets and the horizontal cuts at $y = 0.5$ of the corresponding computed solution. Fig. 2.9 shows the error curves for the exact and estimated errors. Fig. 2.10 and 2.11 show analogous results for the same problem with the parameter $\varepsilon = 10^{-4}$.

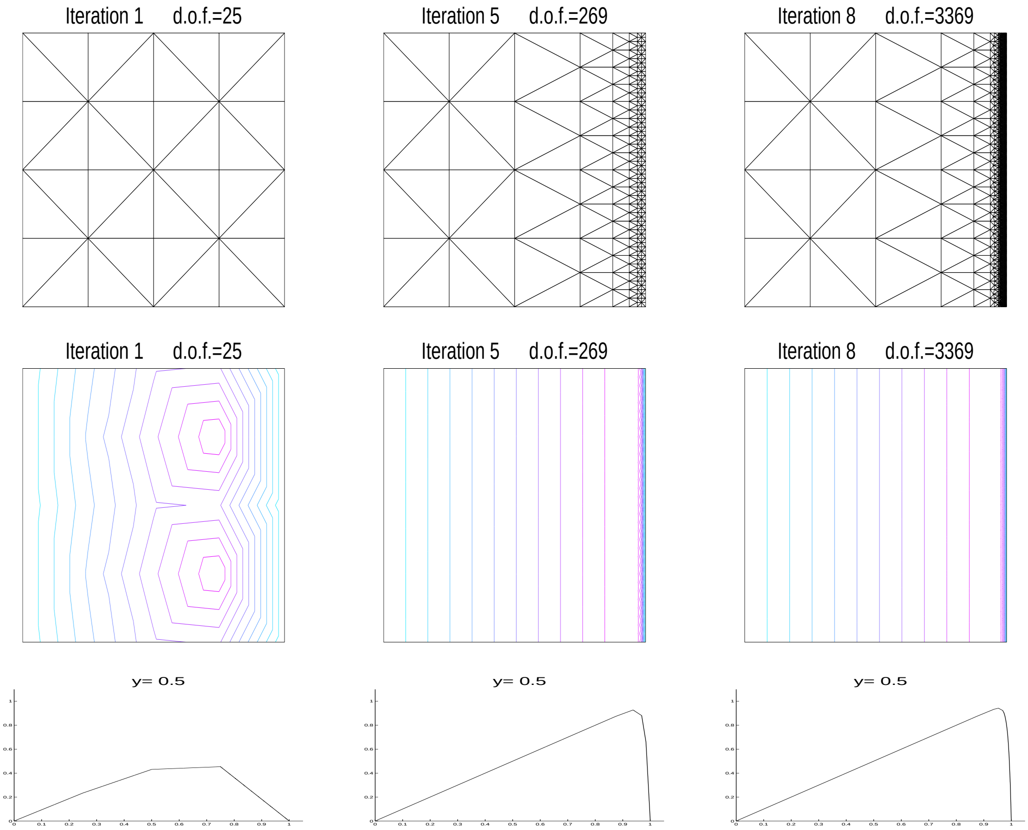

Figure 2.8: Advection-diffusion problem: $\varepsilon = 10^{-2}$. Meshes, level sets, and horizontal cuts of the approximate solutions.

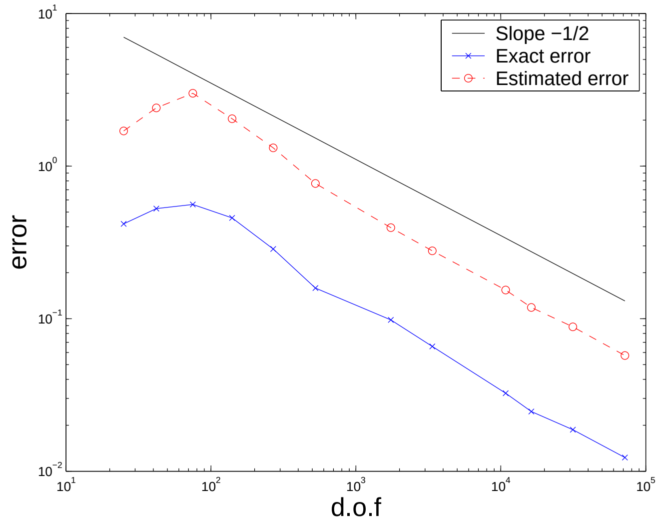

Figure 2.9: Advection-diffusion problem: $\varepsilon = 10^{-2}$. Estimated and exact error curves.

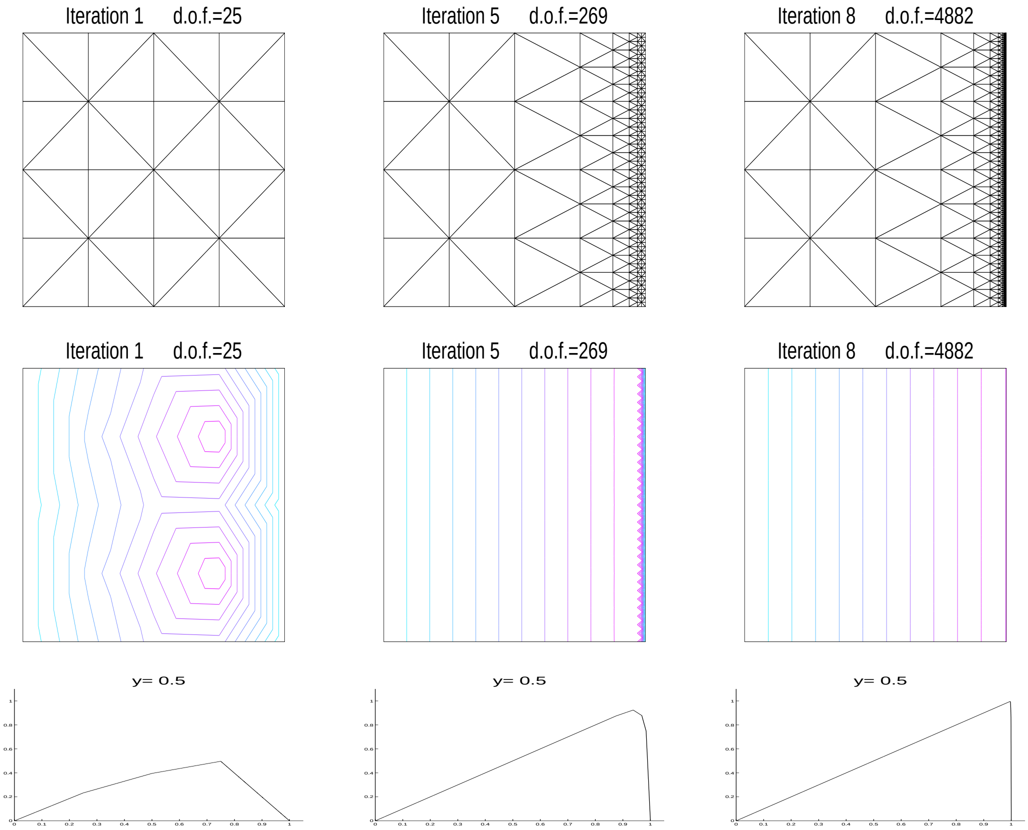

Figure 2.10: Advection-diffusion problem: $\varepsilon = 10^{-4}$. Meshes, level sets, and horizontal cuts of the approximate solutions.

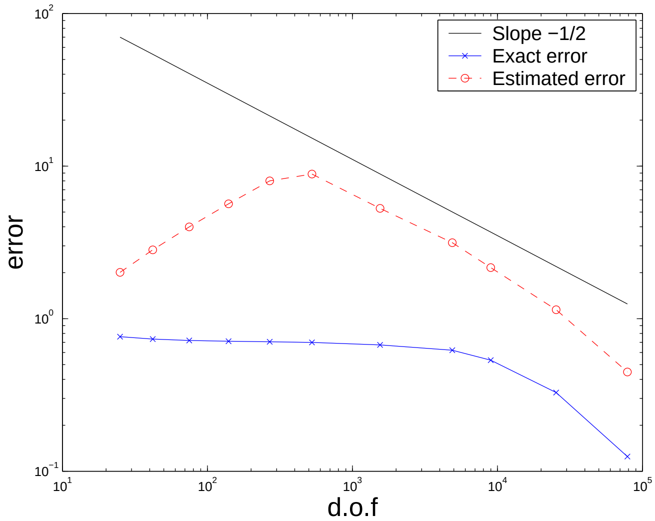

Figure 2.11: Advection-diffusion problem: $\varepsilon = 10^{-4}$. Estimated and exact error curves.

Essentially the same conclusions as in the previous test can be drawn from Fig. 2.8 and 2.10. In spite of the fact that this problem is out of the theory of Sections 2.2 and 2.3, the boundary layers are very sharply captured without any significant oscillation.

On the other hand, the error curves in Fig. 2.9 and 2.11 attain almost optimal slopes $-\frac{1}{2}$, once the meshes are sufficiently refined around the singular zone of the solutions.

2.4.3 An advection-diffusion-reaction problem with an inner layer

The last reported test consists in solving an advection-diffusion-reaction problem whose solution presents an inner layer. We have chosen the same example considered in [32] (*Problem N* in this reference). The corresponding data are: $\boldsymbol{a} = (2, 1)$, $b = 1$, $f = 0$, the boundary conditions shown in Fig. 2.12, and various values of the parameter ε. Let us remark that this problem is not covered by our theoretical results either, since the chosen Dirichlet boundary condition have a jump at the origin; hence, the problem cannot have a solution in $\mathrm{H}^1(\Omega)$. Once more, we report the results obtained for $\varepsilon = 10^{-2}$ and $\varepsilon = 10^{-4}$. We do not include error curves because no analytical solution is known in this case.

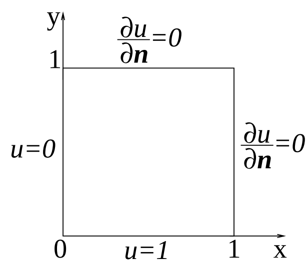

Figure 2.12: Boundary conditions for the advection-reaction-diffusion problem.

Fig. 2.13 and 2.14 show some of the successively refined meshes created in the adaptive process for $\varepsilon = 10^{-2}$ and $\varepsilon = 10^{-4}$, as well as the level sets of the corresponding computed solution.

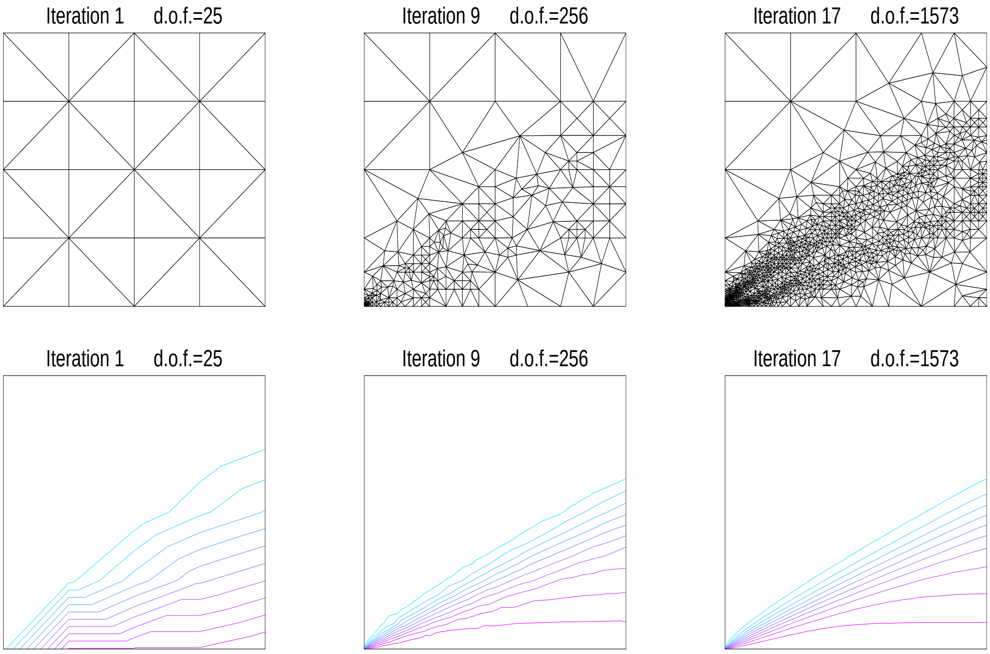

Figure 2.13: Advection-diffusion-reaction problem: $\varepsilon = 10^{-2}$. Meshes and level sets.

These figures show clearly that the adaptive process leads once more to correctly refined meshes. In both cases the adaptive scheme detects both, the corner singularity of the solution and the inner layer, and creates meshes much more concentrated around these zones.

In the first case ($\varepsilon = 10^{-2}$), the inner layer is very mild and the corner singularity of the solution prevails. Hence most of the elements are located in its vicinity (see in particular the mesh corresponding to the iteration number 9 in Fig. 2.13).

In the second case ($\varepsilon = 10^{-4}$), once the corner singularity is resolved, the adaptive scheme detects the inner layer and advance through it refining the mesh (see in particular the meshes corresponding to the iteration numbers 10, 20, and 30, in Fig. 2.14). Finally, the method allows us to capture the inner layer very sharply and without any significant oscillation.

The same problem has been solved in [32] with a very similar adaptive scheme based on an SUPG method. A comparison of the meshes reported in this reference (Fig. 1, top right and bottom left) with Fig. 2.13 and 2.14 of the present paper show clearly the advantage of our approach.

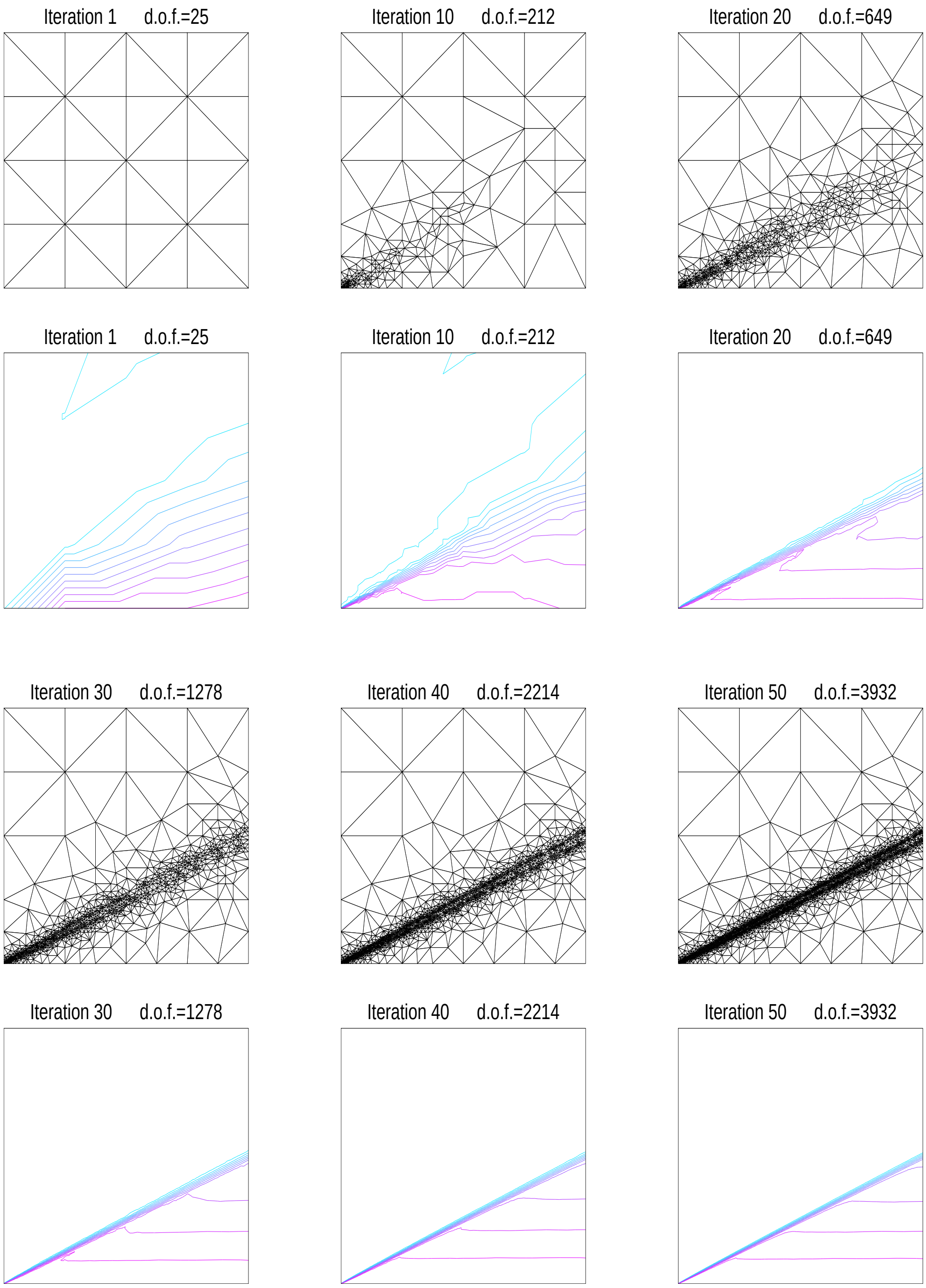

Figure 2.14: Advection-diffusion-reaction problem: $\varepsilon = 10^{-4}$. Meshes and level sets.

2.5 Conclusions

An adaptive finite element scheme for the advection-reaction-diffusion equation has been introduced and analyzed. This scheme is based on a stabilized finite element method combined with a residual error estimator. The estimator is shown to be reliable and efficient in that global upper and local lower error estimates are rigorously proved.

Several numerical experiments are reported. All of them show the effectiveness of this scheme to capture boundary and inner layers very sharply and without significant oscillations. Furthermore, the experiments show that the scheme attains optimal order of convergence.

Chapter 3

Error estimators for advection-reaction-diffusion equations based on the solution of local problems

This chapter deals with a posteriori error estimates for advection-reaction-diffusion equations. In particular, error estimators based on the solution of local problems are derived for a stabilized finite element method. These estimators are proved to be equivalent to the error, with equivalence constants eventually depending on the physical parameters. Numerical experiments illustrating the performance of this approach are reported.

3.1 Introduction

This chapter deals with the advection-diffusion-reaction equations. This kind of problems arise in many application, for instance, to model pollutant transport and degradation in aquatic media, which was the motivation of the present work.

In applications, typically the advective or reactive terms are dominant. In this case, inner or boundary layers arise and stabilization techniques has to be used to avoid spurious oscillations (see [24] and references therein, which include numerical methods). When finite element methods are used, adequately refined meshes are useful to improve the quality of the numerical solution with minimal computational effort. These schemes are typically based on a posteriori error indicators. We refer to [21] for a survey of this kind of techniques applied to advection dominated problems. See also [27, 26] and [34] for error estimates in alternative norms adequately suited to this kind of equations.

In a recent article [4], we have introduced and analyzed from theoretical and experimental points of view an adaptive scheme to efficiently solve the advection-reaction-diffusion equation. This scheme is based on a stabilized finite element method introduced in [19] combined with a residual error estimator, similar to another one introduced by Verfurth in [32]. We have proved global upper and local lower error estimates in the energy norm, with constants which depend on the shape-regularity of the mesh, the polynomial degree of the finite element approximating space, and the local mesh Peclet number.

Following this line, we introduce in this paper a framework to derive error estimators based on the solution of local problems. We prove the equivalence of the resulting estimators with the residual based estimator analyzed in [4] and, hence, with the energy norm of the error.

We report several numerical experiments which allow us to asses the effectiveness of this approach to capture boundary and inner layers very sharply and without significant oscillations. The experiments also show that the schemes lead to optimal orders of convergence.

The paper is organized as follows. In Section 3.2 we recall the advection-diffusion-reaction problem under consideration and the stabilized scheme. In Section 3.3 we recall the main result of [4] and derive *a posteriori* error estimators based on the solution of local problems. Then, we prove their equivalence with the residual error estimator analyzed in [4]. Finally, in Section 3.4, we report the results of some numerical tests, to asses the performance of the estimators.

3.2 A stabilized method for a model problem

Our model problem is the advection-reaction-diffusion problem

$$\left\{ \begin{array}{rcll} -\varepsilon\Delta u + \boldsymbol{a}\cdot\nabla u + bu &=& f & \text{in } \Omega, \\ u &=& 0 & \text{on } \Gamma_{\rm D}, \\ \varepsilon\dfrac{\partial u}{\partial \boldsymbol{n}} &=& g & \text{on } \Gamma_{\rm N}, \end{array} \right. \tag{3.1}$$

where $\Omega \subset \mathbb{R}^2$, is a bounded polygonal domain with a Lipschitz boundary $\Gamma = \bar{\Gamma}_{\rm D} \cup \bar{\Gamma}_{\rm N}$, with $\Gamma_{\rm D} \cap \Gamma_{\rm N} = \emptyset$. We denote by $\boldsymbol{n}$ the outer unit normal vector to Γ.

We are interested in the advection-reaction dominated case and assume that:

(A1) $\varepsilon \in \mathbb{R}:\ 0 < \varepsilon \ll 1$;

(A2) $\boldsymbol{a} \in \mathrm{W}^{1,\infty}(\Omega)^2 :\ \operatorname{div} \boldsymbol{a} = 0$ in Ω;

(A3) $b \geq 1$ in Ω;

(A4) $\Gamma_{\mathrm{D}} \supset \{\boldsymbol{x} \in \Gamma :\ \boldsymbol{a}(\boldsymbol{x}) \cdot \boldsymbol{n}(\boldsymbol{x}) < 0\}$;

(A5) $f \in \mathrm{L}^2(\Omega),\ \ g \in \mathrm{L}^2(\Gamma_{\mathrm{N}})$.

We use standard notation for Sobolev and Lebesgue spaces, norms, and inner products. Moreover, we introduce the following notation: Let

$$\mathrm{H}^1_{\Gamma_{\mathrm{D}}}(\Omega) := \left\{\varphi \in \mathrm{H}^1(\Omega) :\ \varphi = 0 \text{ on } \Gamma_{\mathrm{D}}\right\}$$

and B be the bilinear form defined on $\mathrm{H}^1(\Omega)$ by

$$B(v, w) := \int_\Omega \left(\varepsilon \nabla v \cdot \nabla w + \boldsymbol{a} \cdot \nabla v\ w + bvw\right).$$

Then, the standard variational formulation of problem (3.1) is the following: Find $u \in \mathrm{H}^1_{\Gamma_{\mathrm{D}}}(\Omega)$ such that

$$B(u, v) = \int_\Omega fv + \int_{\Gamma_{\mathrm{N}}} gv \quad \forall v \in \mathrm{H}^1_{\Gamma_{\mathrm{D}}}(\Omega). \tag{3.2}$$

We consider the following (energy) norm on $\mathrm{H}^1(\Omega)$:

$$|||u||| := \left(\varepsilon \left\|\nabla u\right\|^2_{0,\Omega} + \left\|u\right\|^2_{0,\Omega}\right)^{\frac{1}{2}}.$$

Assumptions (A1)–(A4) and integration by parts imply that

$$B(v, v) \geq |||v|||^2 \quad \forall v \in \mathrm{H}^1_{\Gamma_{\mathrm{D}}}(\Omega)$$

and

$$B(v, w) \leq \left(1 + \left\|b\right\|_{\infty,\Omega} + \varepsilon^{-\frac{1}{2}} \left\|\boldsymbol{a}\right\|_{\infty,\Omega}\right) |||v|||\ |||w|||.$$

Hence, as a consequence of Lax-Milgram's Lemma, problem (3.2) has a unique solution.

Let us remark that the same conclusion holds if the assumption (A3) is substituted by the following one, which is slightly weaker: $-\frac{1}{2} \operatorname{div} \boldsymbol{a} + b \geq 1$. Anyway, the difference is meaningless in practice, since typically $\operatorname{div} \boldsymbol{a} = 0$.

Let $\{\mathcal{T}_h\}_{h>0}$, be a family of shape-regular partitions of Ω into triangles. As usual, h denotes the mesh size: $h = \max h_T$, with h_T being the diameter of T.

For $k \in \mathbb{N}$, let

$$V_h := \left\{\varphi \in \mathrm{H}^1_{\Gamma_{\mathrm{D}}}(\Omega) :\ \varphi|_T \in \mathcal{P}_k\ \forall T \in \mathcal{T}_h\right\},$$

where $\mathcal{P}_k$ denotes the space of polynomials of degree at most k.

It is well known that the standard Galerkin method with this finite element space yields poor approximation when $\varepsilon \ll |\boldsymbol{a}|$ or $\varepsilon \ll b$. For this reason we consider the following stabilized formulation introduced in [19]: Find $u_h \in V_h$ such that

$$B_\tau(u_h, v_h) = F_\tau(v_h) \quad \forall v_h \in V_h, \tag{3.3}$$

where, for $v_h, w_h \in V_h$,

$$\begin{aligned} B_\tau(v_h, w_h) &:= B(v_h, w_h) \\ &- \sum_{T \in \mathcal{T}_h} \int_T \tau_T \left(-\varepsilon \Delta v_h + \boldsymbol{a} \cdot \nabla v_h + b v_h\right)\left(-\varepsilon \Delta w_h - \boldsymbol{a} \cdot \nabla w_h + b w_h\right) \end{aligned}$$

and

$$F_\tau(v_h) := \int_\Omega f v_h + \int_{\Gamma_{\mathrm{N}}} g v_h - \sum_{T \in \mathcal{T}_h} \int_T \tau_T f(-\varepsilon \Delta v_h - \boldsymbol{a} \cdot \nabla v_h + b v_h).$$

In the expressions above, the stabilization parameter τ_T is defined as follows:

$$\tau_T(\boldsymbol{x}) := \frac{h_T^2}{b h_T^2 \max\{1, \mathrm{Pe}_T^{\mathrm{R}}(\boldsymbol{x})\} + (2\varepsilon/m_k)\max\{1, \mathrm{Pe}_T^{\mathrm{A}}(\boldsymbol{x})\}},$$

with $\mathrm{Pe}_T^{\mathrm{R}}(\boldsymbol{x})$ and $\mathrm{Pe}_T^{\mathrm{A}}(\boldsymbol{x})$ being the Peclet numbers respectively defined by

$$\mathrm{Pe}_T^{\mathrm{R}}(\boldsymbol{x}) := \frac{2\varepsilon}{m_k b(\boldsymbol{x}) h_T^2} \qquad \text{and} \qquad \mathrm{Pe}_T^{\mathrm{A}}(\boldsymbol{x}) := \frac{m_k \left|\boldsymbol{a}(\boldsymbol{x})\right| h_T}{\varepsilon},$$

where $m_k := \min\{1/3, C_k\}$, with C_k being a positive constant satisfying

$$C_k \sum_{T \in \mathcal{T}_h} h_T^2 \left\|\Delta v_h\right\|_{0,T}^2 \leq \left\|\nabla v_h\right\|_{0,\Omega}^2, \quad \forall v_h \in V_h,$$

which only depends on the polynomial degree k and the shape-regularity of the mesh.

The convergence and stabilization properties of this scheme have been investigated in [19], where numerical experiments proving the effectiveness of this approach have been reported. In particular, the method has been shown to be advantageous in comparison with other more standard stabilization techniques.

However, the experiments reported in [19] also show that the method does not allow a sharp resolution of inner layers when quasi-uniform meshes are used. In the following section we introduce error indicators which will allow us to create in an automatic fashion meshes correctly refined around inner and boundary layers of the solution.

3.3 A posteriori error estimator.

In this section we define error estimators based on the solution of auxiliary local problems. To prove their efficiency and reliability, we will compare it with a residual based estimator analyzed in [4]. In what follows, we recall the definition and main properties of the latter.

Let $\mathcal{E}_h$ denote the set of all edges in $\mathcal{T}_h$ and, for $E \in \mathcal{E}_h$, let h_E be the length of E. We define the respective volumetric and edge residuals by

$$R_T^h(u_h) := f_h + \varepsilon\Delta u_h - \boldsymbol{a}\cdot\nabla u_h - b u_h, \qquad \text{in } T \in \mathcal{T}_h,$$

$$R_E^h(u_h) := \begin{cases} -\left[\!\left[\varepsilon \dfrac{\partial u_h}{\partial \boldsymbol{n}_E}\right]\!\right]_E, & \text{on } E \in \mathcal{E}_h : \ E \not\subset \Gamma, \\ g_h - \varepsilon \dfrac{\partial u_h}{\partial \boldsymbol{n}}, & \text{on } E \in \mathcal{E}_h : \ E \subset \Gamma_{\mathrm{N}}, \\ 0, & \text{on } E \in \mathcal{E}_h : \ E \subset \Gamma_{\mathrm{D}}, \end{cases}$$

where $[\![\cdot]\!]_E$ denotes the jump across E, and $\boldsymbol{n}_E$ is a unit normal vector to E (see for instance [31]). The functions f_h and g_h denote arbitrary but fixed approximations of f and g such that $f_h|_T \in \mathcal{P}_k \ \forall T \in \mathcal{T}_h$ and $g_h|_E \in \mathcal{P}_{k-1} \ \forall E \in \mathcal{E}_h$ such that $E \subset \Gamma_{\mathrm{N}}$.

For each $T \in \mathcal{T}_h$, let $\mathcal{E}_T$ denote the set of edges of T. The following residual based local error estimate η_T was introduced in [4]:

$$\begin{aligned} \eta_T^2 \ &:= \ \alpha_T^2 \left\| R_T^h(u_h) \right\|_{0,T}^2 \\ &\quad + \frac{1}{2} \sum_{E\in\mathcal{E}_T:\, E\not\subset\Gamma} \varepsilon^{-\frac{1}{2}} \alpha_E \left\| R_E^h(u_h) \right\|_{0,E}^2 + \sum_{E\in\mathcal{E}_T:\, E\subset\Gamma_{\mathrm{N}}} \varepsilon^{-\frac{1}{2}} \alpha_E \left\| R_E^h(u_h) \right\|_{0,E}^2, \end{aligned} \tag{3.4}$$

with

$$\alpha_S := \min\left\{ h_S \varepsilon^{-\frac{1}{2}}, 1 \right\}, \quad S = E \text{ or } S = T. \tag{3.5}$$

The equivalence between this estimator and the energy norm of the exact error has been proved in [4], under similar conditions to those of the next theorem:

THEOREM 3.3.1 *Let u and u_h be the solutions of problems (3.2) and (3.3), respectively. Let f_h, g_h, and η_T be defined as above. Then, there holds*

$$\begin{aligned} |\!|\!| u - u_h |\!|\!| \ &\le \ C \left[\left(\sum_{T\in\mathcal{T}_h} \eta_T^2 \right)^{\frac{1}{2}} \right. \\ &\quad \left. + \left(\sum_{T\in\mathcal{T}_h} \alpha_T^2 \left\| f - f_h \right\|_{0,T}^2 + \sum_{E\in\mathcal{E}_h:\, E\subset\Gamma_{\mathrm{N}}} \varepsilon^{-\frac{1}{2}} \alpha_E \left\| g - g_h \right\|_{0,E}^2 \right)^{\frac{1}{2}} \right] \end{aligned}$$

and

$$\eta_T \;\le\; C\left(1 + \|b\|_{\infty,\omega_T} + \varepsilon^{-\frac{1}{2}}\,\|a\|_{\infty,\omega_T}\,\alpha_T\right)|||u-u_h|||_{\omega_T}$$
$$+\,\alpha_T\,\|f-f_h\|_{0,\omega_T} + \left(\sum_{E\in\mathcal{E}_T:\,E\subset\Gamma_{\mathrm{N}}}\varepsilon^{-\frac{1}{2}}\alpha_E\,\|g-g_h\|_{0,E}^2\right)^{\frac{1}{2}} \quad \forall T\in\mathcal{T}_h,$$

where $\omega_T := \bigcup\{T'\in\mathcal{T}_h:\ T'$ *and* T *share an edge*$\}$.

Here and thereafter, C denotes a generic positive constant, not necessarily the same at each occurrence but always independent of the mesh-size and the small parameter ε.

In what follows we introduce some bubble functions and lifting operators which will be used in the sequel. Let ψ_T be the classical cubic bubble function supported in T. Let $\psi_{E,\theta}$, $0<\theta\le 1$, be the piecewise quadratic bubble function introduced in [32]. Let us recall that, for inner edges, the support of $\psi_{E,\theta}$ is the shadowed quadrilateral in Fig. 3.1.

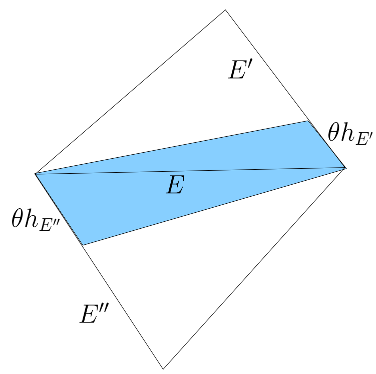

Figure 3.1: Support of $\psi_{E,\theta}$.

Let $\psi_E := \psi_{E,\theta_E}$, with $\theta_E := \min\{\varepsilon^{\frac{1}{2}}h_E^{-1},1\}$. Let P_E be the lifting operator introduced in [32], which associates to each $\sigma\in\mathcal{P}_{k-1}(E)$, a piecewise polynomial function of degree $k-1$ defined on $\omega_E := \bigcup\{T\in\mathcal{T}_h : E\subset T\}$.

From now on we further assume that the coefficients $\boldsymbol{a}$ and b are piecewise polynomial; more precisely,

$$\text{(A6)}\quad \boldsymbol{a}|_T\in\mathcal{P}_1(T)^2\ \forall T\in\mathcal{T}_h,\ \ b|_T\in\mathcal{P}_0(T)\ \forall T\in\mathcal{T}_h.$$

Notice that, because of assumption (A6), $R_T^h(u_h)\in\mathcal{P}_k(T)\ \forall T\in\mathcal{T}_h$. Moreover, $R_E^h(u_h)\in\mathcal{P}_{k-1}(E)\ \forall E\in\mathcal{E}_h$ and then the following estimates follow from Lemma 3.3 in [32]:

LEMMA 3.3.1 *For all $T \in \mathcal{T}_h$, there hold:*

$$\left\|R_T^h(u_h)\right\|_{0,T}^2 \leq C\left(R_T^h(u_h), R_T^h(u_h)\psi_T\right)_T, \tag{3.6}$$

$$\left|\!\left|\!\left|R_T^h(u_h)\psi_T\right|\!\right|\!\right| \leq C\alpha_T^{-1}\left\|R_T^h(u_h)\right\|_{0,T}. \tag{3.7}$$

LEMMA 3.3.2 *For all $E \in \mathcal{E}_h$, there hold:*

$$\left\|R_E^h(u_h)\right\|_{0,E}^2 \leq C\left(R_E^h(u_h), R_E^h(u_h)\psi_E\right)_E, \tag{3.8}$$

$$\left\|P_E\big(R_E^h(u_h)\big)\,\psi_E\right\|_{0,\omega_E} \leq C\varepsilon^{\frac{1}{4}}\alpha_E^{\frac{1}{2}}\left\|R_E^h(u_h)\right\|_{0,E}, \tag{3.9}$$

$$\left|\!\left|\!\left|P_E\big(R_E^h(u_h)\big)\,\psi_E\right|\!\right|\!\right| \leq C\varepsilon^{\frac{1}{4}}\alpha_E^{-\frac{1}{2}}\left\|R_E^h(u_h)\right\|_{0,E}. \tag{3.10}$$

Now we are in position to introduce the local problems that will be used to define the error estimators. Given $T \in \mathcal{T}_h$, let V_T be the finite dimensional space defined by

$$V_T := \operatorname{span}\left(\{\psi_T v : v \in \mathcal{P}_k(T)\} \cup \{\psi_E P_E\sigma : \sigma \in \mathcal{P}_{k-1}(E),\ E \in \mathcal{E}_T : E \not\subset \Gamma_{\mathrm{D}}\}\right).$$

Let β_T be a bilinear form defined on V_T such that there exist positive constants γ and β, eventually depending on ε, such that

$$|\beta_T(v,w)| \leq \beta\,|\!|\!|v|\!|\!|\,|\!|\!|w|\!|\!| \quad \forall v,w \in V_T, \tag{3.11}$$

$$\beta_T(v,v) \geq \gamma\,|\!|\!|v|\!|\!|^2 \quad \forall v \in V_T. \tag{3.12}$$

Two different particular bilinear forms β_T will be tested in the following section. The first one is the same bilinear form B of the original problem:

$$\beta_T^{(1)}(v,w) := \int_{\omega_T}\left(\varepsilon\nabla v\cdot\nabla w + \boldsymbol{a}\cdot\nabla v\; w + bvw\right), \tag{3.13}$$

which satisfies (3.11) with $\beta = 1 + \|b\|_{\infty,\omega_T} + \varepsilon^{-\frac{1}{2}}\|\boldsymbol{a}\|_{\infty,\omega_T}$. The second one is the bilinear form B without the advective term:

$$\beta_T^{(2)}(v,w) := \int_{\omega_T}\left(\varepsilon\nabla v\cdot\nabla w + bvw\right), \tag{3.14}$$

which satisfies (3.11) with $\beta = 1 + \|b\|_{\infty,\omega_T}$. Notice that in this case β does not depend on ε. Both, $\beta_T^{(1)}$ and $\beta_T^{(2)}$, clearly satisfy (3.12), with $\gamma = 1$ independently of ε, too.

Given $T \in \mathcal{T}_h$, consider the following finite dimensional problem: Find $v_T \in V_T$:

$$\beta_T(v_T,w) = (R_T^h(u_h),w)_T + \sum_{E\in\mathcal{E}_T}(R_E^h(u_h),w)_E \quad \forall w \in V_T. \tag{3.15}$$

From (3.11) and (3.12), problem (3.15) is well posed on V_T, as a consequence of Lax-Milgram Lemma.

Finally, we define the local error estimate $\tilde{\eta}_T$ by

$$\tilde{\eta}_T := |||v_T||| \,. \tag{3.16}$$

The following is the main theoretical result of this paper:

THEOREM 3.3.2 *Given T in $\mathcal{T}_h$, let η_T and $\tilde{\eta}_T$ be the estimators defined by (3.4) and (3.16), respectively. Then, there exist positive constants C and C' such that*

$$C'\gamma\tilde{\eta}_T \le \eta_T \le C\beta\tilde{\eta}_T,$$

where β and γ are the continuity and ellipticity constants in (3.11) and (3.12), respectively.

PROOF. For the lower bound of the theorem, we take $w = v_T$ in (3.15) and we use (3.12) and Cauchy-Schwartz inequality to obtain

$$\begin{aligned}
\gamma\, |||v_T|||^2 &\le \beta_T(v_T, v_T) \\
&= (R_T^h(u_h), v_T)_T + \sum_{E\in\mathcal{E}_T} (R_E^h(u_h), v_T)_E \\
&\le \left\|R_T^h(u_h)\right\|_{0,T} \|v_T\|_{0,T} + \sum_{E\in\mathcal{E}_T} \left\|R_E^h(u_h)\right\|_{0,E} \|v_T\|_{0,E} \,.
\end{aligned}$$

Next we use the following inverse inequalities which can be proved by following some arguments in [32] (see (5.6) and the proof of (5.4) in this reference):

$$\begin{aligned}
\|v_T\|_{0,T} &\le C\alpha_T\, |||v_T||| \,, \\
\|v_T\|_{0,E} &\le C\varepsilon^{-\frac{1}{4}}\alpha_E^{\frac{1}{2}}\, |||v_T||| \quad \forall E \in \mathcal{E}_T.
\end{aligned}$$

Thus, from (3.4), we obtain

$$\gamma\, |||v_T|||^2 \le C \left[\alpha_T \left\|R_T^h(u_h)\right\|_{0,T} + \sum_{E\in\mathcal{E}_T} \varepsilon^{-\frac{1}{4}}\alpha_E^{\frac{1}{2}} \left\|R_E^h(u_h)\right\|_{0,E}\right] |||v_T||| \le C\eta_T\, |||v_T||| \,,$$

and we conclude the lower bound of the theorem.

To prove the upper bound, first let $w_T := R_T^h(u_h)\psi_T \in V_T$. Using (3.6), (3.15) with $w = w_T$, (3.11), and (3.7), we have

$$\begin{aligned}
\left\|R_T^h(u_h)\right\|_{0,T}^2 &\le C(R_T^h(u_h), w_T) \\
&= C\beta_T(v_T, w_T) \\
&\le C\beta\, |||v_T|||\, |||w_T||| \\
&\le C\beta\, |||v_T|||\, \alpha_T^{-1} \left\|R_T^h(u_h)\right\|_{0,T} .
\end{aligned}$$

Consequently,

$$\alpha_T \left\| R_T^h(u_h) \right\|_{0,T} \leq C\beta \left|\left|\left| v_T \right|\right|\right| . \tag{3.17}$$

Next, given $E \in \mathcal{E}_T$, such that $E \not\subset \Gamma_{\mathrm{D}}$, let $w_E := P_E\big(R_E^h(u_h)\big)\, \psi_E \in V_T$. Taking $w = w_E$ in (3.15) we have

$$\beta_T(v_T, w_E) = (R_T^h(u_h), w_E)_T + (R_E^h(u_h), w_E)_E.$$

Hence, using (3.8), (3.11), Cauchy-Schwartz inequality, (3.9), (3.17), and (3.10), we have

$$\begin{aligned}
\left\| R_E^h(u_h) \right\|_{0,E}^2 &\leq C(R_E^h(u_h), R_E^h(u_h)\psi_E)_E = C(R_E^h(u_h), w_E)_E \\
&= C\left[\beta_T\left(v_T, P_E\big(R_E^h(u_h)\big)\,\psi_E\right) - \left(R_T^h(u_h), P_E\big(R_E^h(u_h)\big)\,\psi_E\right)_T\right] \\
&\leq C\left[\beta \left|\left|\left| v_T \right|\right|\right| \left|\left|\left| P_E\big(R_E^h(u_h)\big)\,\psi_E \right|\right|\right| + \left\| R_T^h(u_h) \right\|_{0,T} \left\| P_E\big(R_E^h(u_h)\big)\,\psi_E \right\|_{0,T}\right] \\
&\leq C\left[\beta \left|\left|\left| v_T \right|\right|\right| \varepsilon^{\frac14}\alpha_E^{-\frac12} \left\| R_E^h(u_h) \right\|_{0,E} + \beta\alpha_T^{-1} \left|\left|\left| v_T \right|\right|\right| \varepsilon^{\frac14}\alpha_E^{\frac12} \left\| R_E^h(u_h) \right\|_{0,E}\right]
\end{aligned}$$

Now, because of the regularity of the mesh, $\alpha_E \leq C\alpha_T$, and, consequently,

$$\varepsilon^{-\frac14}\alpha_E^{\frac12} \left\| R_E^h(u_h) \right\|_{0,E} \leq C\beta \left|\left|\left| v_T \right|\right|\right| .$$

Finally, from (3.17) and the last inequality we conclude the proof. □

As a consequence of Theorems 3.3.1 and 3.3.2, we obtain error estimates similar to those of Theorem 3.3.1, with $\tilde{\eta}_T$ instead of η_T, although with the constants of the estimates depending on ε, whenever β or γ do it.

3.4 Numerical experiments

In this section we report three series of numerical experiments with the stabilized method described in Section 3.2 and an h-adaptive mesh-refinement strategy based on the error estimators analyzed in Section 3.3. In all the experiments we have used piecewise linear finite elements (i.e., polynomial degree $k = 1$) and we have taken as geometric domain the unit square $\Omega := (0,1) \times (0,1)$, although with different boundary conditions. We have considered different values of the coefficients ε, $\boldsymbol{a}$, and b of the advection-reaction-diffusion equation (3.1), too.

The adaptive procedure consists in solving problem (3.3) on a sequence of meshes up to finally attain a solution with an estimated error within a prescribed tolerance. To attain this purpose, the process is initiated with a quasi-uniform mesh and, at each step, a new mesh better adapted to the solution of problem (3.2) is created. This is done by computing the local error estimators $\tilde{\eta}_T$ for all T in the "old" mesh $\mathcal{T}_h$, and refining those elements T with $\tilde{\eta}_T \geq \mu \max\{\tilde{\eta}_T : T \in \mathcal{T}_h\}$, where $\mu \in (0,1)$ is a prescribed parameter. In all our experiments we have chosen $\mu = \frac{1}{2}$. To refine the meshes we have used the red-green-blue strategy described in [31].

We have considered two estimators: $\tilde{\eta}_T^{(1)}$, associated with the local bilinear form $\beta_T^{(1)}$ as defined in (3.13), and $\tilde{\eta}_T^{(2)}$, associated with $\beta_T^{(2)}$ as defined in (3.14). Let us remark that the constants β and γ in Theorem 3.3.2 do not depend on ε for $\beta_T^{(1)}$ and, consequently, $\tilde{\eta}_T^{(1)}$ is equivalent to the estimator η_T with constants independent of ε.

3.4.1 A reaction-diffusion problem

The first test consists in solving a purely reaction-diffusion problem. We have chosen the following data: $\boldsymbol{a} = \mathbf{0}$, $b = 1$, $f = 1$, and $\varepsilon = 10^{-4}$. We have used the boundary conditions shown in Fig. 3.2.

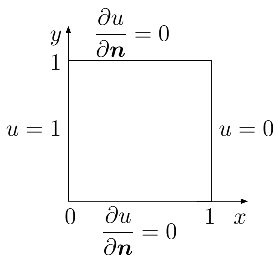

Figure 3.2: Reaction-diffusion problem: Boundary conditions.

The exact solution of this problem is analytically known:

$$u(x,y) = 1 - \frac{\sinh(\varepsilon^{-1/2}x)}{\sinh(\varepsilon^{-1/2})};$$

thus, we have been able to compute the exact errors of our finite element approximations.

Notice that for this problem, $\tilde{\eta}_T^{(1)} = \tilde{\eta}_T^{(2)}$ because the advective term is not present.

Fig. 3.3 shows some of the successively refined meshes created in the adaptive process. This figure also shows the level sets and the vertical sections at $y = 0.5$ of the corresponding computed solution. The iteration number and the number of degrees of freedom (d.o.f.) of each mesh are also reported in this figure.

Fig. 3.4 shows the error curves of the whole process for the estimated errors $\tilde{\eta} = \left(\sum_{T\in\mathcal{T}_h} \tilde{\eta}_T^2\right)^{1/2}$ and $\eta = \left(\sum_{T\in\mathcal{T}_h} \eta_T^2\right)^{1/2}$. We also include in this figure the exact errors of the adaptive schemes guided by $\tilde{\eta}_T$ and η_T, which are labelled "Error $(\tilde{\eta}_T)$" and "Error (η_T)", respectively. The figure also includes a line with slope $-\frac{1}{2}$, which corresponds to the theoretically optimal order of convergence for piecewise linear elements.

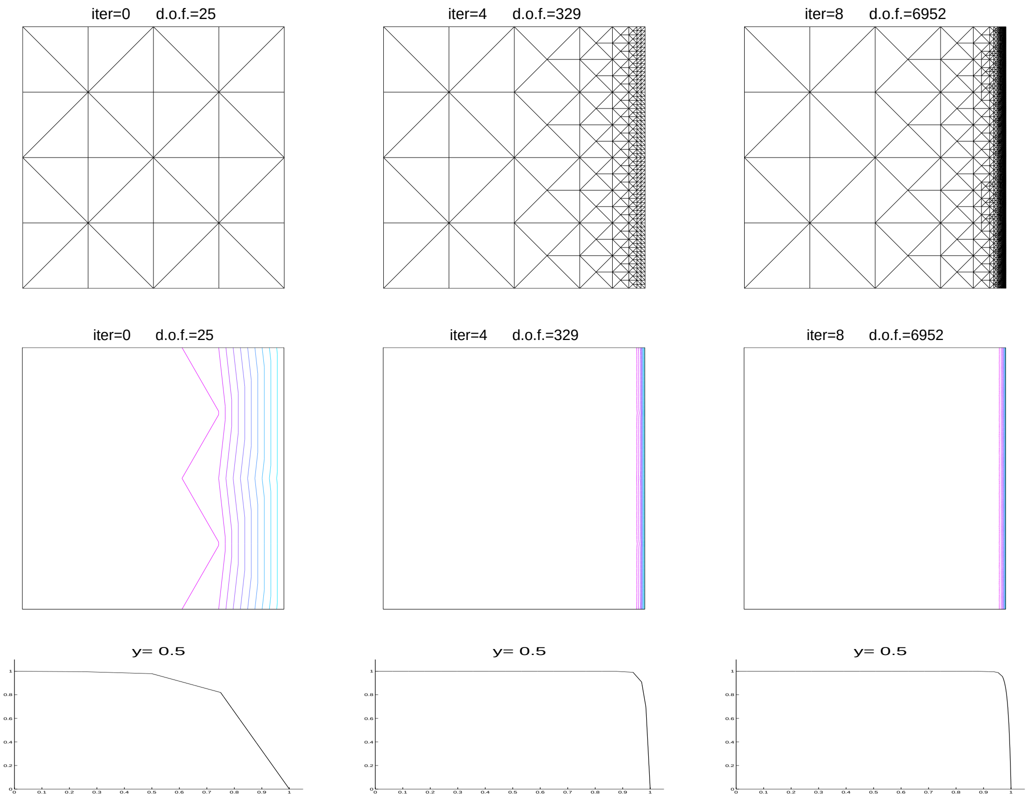

Figure 3.3: Reaction-diffusion problem: Meshes, level sets, and vertical sections of the approximate solutions.

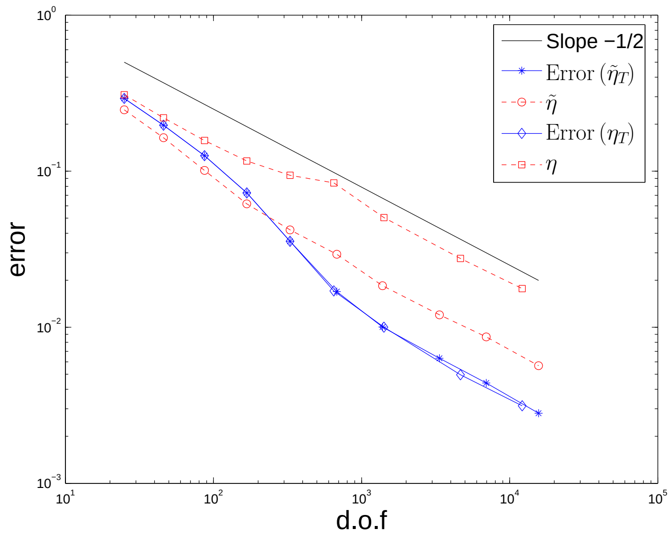

Figure 3.4: Reaction-diffusion problem: Estimated and exact error curves.

It can be seen from Fig. 3.3 that the adaptive process leads to meshes correctly refined in the boundary layer zone. In fact, both estimators lead almost to the same meshes.

On the other hand, the error curves show that the adaptive process yields optimal order convergence: the exact and estimated error curves have approximately the same optimal slope $-\frac{1}{2}$. Furthermore, Fig. 3.4 shows that the error estimator $\tilde{\eta}$ have a significantly better effectivity index than the residual error estimator η.

3.4.2 An advection-diffusion problem

The second test consists in solving a purely advection-diffusion problem. We have chosen the following data: $\boldsymbol{a} = (1, 0)$, $b = 0$, $f = 1$, $\varepsilon = 10^{-4}$, and the boundary conditions shown in Fig. 3.5. Let us remark that this problem is not covered by our theoretical results, since the chosen value of b violates assumption (A3).

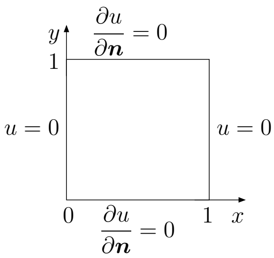

Figure 3.5: Advection-diffusion problem: Boundary conditions.

The exact solution of this problem is also analytically known:

$$u(x, y) = x - \frac{\mathrm{e}^{-\frac{1-x}{\varepsilon}} - \mathrm{e}^{-\frac{1}{\varepsilon}}}{1 - \mathrm{e}^{-\frac{1}{\varepsilon}}};$$

thus, we have been able to compute the exact errors, too.

Both estimators, $\tilde{\eta}_T^{(1)}$ and $\tilde{\eta}_T^{(2)}$, lead to similar adapted meshes. Fig. 3.6 shows some of the successively refined meshes created in the adaptive process guided by the error indicators $\tilde{\eta}_T^{(1)}$. This figure also includes the level sets and the vertical sections at $y = 0.5$ of the corresponding computed solution.

Fig. 3.7 shows the error curves for the exact and the estimated errors. Once more, "Error ($\tilde{\eta}_T^{(k)}$)" denotes the exact error of the adaptive scheme guided by $\tilde{\eta}_T^{(k)}$, $k = 1, 2$, and $\tilde{\eta}^{(k)} := \left(\sum_{T \in \mathcal{T}_h} \tilde{\eta}_T^{(k)}\right)^{1/2}$, the corresponding estimated errors.

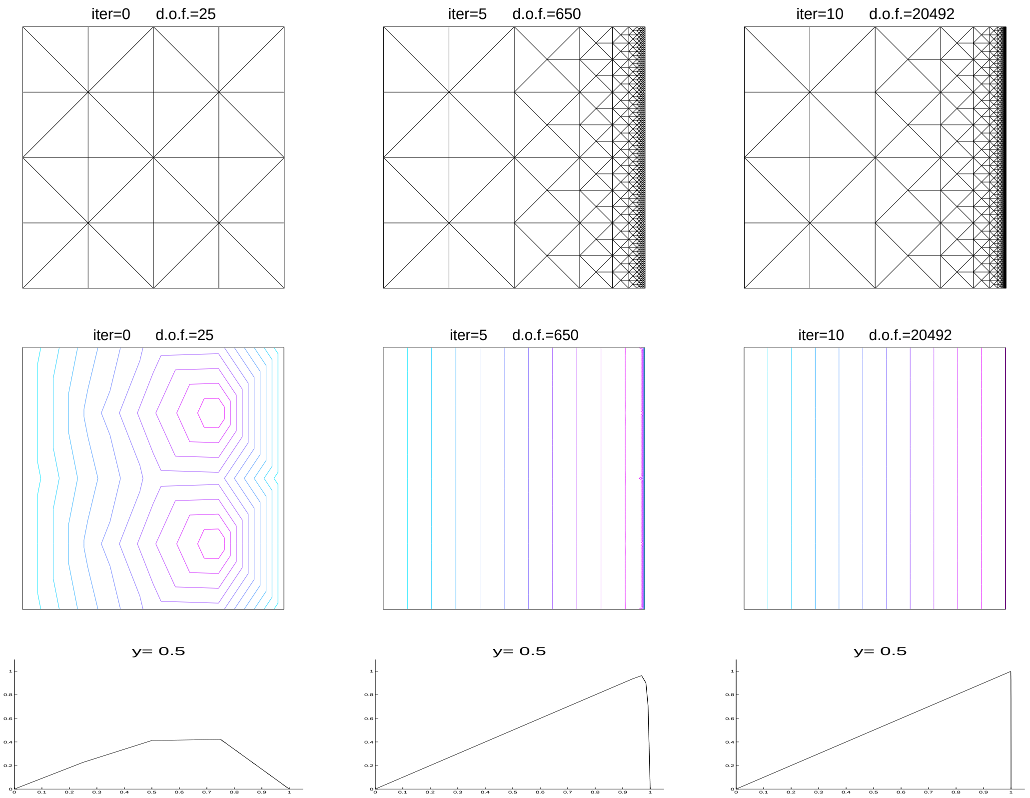

Figure 3.6: Advection-diffusion problem: Meshes, level sets, and vertical sections of the approximate solutions.

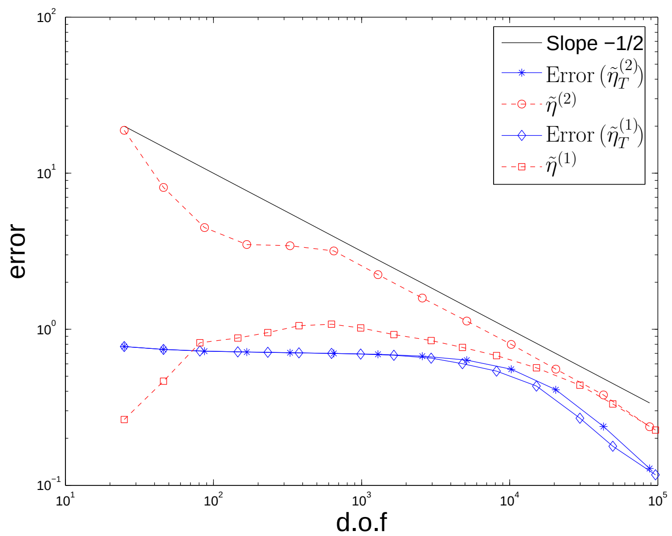

Figure 3.7: Advection-diffusion problem: Estimated and exact error curves.

Essentially the same conclusions as in the previous test can be drawn from Fig. 3.6. In spite of the fact that this problem is out of the theory of Sections 3.2 and 3.3, the boundary layers are very sharply captured without any significant oscillation.

Fig. 3.7 shows that the error estimators $\tilde{\eta}^{(1)}$ and $\tilde{\eta}^{(2)}$ have a very different behavior in the first steps of the adaptive process. However, once the meshes are sufficiently refined around the boundary layer, both error curves attain almost optimal slopes $-\frac{1}{2}$, which shows that optimal orders of convergence are again attained in both cases.

Fig. 3.7 also shows that $\tilde{\eta}_T^{(1)}$ leads to slightly better adapted meshes than $\tilde{\eta}_T^{(2)}$, despite the fact that the theoretical results are poorer for $\tilde{\eta}_T^{(1)}$, because the constant β in Theorem 3.3.2 for this estimator actually depends on ε; namely, $\beta = 1 + \|b\|_{\infty,\omega_T} + \varepsilon^{-\frac{1}{2}} \|\boldsymbol{a}\|_{\infty,\omega_T}$.

3.4.3 An advection-diffusion-reaction problem with an inner layer

The last reported test consists in solving an advection-diffusion-reaction problem whose solution presents an inner layer. The corresponding data are: $\boldsymbol{a} = (2,1)$, $b = 1$, $f = 0$, $\varepsilon = 10^{-4}$, and the boundary conditions shown in Fig. 3.8.

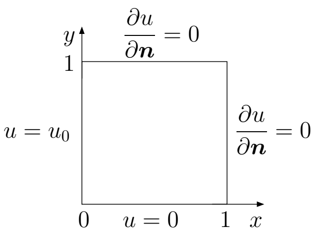

$$u_0(y) = \begin{cases} \varepsilon^{-1/2} y, & 0 \le y < \varepsilon^{1/2}, \\ 1, & \varepsilon^{1/2} \le y \le 1. \end{cases}$$

Figure 3.8: Advection-reaction-diffusion problem: Boundary conditions.

Fig. 3.9 shows some of the successively refined meshes created in the adaptive process, as well as the level sets of the corresponding computed solution. This figure clearly shows that the adaptive process leads once more to correctly refined meshes. The adaptive scheme detects both, the corner singularity of the solution and the inner layer, and leads to meshes much more concentrated around these zones. Once the corner singularity is resolved, the adaptive scheme detects the inner layer and advances through it refining the mesh (see in particular the meshes corresponding to the iteration numbers 10, 15, and 20). At the last iteration, the method captures the inner layer very sharply and without any significant oscillation.

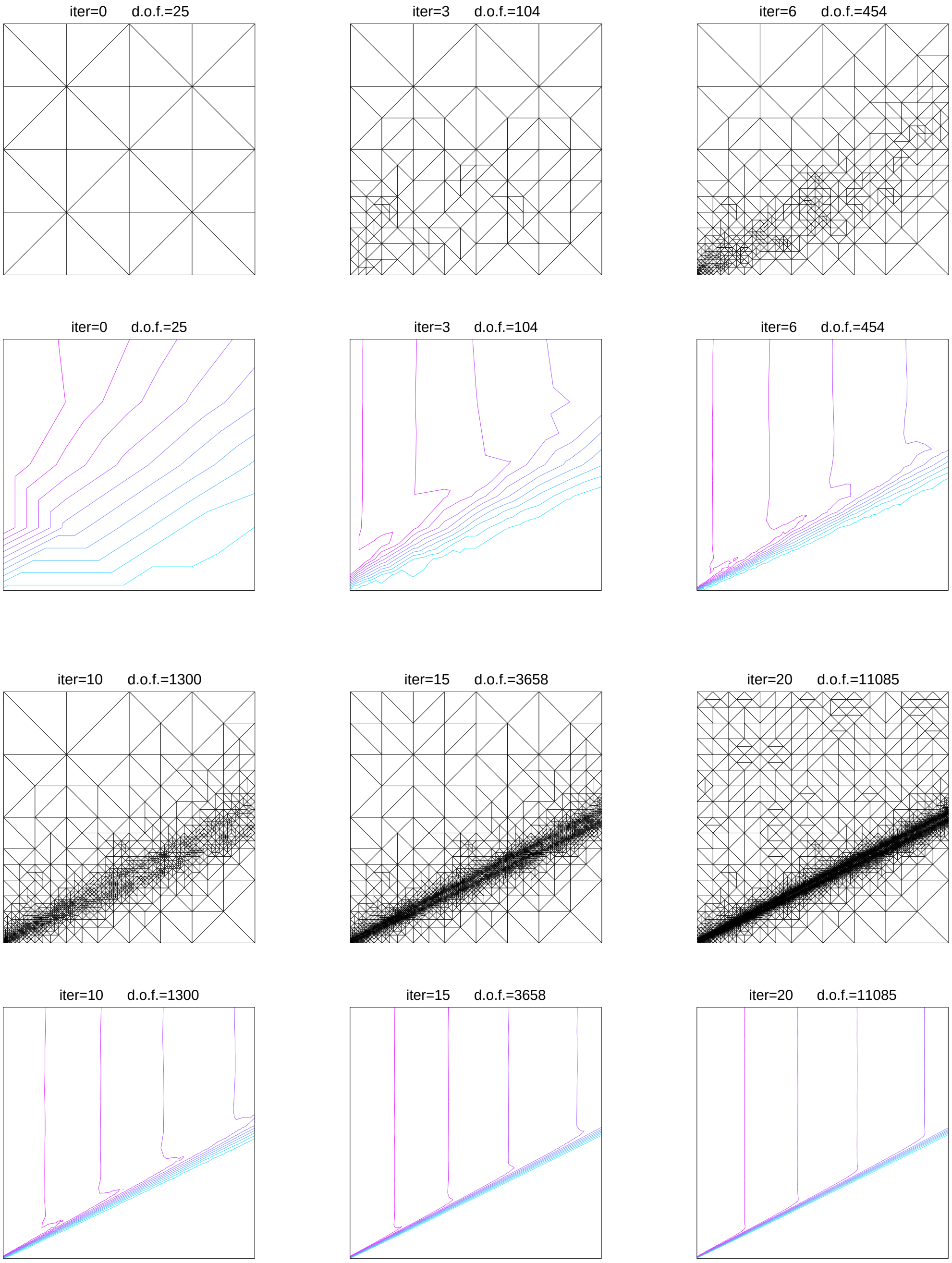

Figure 3.9: Advection-diffusion-reaction problem: Meshes and level sets.

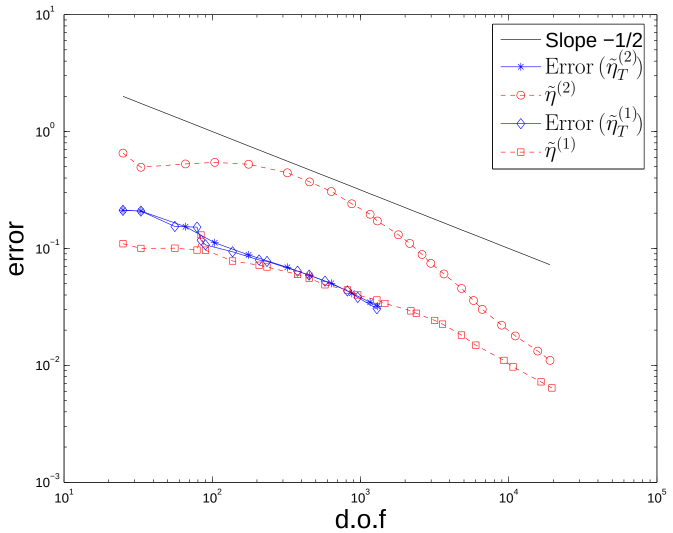

Figure 3.10: Advection-reaction-diffusion problem: Estimated and exact error curves.

Fig. 3.10 shows the error curves for the exact and the estimated errors. Here, the 'exact' errors, "Error $(\tilde{\eta}_T^{(1)})$" and "Error $(\tilde{\eta}_T^{(2)})$", have been computed by considering as 'exact' the numerical solution obtained with the last mesh of the adaptive process. Because of this, we do not include the 'exact' error for the finer meshes which should be heavily affected by the error of the 'exact' solution. No significant difference between "Error $(\tilde{\eta}_T^{(1)})$" and "Error $(\tilde{\eta}_T^{(2)})$" can be appreciated, because both estimators lead to almost to the same meshes. However, Fig. 3.10 shows that in spite of the fact that the theoretical results are poorer for $\tilde{\eta}_T^{(1)}$, its effectivity indices are better than those of $\tilde{\eta}_T^{(2)}$.

3.5 Conclusions

A framework to derive error estimators based on the solution of local problems has been introduced for advection-reaction-diffusion equations. The equivalence of the resulting estimators depend on the continuity and coercivity constants of the bilinear forms used for the local problems.

In particular, two bilinear forms have been analyzed from theoretical and experimental viewpoints. Although the theoretical results are better for one of the estimators, the numerical experiments show similar performances. In both cases, the effectivity indices of the estimators are significantly better than those of a previously known residual based estimator.

Chapter 4

A posteriori error estimates for elliptic problems with Dirac delta source terms

In this chapter are introduced residual type *a posteriori* error estimators for a Poisson problem with a Dirac delta source term, in L^p norm and $W^{1,p}$ seminorm. The estimators are proved to yield global upper and local lower bounds for the corresponding norms of the error. They are used to guide adaptive procedures, which are experimentally shown to lead to optimal orders of convergence.

4.1 Introduction

In this chapter are derived an *a posteriori* error estimator for elliptic problems with Dirac delta source terms. This kind of problems arise in different applications as, for instance, the electric field generated by a point charge, modeling of acoustic monopoles, transport equations for effluent discharge in aquatic media, etc.

In spite of the fact that the solution of one such problem typically does not belong to H^1, it can be numerically approximated by standard finite elements. A priori estimates in L^2 can be found in [29, 12], whereas interior maximum norm error estimates have been proved in [28].

The singular character of the solution of such problems suggests that meshes adequately refined around the delta support should be used to improve the quality of the approximation. Adaptive schemes based on some *a posteriori* error indicators should be used with this purpose. However, to the best of the authors knowledge, no *a posteriori* error analysis has been performed for such problem.

In this paper we consider the simplest minded model example: the approximation by piecewise linear continuous elements of the Laplace equation on a polygonal domain with a homogeneous Dirichlet boundary condition and a Dirac delta source term.

The solution of this problem belongs to L^p for $p < \infty$ and to $\mathrm{W}^{1,p}$ for $p < 2$. We introduce error estimators for the norms of each one of these spaces. When the Dirac delta support is a vertex of the triangulation, the estimators depend only on the edge residuals, conveniently scaled. Otherwise, an additional term depending on the size of the element containing the delta support must be added. We prove reliability and efficiency estimates, for p ranging on some intervals which depend on the geometry of the domain.

We have used these error indicators to guide adaptive schemes, which experimentally show optimal orders of convergence. This happens even for the L^2 norm of the error on non-convex domains, which is not covered by the theory. Moreover, we have shown that the estimator is not equivalent to the error in this case on quasiuniform meshes, even for smooth source terms. This is a well-know fact, however, the adaptive process allows us to attain an optimal order of convergence in this case, too.

The paper is organized as follows. We introduce the model problem in Section 4.2. In Section 4.3, we introduce some generalized bubble functions and prove some technical lemmas, which will be used in the sequel. The main results are presented in Sections 4.4 and 4.5, where we prove the equivalence between our error estimates and the error in L^p norm and $\mathrm{W}^{1,p}$ seminorm, respectively. Finally, in Section 4.6, we report some numerical results, which allow assessing the performance of the adaptive scheme.

4.2 Model problem

Our model problem will be the Laplace equation with the Dirac delta measure as source term and homogeneous Dirichlet boundary condition:

$$\left\{ \begin{array}{rcll} -\Delta u & = & \delta_{x_0} & \text{in } \Omega, \\ u & = & 0 & \text{on } \partial\Omega, \end{array} \right. \tag{4.1}$$

where $\Omega \subset \mathbb{R}^2$ is a bounded polygonal domain and x_0 is an inner point of Ω.

Throughout the paper we will use standard notation for Sobolev spaces, norms, and seminorms.

Let us remark that problem (4.1) has a unique solution. In fact, consider the fundamental solution of the problem $G(x) := \frac{1}{2\pi} \log |x - x_0|$; i. e.,

$$-\Delta G = \delta_{x_0} \qquad \text{in } \Omega.$$

Straightforward calculations show that $G \in \mathrm{W}^{1,p}(\Omega)\ \forall p \in [1,2)$. Hence, u is a solution of problem (4.1) if and only if $u = w + G$, with w being a solution of

$$\left\{\begin{array}{rcll} -\Delta w &=& 0 & \text{in } \Omega, \\ w &=& -G & \text{on } \partial\Omega. \end{array}\right. \tag{4.2}$$

Since $x_0 \notin \partial\Omega$, G is smooth on $\partial\Omega$ and, thus, problem (4.2) has a unique solution $w \in \mathrm{H}^1(\Omega)$. Therefore, problem (4.1) has a unique solution $u \in \mathrm{W}_0^{1,p}(\Omega)$, $1 \le p < 2$.

Problem (4.1) can be written in a weak form as follows:

$$\text{Find } u \in \mathrm{W}_0^{1,p}(\Omega): \qquad \int_\Omega \nabla u \cdot \nabla v = \langle \delta_{x_0}, v\rangle \qquad \forall v \in \mathrm{W}_0^{1,q}(\Omega), \tag{4.3}$$

with $\frac{1}{p} + \frac{1}{q} = 1$. The right-hand side is well defined because, for $q > 2$, $\mathrm{W}^{1,q}(\Omega) \subset \mathcal{C}(\Omega)$.

We consider a regular family $\{\mathcal{T}_h\}$ of meshes of Ω (see for instance [13]). As usual, h denotes the mesh size: $h := \max_{T\in\mathcal{T}_h} h_T$, with h_T being the diameter of T.

Let $S_h := \{v_h \in \mathcal{C}(\Omega):\ v_h|_T \in \mathcal{P}_1\ \forall T \in \mathcal{T}_h\}$ and $S_h^0 := \{v_h \in S_h:\ v_h|_{\partial\Omega} = 0\}$ be the spaces of standard piecewise linear continuous elements. Notice that $S_h^0 \subset \mathrm{W}_0^{1,q}(\Omega) \subset \mathrm{W}_0^{1,p}(\Omega)$. So, the following discrete version of (4.3) is well defined:

$$\text{Find } u_h \in S_h^0: \qquad \int_\Omega \nabla u_h \cdot \nabla v_h = \langle \delta_{x_0}, v_h\rangle \qquad \forall v_h \in S_h^0. \tag{4.4}$$

Clearly, the approximation error satisfies the orthogonality relation

$$\int_\Omega \nabla(u - u_h) \cdot \nabla v_h = 0 \qquad \forall v_h \in S_h^0. \tag{4.5}$$

The following *a priori* error estimate in L^2 norm has been proved in [29] and [12]:

$$\|u - u_h\|_{0,2,\Omega} \le Ch.$$

Here and thereafter C, as well as C', denote strictly positive generic constants, not necessarily the same at each occurrence, but always independent of the mesh size h.

The goals of this paper are to define *a posteriori* estimators of the error $(u - u_h)$ in adequate Sobolev norms, to prove their equivalence with the corresponding norm of the error, and to use them to guide adaptive procedures, in order to attain optimal orders of convergence in terms of the number of degrees of freedom.

4.3 Preliminary results

To prove the equivalence of the estimators, we will have to deal with two kind of bubble functions, one associated with inner edges and the other with the point x_0. In this section we define these bubble functions and prove some properties that will be used in the sequel.

Let $\mathcal{E}_h$ be the set of all the inner edges of the triangulation $\mathcal{T}_h$. Given $\ell \in \mathcal{E}_h$, let b_ℓ be the bubble function defined in Ω, with support

$$\omega_\ell := \bigcup \{T : \ \partial T \supset \ell\}$$

(see Fig. 4.1), defined for $x \in \omega_\ell$ by

$$b_\ell(x) := \begin{cases} \left[\lambda_{P_2}^{T_1}\lambda_{P_3}^{T_1}\lambda_{P_2}^{T_2}\lambda_{P_3}^{T_2}\right]^2 \dfrac{|x-x_0|^2}{|\ell|^2}, & \text{if } \omega_\ell^\circ \ni x_0, \\ \left[\lambda_{P_2}^{T_1}\lambda_{P_3}^{T_1}\lambda_{P_2}^{T_2}\lambda_{P_3}^{T_2}\right]^2, & \text{otherwise.} \end{cases} \tag{4.6}$$

In this definition, we have used the notation given in Fig. 4.1. Moreover, ω_ℓ° is the interior of ω_ℓ and $\lambda_{P_i}^{T_j}$ is the barycentric coordinate of x associated with the triangle T_j and the point P_i, extended to the whole ω_ℓ.

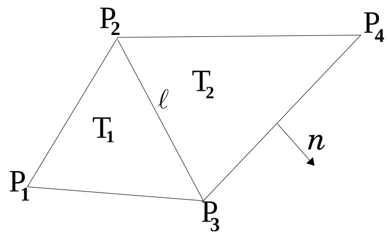

Figure 4.1: Support ω_ℓ of b_ℓ

In what follows we will prove several properties involving conjugate numbers $p, q \in (1, \infty)$ such that $\frac{1}{p} + \frac{1}{q} = 1$.

Lemma 4.3.1 *Given $\ell \in \mathcal{E}_h$, let b_ℓ and ω_ℓ be defined as above. Then*

$$\frac{\partial b_\ell}{\partial n} = 0 \qquad \text{on } \partial\omega_\ell, \tag{4.7}$$

$$C' |\ell| \leq \int_\ell b_\ell \leq C |\ell|, \tag{4.8}$$

$$|b_\ell|_{m,q,\omega_\ell} \leq C |\ell|^{2-m-2/p}, \qquad m = 1, 2. \tag{4.9}$$

Proof. Equation (4.7) is an immediate consequence of the definition of b_ℓ. Estimate (4.8) is obtained by straightforward computations. Estimate (4.9) follows from standard scaling arguments and the regularity of the mesh; in fact, for $m = 1, 2$, we have

$$|b_\ell|_{m,q,\omega_\ell} \leq C |\ell|^{-m} |b_\ell|_{0,q,\omega_\ell} \leq C |\ell|^{-m} |\omega_\ell|^{1/q} \leq C |\ell|^{2-m-2/p}.$$

□

Although in practice the meshes are usually constructed in such a way that x_0 is a vertex of all the triangulations, we do not need to assume this for our analysis. However, when x_0 is not a vertex, the definition of the estimator will include an additional term. In this case, we will use another bubble function. Let T be a triangle of $\mathcal{T}_h$ containing x_0 (if x_0 lies on an inner edge, any of the two triangles sharing the edge can be chosen as T). Let

$$w_T := \bigcup \{T' \in \mathcal{T}_h : \ T' \cap T \neq \emptyset\}$$

and $d := \mathrm{dist}(x_0, \partial w_T)$ (see Fig. 4.2). Notice that, because of the regularity of the mesh, $h_T \leq Cd$. Let b_{x_0} be a smooth bubble function defined in Ω, with support in w_T and satisfying

$$0 \leq b_{x_0}(x) \leq 1 \qquad \forall x \in \Omega, \tag{4.10}$$

$$b_{x_0}(x) = 1 \qquad \forall x \in \Omega : \ |x - x_0| \leq \frac{d}{4}, \tag{4.11}$$

$$b_{x_0}(x) = 0 \qquad \forall x \in \Omega : \ |x - x_0| \geq \frac{3d}{4}, \tag{4.12}$$

$$|b_{x_0}|_{m,\infty,w_T} \leq Cd^{-m}, \qquad m = 1, 2. \tag{4.13}$$

Such a function can be easily obtained by convolution of the characteristic function of the set $\{x \in \Omega : \ |x - x_0| < d/4\}$ with a mollifier.

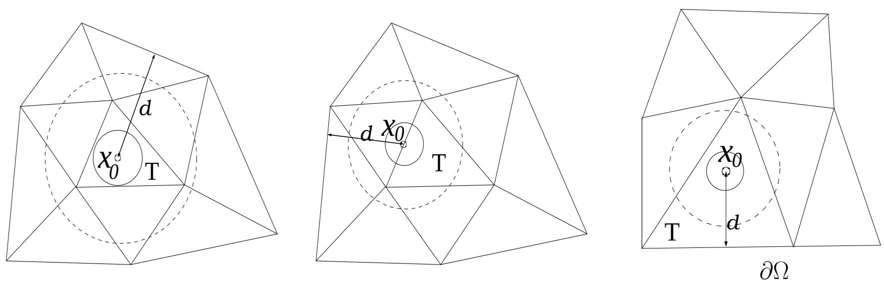

Figure 4.2: Domains w_T for different locations of x_0. Circles $|x - x_0| = \frac{d}{4}$ (solid line) and $|x - x_0| = \frac{3d}{4}$ (dashed line).

Lemma 4.3.2 *Let $T \ni x_0$. Let b_{x_0} and w_T be defined as above. Then*

$$|b_{x_0}|_{m,q,w_T} \leq Ch_T^{2-m-2/p}, \qquad m = 1, 2.$$

PROOF. Using (4.13) and the fact that $h_T \le Cd$, the definition of $|\cdot|_{m,q,w_T}$ yields
$$|b_{x_0}|_{m,q,w_T} \le Cd^{-m} h_T^{2/q} \le C h_T^{2-m-2/p}.$$
□

To define the error estimators in the next sections, we will use the jumps of the normal derivative of the finite element solution across the inner edges ℓ, which we denote by
$$J_\ell := \left[\!\left[\frac{\partial u_h}{\partial n} \right]\!\right]_\ell, \qquad \ell \in \mathcal{E}_h.$$

The following bounds will be used to prove the efficiency of the estimators.

LEMMA 4.3.3 *Let $T \ni x_0$ and w_T be defined as above. Let $\mathcal{F}_h^T$ be the set of edges ℓ of triangles $T \subset w_T$, such that $\ell \not\subset \partial w_T$. Then*
$$h_T^{2/p} \le C \left(\|u-u_h\|_{0,p,w_T} + \sum_{\ell \in \mathcal{F}_h^T} |J_\ell| \, |\ell|^{1+2/p} \right),$$
$$h_T^{2/p-1} \le C \left(|u-u_h|_{1,p,w_T} + \sum_{\ell \in \mathcal{F}_h^T} |J_\ell| \, |\ell|^{2/p} \right).$$

PROOF. Let b_{x_0} be the above defined bubble function. By using (4.3), integration by parts, (4.7), Hölder inequality, (4.10), Lemma 4.3.2, and the regularity of the mesh, we have
$$\begin{aligned}
1 = \langle \delta_{x_0}, b_{x_0} \rangle &= \int_\Omega \nabla(u-u_h)\cdot\nabla b_{x_0} + \int_\Omega \nabla u_h \cdot \nabla b_{x_0} \\
&= -\int_{w_T} (u-u_h)\Delta b_{x_0} - \sum_{\ell \in \mathcal{F}_h^T} \int_\ell J_\ell b_{x_0} \\
&\le \|u-u_h\|_{0,p,w_T} |b_{x_0}|_{2,q,w_T} + \sum_{\ell \in \mathcal{F}_h^T} |J_\ell| \, |\ell| \\
&\le C \left(\|u-u_h\|_{0,p,w_T} h_T^{-2/p} + \sum_{\ell \in \mathcal{F}_h^T} |J_\ell| \, |\ell|^{1+2/p} h_T^{-2/p} \right),
\end{aligned}$$
which leads to the first estimate.

The same arguments give
$$\begin{aligned}
1 = \langle \delta_{x_0}, b_{x_0} \rangle &= \int_\Omega \nabla(u-u_h)\cdot\nabla b_{x_0} + \int_\Omega \nabla u_h \cdot \nabla b_{x_0} \\
&\le |u-u_h|_{1,p,w_T} |b_{x_0}|_{1,q,w_T} - \sum_{\ell \in \mathcal{F}_h^T} \int_\ell J_\ell b_{x_0} \\
&\le C \left(|u-u_h|_{1,p,w_T} h_T^{1-2/p} + \sum_{\ell \in \mathcal{F}_h^T} |J_\ell| \, |\ell|^{2/p} h_T^{1-2/p} \right),
\end{aligned}$$

which allow us to prove the second estimate. □

To end this section, we settle some error estimates for the Lagrange interpolant $v^I \in S_h$ of a function $v \in \mathcal{C}(\Omega)$, which will be also used in the sequel.

LEMMA 4.3.4 *Given $\ell \in \mathcal{E}_h$, let ω_ℓ be defined as above. Then*

$$\begin{aligned} \left\|v - v^I\right\|_{0,q,\ell} &\leq C\,|\ell|^{1+1/p}\,|v|_{2,q,\omega_\ell} \qquad \forall v \in \mathrm{W}^{2,q}(\omega_\ell), \qquad 1 < q < \infty, \\ \left\|v - v^I\right\|_{0,q,\ell} &\leq C\,|\ell|^{1/p}\,|v|_{1,q,\omega_\ell} \qquad \forall v \in \mathrm{W}^{1,q}(\omega_\ell), \qquad 2 < q < \infty. \end{aligned}$$

PROOF. Scaling arguments lead to

$$\left\|v - v^I\right\|_{0,q,\ell} \leq C\left(|\ell|^{-1/q}\left\|v - v^I\right\|_{0,q,\omega_\ell} + |\ell|^{1-1/q}\left|v - v^I\right|_{1,q,\omega_\ell}\right). \tag{4.14}$$

Next, we use the standard error estimate for the Lagrange interpolant (see for instance [13])

$$\left|v - v^I\right|_{k,q,\omega_\ell} \leq C\,|\ell|^{2-k}\,|v|_{2,q,\omega_\ell}\,, \qquad k = 0, 1,$$

to estimate both terms in the right-hand side of (4.14). Thus we obtain the first estimate of the lemma.

On the other hand, for $q > 2$, the following estimate also holds true (see again [13]):

$$\left|v - v^I\right|_{k,q,\omega_\ell} \leq C\,|\ell|^{1-k}\,|v|_{1,q,\omega_\ell}\,, \qquad k = 0, 1.$$

Finally, from this and (4.14), we conclude the second estimate of the lemma. □

4.4 An *a posteriori* error estimator equivalent to $\|u - u_h\|_{0,p,\Omega}$

Notice that the solution u of (4.1) belongs to $\mathrm{L}^p(\Omega)$ for all $p < \infty$. In this section, we will define an estimator for the $\mathrm{L}^p(\Omega)$ norm of the finite element approximation error $(u - u_h)$ and will prove the equivalence of exact and estimated errors for all $p \in (1, p_\Omega)$, with $p_\Omega > 1$ as shown below.

In the proof of Theorem 4.4.1 below we will use a duality argument. With this purpose we consider the following problem:

$$\begin{cases} -\Delta v = \psi & \text{in } \Omega, \\ \quad\; v = 0 & \text{on } \partial\Omega, \end{cases} \tag{4.15}$$

where $\psi \in \mathrm{L}^q(\Omega)$ and $\frac{1}{p} + \frac{1}{q} = 1$. According to [20], if

$$\left(2 - \frac{\pi}{\theta}\right) p < 2, \tag{4.16}$$

with θ being the largest inner angle of Ω, then the solution of (4.15) satisfies $v \in \mathrm{W}^{2,q}(\Omega)$ and

$$|v|_{2,q,\Omega} \leq C \, \|\psi\|_{0,q,\Omega} \,. \tag{4.17}$$

If Ω were either a triangle with three acute angles or a rectangle, then $\theta \leq \frac{\pi}{2}$ and (4.16) would hold true for all $p < \infty$. Exception made of these very particular cases, the largest angle of Ω satisfies $\theta > \frac{\pi}{2}$ and, consequently, (4.16) holds true only if $p < 2/(2-\frac{\pi}{\theta})$. Hence, let

$$p_\Omega := \begin{cases} \dfrac{2}{2 - \dfrac{\pi}{\theta}}, & \text{if } \theta > \frac{\pi}{2}, \\ \infty, & \text{otherwise.} \end{cases} \tag{4.18}$$

For all $T \in \mathcal{T}_h$, let $\mathcal{E}_h^T$ be the set of inner edges $\ell \in \mathcal{E}_h$ such that $\ell \subset \partial T$. If x_0 is a vertex of the triangulation, we define the local *a posteriori* error indicator by

$$\eta_{T,p} := \left(\sum_{\ell \in \mathcal{E}_h^T} |J_\ell|^p \, |\ell|^{p+2} \right)^{1/p},$$

for all the triangles $T \in \mathcal{T}_h$. Instead, if x_0 is not a vertex of the triangulation, the indicators corresponding to the triangles $T \ni x_0$ include an additional term. In this case, we define

$$\eta_{T,p} := \begin{cases} \left(h_T^2 + \displaystyle\sum_{\ell \in \mathcal{E}_h^T} |J_\ell|^p \, |\ell|^{p+2} \right)^{1/p}, & \text{if } T \ni x_0, \\ \left(\displaystyle\sum_{\ell \in \mathcal{E}_h^T} |J_\ell|^p \, |\ell|^{p+2} \right)^{1/p}, & \text{otherwise.} \end{cases}$$

In both cases, we define the global error estimator with these indicators as follows:

$$\eta_p := \left(\sum_{T \in \mathcal{T}_h} \eta_{T,p}^p \right)^{1/p}.$$

THEOREM 4.4.1 *For $p \in (1, p_\Omega)$, let $\eta_{T,p}$ and η_p be defined as above. Then the following estimates hold true:*

$$\begin{aligned} \|u - u_h\|_{0,p,\Omega} &\leq C\eta_p, \\ \eta_{T,p} &\leq C \, \|u - u_h\|_{0,p,w_T} \qquad \forall T \in \mathcal{T}_h. \end{aligned}$$

PROOF. Let $T \in \mathcal{T}_h$ be such that $T \ni x_0$. (If x_0 is a vertex of the triangulation, see Remark 4.4.1 below).

Given $\psi \in \mathrm{L}^q(\Omega)$, let $v \in \mathrm{W}^{2,q}(\Omega)$ be the solution of (4.15). By using integration by parts, (4.5), (4.3), Hölder inequality, standard interpolation error estimates (see for instance [13]), Lemma 4.3.4, and (4.17), we have

$$
\begin{aligned}
\int_\Omega (u-u_h)\psi &= -\int_\Omega (u-u_h)\Delta v \\
&= \int_\Omega \nabla(u-u_h)\cdot\nabla v \\
&= \int_\Omega \nabla(u-u_h)\cdot\nabla(v-v^I) \\
&= \langle \delta_{x_0}, v-v^I\rangle + \sum_{\ell\in\mathcal{E}_h}\int_\ell J_\ell(v-v^I) \\
&\leq \left\|v-v^I\right\|_{0,\infty,T} + \sum_{\ell\in\mathcal{E}_h}\|J_\ell\|_{0,p,\ell}\left\|v-v^I\right\|_{0,q,\ell} \\
&\leq C\left(h_T^{2-2/q}\,|v|_{2,q,T} + \sum_{\ell\in\mathcal{E}_h}\|J_\ell\|_{0,p,\ell}\,|\ell|^{1+1/p}\,|v|_{2,q,\omega_\ell}\right) \\
&\leq C\left(h_T^2 + \sum_{\ell\in\mathcal{E}_h}\|J_\ell\|_{0,p,\ell}^p\,|\ell|^{p+1}\right)^{1/p}\left(\sum_{\ell\in\mathcal{E}_h}|v|_{2,q,\omega_\ell}^q\right)^{1/q} \\
&\leq C\left(h_T^2 + \sum_{\ell\in\mathcal{E}_h}|J_\ell|^p\,|\ell|^{p+2}\right)^{1/p}\|\psi\|_{0,q,\Omega}\,.
\end{aligned}
\tag{4.19}
$$

Therefore,

$$
\|u-u_h\|_{0,p,\Omega} = \sup_{\psi\in\mathrm{L}^q(\Omega)}\frac{\displaystyle\int_\Omega (u-u_h)\,\psi}{\|\psi\|_{0,q,\Omega}} \leq C\left(h_T^2 + \sum_{\ell\in\mathcal{E}_h}|J_\ell|^p\,|\ell|^{p+2}\right)^{1/p},
$$

which together with the definition of η_p yield the first estimate.

To prove the second estimate, we test (4.3) with the bubble function b_ℓ and use that $b_\ell(x_0)=0$ and integration by parts to obtain

$$
\int_\Omega \nabla(u-u_h)\cdot\nabla b_\ell = \langle\delta_{x_0}, b_\ell\rangle - \int_\Omega \nabla u_h\cdot\nabla b_\ell = \int_\ell J_\ell b_\ell. \tag{4.20}
$$

Therefore, integration by parts, (4.7), Hölder inequality, and (4.9) yield

$$
\begin{aligned}
\int_\ell J_\ell b_\ell &= \int_\Omega \nabla(u-u_h)\cdot\nabla b_\ell = \int_{\omega_\ell}(u-u_h)\Delta b_\ell \\
&\leq \|u-u_h\|_{0,p,\omega_\ell}\,|b_\ell|_{2,q,\omega_\ell} \leq \|u-u_h\|_{0,p,\omega_\ell}\,|\ell|^{-2/p}\,.
\end{aligned}
$$

On the other hand, from (4.8) we have

$$\left|\int_\ell J_\ell b_\ell\right| = |J_\ell| \int_\ell b_\ell \geq C' |\ell| \, |J_\ell| \,. \tag{4.21}$$

The two last inequalities yield

$$|J_\ell| \, |\ell|^{(p+2)/p} \leq C \, \|u - u_h\|_{0,p,\omega_\ell}$$

and, consequently,

$$\left(\sum_{\ell \in \mathcal{E}_h^T} |J_\ell|^p \, |\ell|^{p+2}\right)^{1/p} \leq C \, \|u - u_h\|_{0,p,w_T} \,, \tag{4.22}$$

which together with Lemma 4.3.3 allow us to conclude the theorem. □

REMARK 4.4.1 *The proof is still valid when x_0 is a vertex of the triangulation. Indeed, in this case, the term $\langle \delta_{x_0}, v - v^I \rangle$ vanishes and (4.19) reduces to*

$$\int_\Omega (u - u_h)\psi \leq C \left(\sum_{\ell \in \mathcal{E}_h} |J_\ell|^p \, |\ell|^{p+2}\right)^{1/p} \|\psi\|_{0,q,\Omega} \,.$$

This allows us to conclude the first estimate of the theorem, whereas the second estimate is given directly by (4.22).

REMARK 4.4.2 *When Ω is convex, according to (4.18), $p_\Omega > 2$. Hence, in this case, the estimator η_2 turns out to be equivalent to the $\mathrm{L}^2(\Omega)$ norm of the error.*

4.5 An *a posteriori* error estimator equivalent to $|u - u_h|_{1,p,\Omega}$

Since the solution of (4.1) also belongs to $\mathrm{W}_0^{1,p}(\Omega)$ for all $p < 2$, it makes sense to estimate the $\mathrm{W}^{1,p}(\Omega)$ seminorm of the finite element approximation error $(u - u_h)$, as well. In this section, we will define one such estimator and will prove that it is equivalent to the error for any $p \in (p^\Omega, 2)$, with $p^\Omega > 1$ as shown below.

Given $\Psi \in \mathrm{L}^q(\Omega)^2$, with $\frac{1}{p} + \frac{1}{q} = 1$, consider now the following problem:

$$\text{Find } v \in \mathrm{W}_0^{1,q}(\Omega): \qquad \int_\Omega \nabla v \cdot \nabla w = \int_\Omega \Psi \cdot \nabla w \qquad \forall w \in \mathrm{W}_0^{1,p}(\Omega). \tag{4.23}$$

According to [15], for any polygonal domain Ω, there exists a neighborhood of 2 such that, for all p in this neighborhood, problem (4.23) has a unique solution v. Furthermore, in such case, the following estimate holds true:

$$|v|_{1,q,\Omega} \leq C \|\Psi\|_{0,q,\Omega}. \tag{4.24}$$

This happens for all $p \in (1,\infty)$ when Ω is convex. In general, let $p^\Omega \in [1,2)$ be the smallest number such that, if $p^\Omega < p < 2$, then (4.23) has a unique solution satisfying (4.24).

If x_0 is a vertex of the triangulation, the local *a posteriori* error indicator is given by

$$\varepsilon_{T,p} := \left(\sum_{\ell \in \mathcal{E}_h^T} |J_\ell|^p \, |\ell|^2 \right)^{1/p},$$

for all triangles $T \in \mathcal{T}_h$. (We recall that $\mathcal{E}_h^T$ is the set of inner edges $\ell \in \mathcal{E}_h$ such that $\ell \subset \partial T$.) As in the previous section, if x_0 is not a vertex of the triangulation, an additional term appears in the indicators corresponding to the triangles $T \ni x_0$:

$$\varepsilon_{T,p} := \begin{cases} \left(h_T^{2-p} + \displaystyle\sum_{\ell \in \mathcal{E}_h^T} |J_\ell|^p \, |\ell|^2 \right)^{1/p}, & \text{if } T \ni x_0, \\ \left(\displaystyle\sum_{\ell \in \mathcal{E}_h^T} |J_\ell|^p \, |\ell|^2 \right)^{1/p}, & \text{otherwise.} \end{cases}$$

In both cases, the corresponding global error estimator is given by

$$\varepsilon_p := \left(\sum_{T \in \mathcal{T}_h} \varepsilon_{T,p}^p \right)^{1/p}.$$

THEOREM 4.5.1 *For $p \in (p^\Omega, 2)$, let $\varepsilon_{T,p}$ and ε_p be defined as above. Then the following estimates hold true:*

$$\begin{aligned} |u-u_h|_{1,p,\Omega} &\leq C\varepsilon_p, \\ \varepsilon_{T,p} &\leq C\,|u-u_h|_{1,p,w_T} \qquad \forall T \in \mathcal{T}_h. \end{aligned}$$

PROOF. Let $T \in \mathcal{T}_h$ be such that $T \ni x_0$. (As in the proof of previous theorem, we postpone the case of x_0 being a vertex of the triangulation to Remark 4.5.1 below). Given $\Psi \in \mathrm{L}^q(\Omega)^2$, with $\frac{1}{p} + \frac{1}{q} = 1$, let $v \in \mathrm{W}_0^{1,q}(\Omega)$ be the solution of (4.23). Since $u - u_h \in \mathrm{W}_0^{1,p}(\Omega)$, it can be used as a test function w in (4.23). Hence, (4.5), (4.3), integration by parts, Hölder inequality, standard interpolation error estimates (see for instance [13]), Lemma 4.3.4, and (4.24) lead to

$$\begin{aligned}
\int_\Omega \nabla(u-u_h)\cdot\Psi &= \int_\Omega \nabla(u-u_h)\cdot\nabla v \\
&= \int_\Omega \nabla(u-u_h)\cdot\nabla(v-v^I) \\
&= \langle\delta_{x_0}, v-v^I\rangle + \sum_{\ell\in\mathcal{E}_h}\int_\ell J_\ell(v-v^I) \\
&\le \left\|v-v^I\right\|_{0,\infty,T} + \sum_{\ell\in\mathcal{E}_h}\|J_\ell\|_{0,p,\ell}\left\|v-v^I\right\|_{0,q,\ell} \\
&\le C\left(h_T^{1-2/q}\,|v|_{1,q,T} + \sum_{\ell\in\mathcal{E}_h}\|J_\ell\|_{0,p,\ell}\,|\ell|^{1/p}\,|v|_{1,q,\omega_\ell}\right) \\
&\le C\left(h_T^{2-p} + \sum_{\ell\in\mathcal{E}_h}\|J_\ell\|_{0,p,\ell}^p\,|\ell|\right)^{1/p}\left(\sum_{\ell\in\mathcal{E}_h}|v|_{1,q,\omega_\ell}^q\right)^{1/q} \\
&\le C\left(h_T^{2-p} + \sum_{\ell\in\mathcal{E}_h}|J_\ell|^p\,|\ell|^2\right)^{1/p}\|\Psi\|_{0,q,\Omega}\,. \qquad (4.25)
\end{aligned}$$

Therefore

$$|u-u_h|_{1,p,\Omega} = \sup_{\Psi\in\mathrm{L}^q(\Omega)^2}\frac{\displaystyle\int_\Omega \nabla(u-u_h)\cdot\Psi}{\|\Psi\|_{0,q,\Omega}} \le C\left(h_T^{2-p} + \sum_{\ell\in\mathcal{E}_h}|J_\ell|^p\,|\ell|^2\right)^{1/p},$$

which together with the definition of ε_p yield the first estimate.

To prove the second estimate, we proceed as in the proof of Theorem 4.4.1; thus, from (4.20) and (4.21) we have

$$C'\,|\ell|\,|J_\ell| \le \int_\Omega \nabla(u-u_h)\cdot\nabla b_\ell.$$

Hence, from Hölder inequality and (4.9) we obtain

$$|J_\ell|\,|\ell| \le C\,|u-u_h|_{1,p,\omega_\ell}\,|b_\ell|_{1,q,\omega_\ell} \le C\,|u-u_h|_{1,p,\omega_\ell}\,|\ell|^{1-2/p}\,.$$

Therefore, we have

$$\left(\sum_{\ell\in\mathcal{E}_h^T}|J_\ell|^p\,|\ell|^2\right)^{1/p} \le C\,|u-u_h|_{1,p,w_T}\,,$$

which together with Lemma 4.3.3 allow us to conclude the theorem. □

Remark 4.5.1 *The proof of this theorem also remains valid if x_0 is a vertex of the triangulation. Indeed, the only difference is that the term $\langle \delta_{x_0}, v - v^I \rangle$ vanishes in this case, and thus the term h_T^{2-p} does not appear in (4.25).*

Remark 4.5.2 *When Ω is convex, according to [15], $p^\Omega = 1$. Hence, in this case, the estimator ε_p turns out to be equivalent to the error in $\mathrm{W}^{1,p}(\Omega)$ norm for all $p \in (1,2)$.*

4.6 Numerical experiments

In this section we report several numerical experiments to assess the performance of an h-adaptive mesh-refinement strategy based on the error indicators $\eta_{T,p}$ and $\varepsilon_{T,p}$ analyzed in Sections 4.4 and 4.5.

The adaptive procedure consists in solving problem (4.4) on a sequence of meshes up to finally attain a solution with an estimated error within a prescribed tolerance. With this purpose, we initiate the process with a quasiuniform mesh and create, at each step, a new mesh better adapted to the solution of problem (4.4). This is done by computing the local error estimators $\eta_{T,p}$ or $\varepsilon_{T,p}$ for all T in the 'old' mesh $\mathcal{T}_h$, and refining those elements T with $\eta_{T,p} \geq \theta \max\{\eta_{T,p} : \ T \in \mathcal{T}_h\}$, (resp. $\varepsilon_{T,p} \geq \theta \max\{\varepsilon_{T,p} : \ T \in \mathcal{T}_h\}$) where $\theta \in (0,1)$ is a prescribed parameter. In all our experiments we have chosen $\theta = \frac{1}{2}$.

We have used a `Matlab` code adapted by us from [2] and the mesh generator `Triangle`. This generator allows creating successively refined meshes based on a hybrid Delaunay refinement algorithm (see [30]).

4.6.1 Test 1: A convex domain

The first set of tests consists of solving the problem $-\Delta u = \delta_{x_0}$ in the unit square $\Omega := (0,1) \times (0,1)$, with $x_0 = (0.5, 0.5)$. We choose Dirichlet boundary conditions such that the exact solution is given by $u(x,y) = \frac{1}{2\pi} \log |x - x_0|$.

We show first the results obtained for the adaptive process guided by the error estimator $\eta_{T,p}$.

Fig. 4.3 shows some of the successively refined meshes created in the process guided by $\eta_{T,p}$, with $p = 2$, and under the constraint that x_0 be a vertex of all the triangulations. This figure also shows the computed solution, the iteration number, and the number of degrees of freedom (d.o.f.) of each mesh. Fig. 4.4 shows the error curves of the whole process for the exact and estimated errors. This figure also includes a line with slope -1, which corresponds to the theoretically optimal order of convergence for piecewise linear elements.

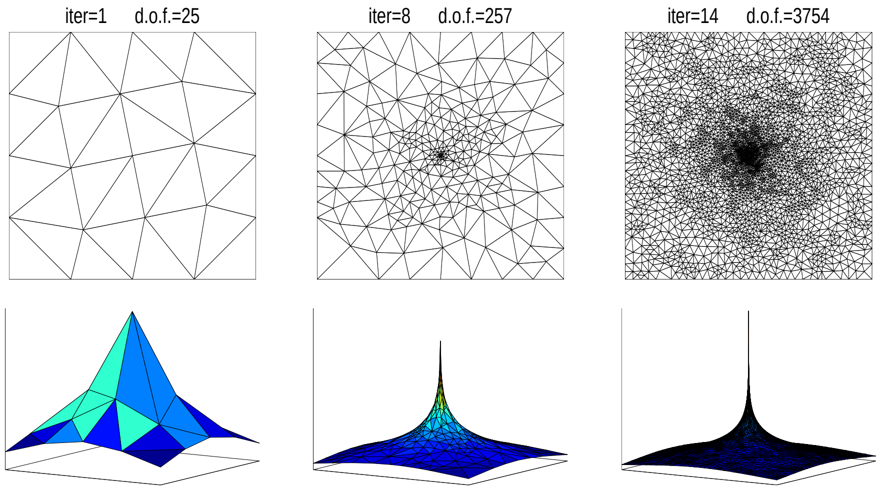

Figure 4.3: Convex domain with x_0 being a vertex of the triangulations. Meshes and approximate solutions obtained with $\eta_{T,p}$; $p = 2$.

It can be seen from Fig. 4.3 that the adaptive process leads to meshes correctly refined around x_0. On the other hand, the error curves show that the process yields optimal order convergence. This happens in spite of the fact that the effectivity indices are very poor. Indeed, it can be observed in Fig. 4.4 that the exact error is severely overestimated. Anyway, the exact and estimated error curves have approximately the same optimal slope -1.

Fig. 4.5 shows some of the successively refined meshes created with the adaptive process guided again by $\eta_{T,p}$, with $p = 2$, but without the constraint that x_0 be a vertex of the triangulations. The same conclusions as in the previous test can be drawn from Fig. 4.5 and 4.6.

It can be seen that the constraint of x_0 being a vertex of the triangulations does not make any significant difference.

Next, we report the results obtained with the adaptive process guided by $\varepsilon_{T,p}$ as error estimator. Fig. 4.7 shows some of the successively refined meshes created with the adaptive process guided by $\varepsilon_{T,p}$, with $p = 1.5$, and x_0 being a vertex of the triangulations, as well as the computed solution. Fig. 4.8 shows successive zooms of the last final adapted mesh around x_0. The second square corresponds to a zoom of the white inner square in the first one, amplified 10 times around x_0, and so on. Fig. 4.9 shows the error curves for the exact and estimated errors. It also includes a line with slope $-\frac{1}{2}$, which corresponds to the theoretically optimal order of convergence for piecewise linear elements in problems with a smooth solution.

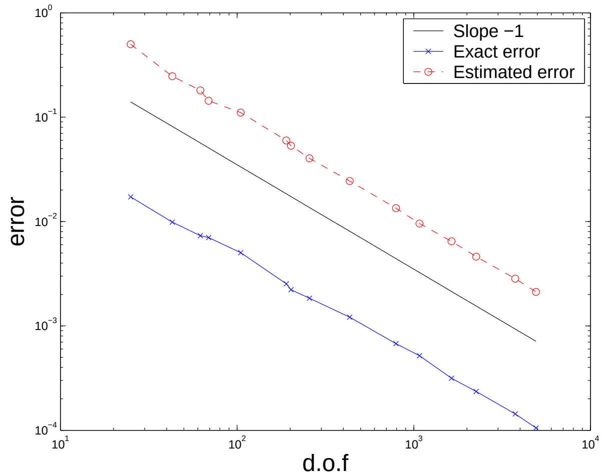

Figure 4.4: Convex domain with x_0 being a vertex of the triangulations. Estimator η_p and exact L^p norm error curves; $p = 2$.

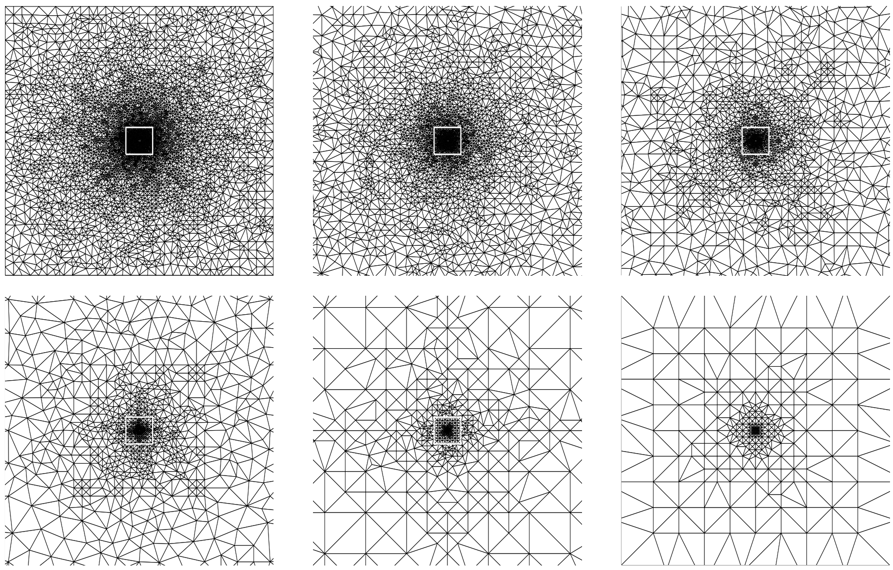

Figure 4.8: Convex domain. Successive zooms of the final adapted mesh obtained with $\varepsilon_{T,p}$; $p = 1.5$.

These figures clearly show that the adaptive process leads again to correctly refined meshes around x_0. On the other hand, the error curves in Fig. 4.9 have almost the optimal slope $-\frac{1}{2}$.

Once more, essentially identical results were obtained for the same estimator ε_p, when

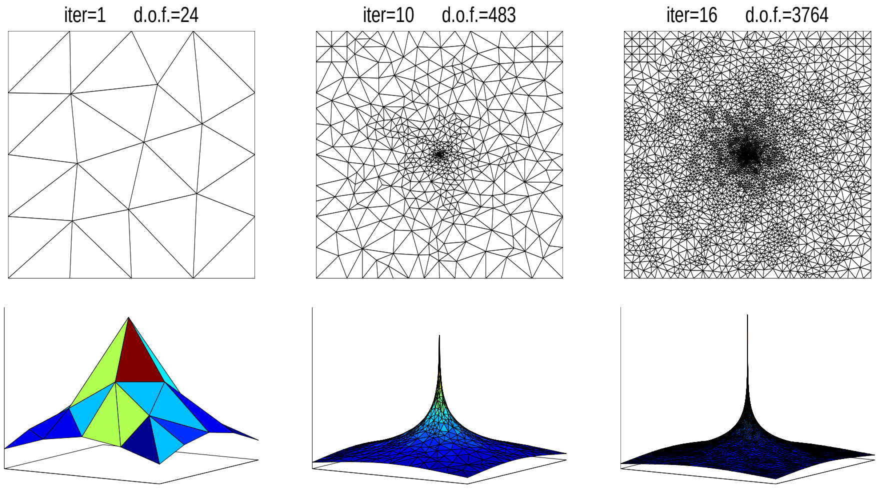

Figure 4.5: Convex domain with x_0 not being a vertex of the triangulations. Meshes and approximate solutions obtained with $\eta_{T,p}$; $p = 2$.

x_0 is not a vertex of the triangulations.

4.6.2 Test 2: A non convex domain

We will solve the problem $-\Delta u = \delta_{x_0}$ in the L-shape domain shown in Fig. 4.10.

We choose Dirichlet boundary conditions such that the exact solution be $u(x, y) = u_1(x, y) + u_2(x, y)$ where

$$u_1(x, y) = \frac{1}{2\pi} \log |x - x_0| \qquad \text{and} \qquad u_2(x, y) = r^{2/3} \sin\left(\frac{2}{3}\theta\right). \tag{4.26}$$

Here (r, θ) are the polar coordinates corresponding to (x, y) with $\theta \in [0, 2\pi)$.

Fig. 4.11 shows some of the successively refined meshes created in the adaptive process guided by $\varepsilon_{T,p}$, with $p = 1.5$. It can be seen that the adaptive process leads to meshes refined around both, x_0 and the corner singularity.

On the other hand, Fig.4.12 shows the corresponding exact and estimated error curves. Once more, it can be seen that the adaptive process yields optimal order convergence: the exact and estimated error curves have both again approximately the same optimal slope $-\frac{1}{2}$.

Next, we report results obtained with the adaptive procedure guided by $\eta_{T,2}$ as error estimator for the same problem. Notice that this example is not covered by Theorem 4.4.1. Indeed, according to (4.18), for a non convex polygonal domain, $p_\Omega < 2$. Moreover, as shown below, the estimator η_2 is not expected to be equivalent to the $L_2(\Omega)$ error for non

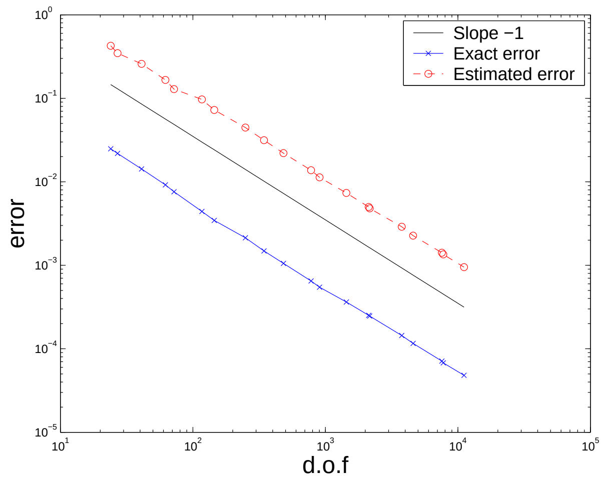

Figure 4.6: Convex domain with x_0 not being a vertex of the triangulations. Estimator η_p and exact L^p norm error curves; $p = 2$.

convex domains. In spite of this fact, the adaptive process succeeds in yielding well refined meshes and an optimal order of convergence, as shown in Fig 4.13 and 4.14, respectively.

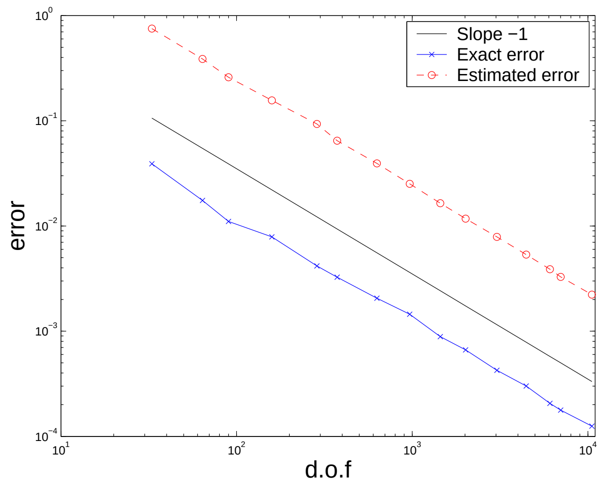

Figure 4.14: Non convex domain. Estimator η_p and exact L^p norm error curves; $p = 2$.

Let us remark that the non equivalence of η_2 and $\|u - u_h\|_{0,2,\Omega}$ is not related with the singular character of the right-hand side of problem (4.1), but with the non convexity of

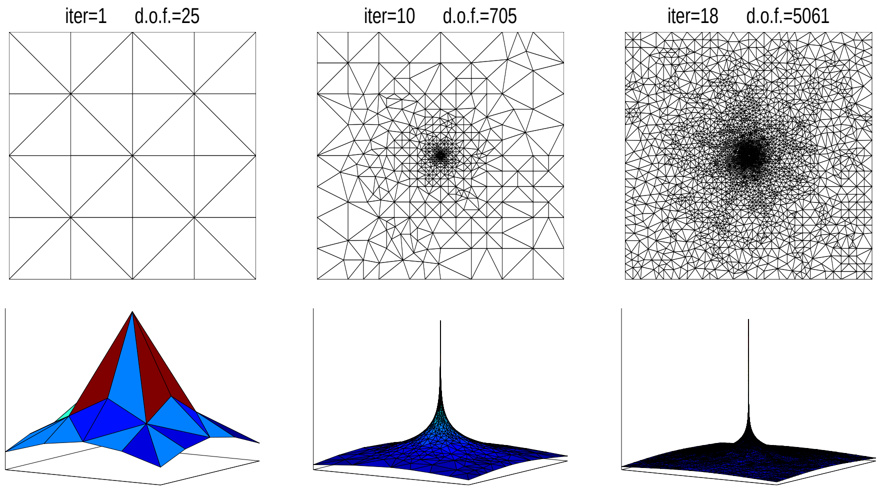

Figure 4.7: Convex domain. Meshes and approximate solutions obtained with $\varepsilon_{T,p}$; $p = 1.5$.

the domain. Indeed, consider the following problem with a piecewise constant f:

$$\begin{cases} -\Delta v &= f \quad \text{in } \Omega, \\ v &= 0 \quad \text{on } \partial\Omega. \end{cases}$$

Let v_h be the corresponding finite element approximate solution. The estimator analogous to $\eta_{T,2}$ for this problem is (see [31])

$$\widehat{\eta}_{T,2}^2 := h_T^4 \, \|f\|_{0,2,T}^2 + \sum_{\ell \in \mathcal{E}_h^T} |J_\ell|^2 |\ell|^4,$$

whereas the analogous to $\varepsilon_{T,2}$ is

$$\widehat{\varepsilon}_{T,2}^2 := h_T^2 \, \|f\|_{0,2,T}^2 + \sum_{\ell \in \mathcal{E}_h^T} |J_\ell|^2 |\ell|^2,$$

which defines a global estimator equivalent to $|v - v_h|_{1,2,\Omega}$ (see for instance [31] again). Hence, from the standard theory of finite element approximation on fractional Sobolev spaces (see for instance [9]), we have

$$\begin{aligned} \widehat{\eta}_2 \;&:=\; \left(\sum_{T \in \mathcal{T}_h} \widehat{\eta}_{T,2}^2 \right)^{1/2} \leq Ch \left(\sum_{T \in \mathcal{T}_h} \widehat{\varepsilon}_{T,2}^2 \right)^{1/2} \\ &\leq\; Ch \, |v - v_h|_{1,2,\Omega} \leq C \, \|v\|_{1+\alpha,2,\Omega} \, h^{1+\alpha} \end{aligned} \tag{4.27}$$

$\forall \alpha < \frac{\pi}{\theta}$, where θ is the largest reentrant corner of Ω.

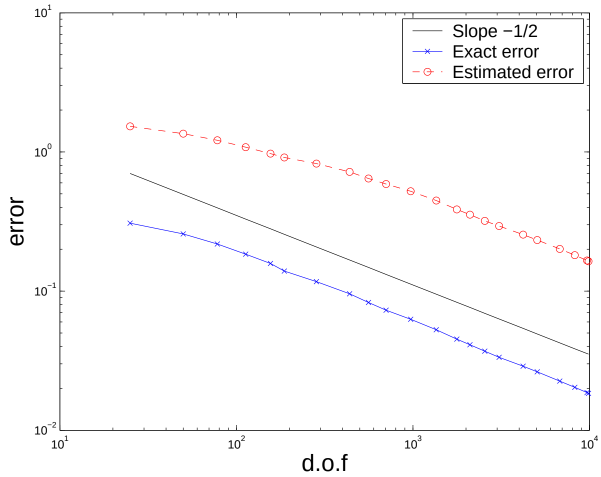

Figure 4.9: Convex domain. Estimator ε_p and exact $\mathrm{W}^{1,p}$ seminorm error curves; $p = 1.5$.

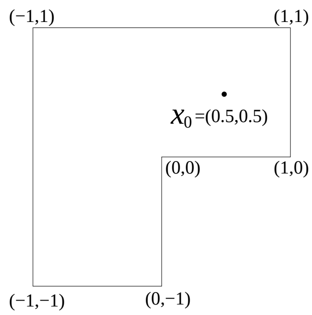

Figure 4.10: L-shape non convex domain.

On the other hand, using the orthogonality of the error, integration by parts, and Cauchy-Schwarz inequality, we have

$$\int_\Omega |\nabla(v - v_h)|^2 = \int_\Omega \nabla(v - v_h) \cdot \nabla v = \int_\Omega (v - v_h)\Delta v \leq \|v - v_h\|_{0,2,\Omega} \|f\|_{0,2,\Omega},$$

which yields

$$\|v - v_h\|_{0,2,\Omega} \geq C\, |v - v_h|^2_{1,2,\Omega}.$$

In general, for quasiuniform meshes, $\exists C > 0$ such that $|v - v_h|_{1,2,\Omega} \geq Ch^{\pi/\theta}$ (see [7]); hence,

$$\|v - v_h\|_{0,2,\Omega} \geq Ch^{2\pi/\theta}. \tag{4.28}$$

Therefore, from (4.27) and (4.28), we have that in general, for quasiuniform meshes,

$$\widehat{\eta}_2 \not\leq C\, \|v - v_h\|_{0,2,\Omega},$$

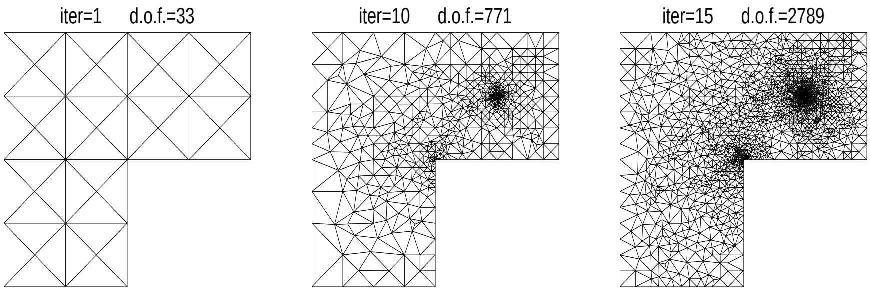

Figure 4.11: Non convex domain. Meshes obtained with $\varepsilon_{T,p}$; $p = 1.5$.

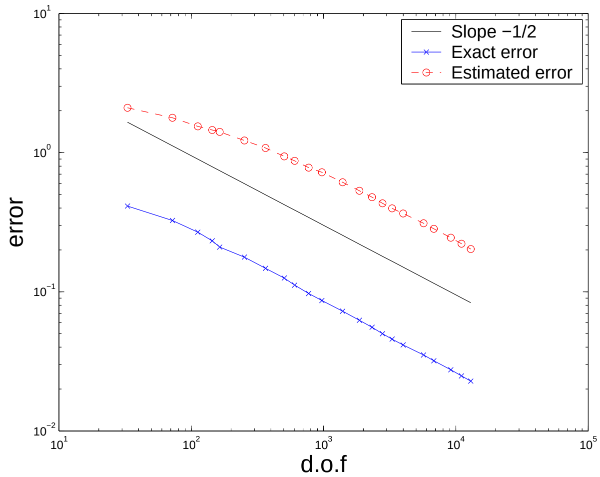

Figure 4.12: Non convex domain. Estimator ε_p and exact $\mathrm{W}^{1,p}$ seminorm error curves; p=1.5.

with a constant C independent of h. This lack of equivalence was somehow circumvented in [23], where other estimator depending on the distance of the element to the singular points of the solution and on the strength of the singularity was proposed.

Despite this lack of equivalence, if we use $\widehat{\eta}_{T,2}$ as an indicator to refine the meshes, we recover an optimal order of convergence in $\mathrm{L}^2(\Omega)$ norm. This can be seen in Fig. 4.15, which shows the error curves for this approach applied to $\Delta v = 0$ with Dirichlet boundary conditions such that the solution be $v = u_2$ as in (4.26).

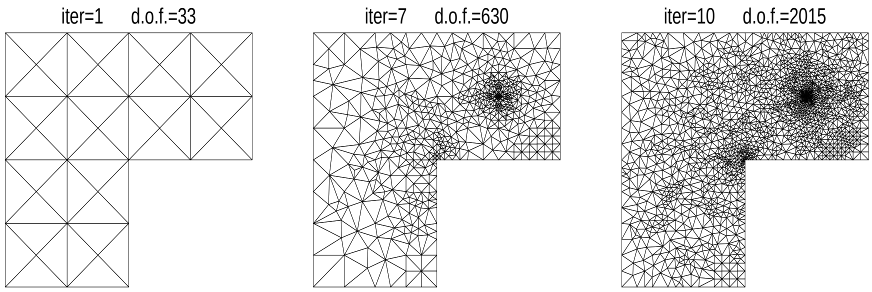

Figure 4.13: Non convex domain. Meshes obtained with $\eta_{T,p}$; $p = 2$.

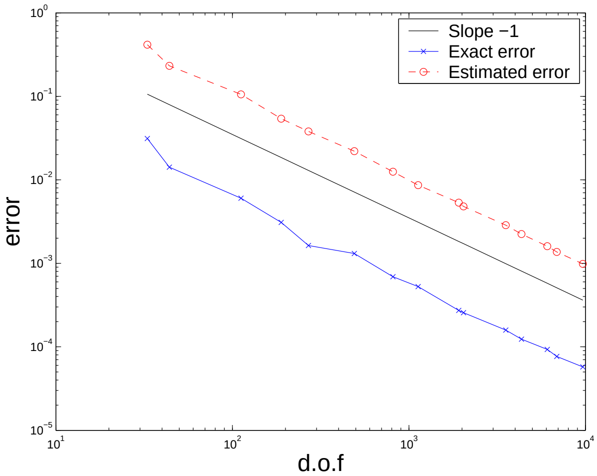

Figure 4.15: Non convex domain; source term $f = 0$. Estimator $\widehat{\eta}_2$ and exact L^2 norm error curves.

4.7 Conclusions

We have introduced residual type *a posteriori* error estimators for the standard finite element approximation of the Poisson problem with a Dirac delta source term. We have proved that these estimators are equivalent to the L^p norm or the $W^{1,p}$ seminorm of the error, for particular ranges of p. In particular, for convex domains, this includes L^2 and $\mathrm{W}^{1,p}$ norms for all $p \in (1, 2)$.

The estimators provide global upper and local lower bounds of the error norms. Because of this, we have used them to guide adaptive refinement schemes. We have shown experimentally that these schemes yield optimal orders of convergence in terms of the number of degrees of freedom. This happens even for the L^2 norm of the error on non-convex domains, which is not covered by the theory because error and estimator are not equivalent in such case.

The extension of this approach to advection dominated advection-diffusion-reaction equations modeling pollutant transport and degradation in aquatic media is currently under investigation.

Chapter 5

An adaptive stabilized finite element scheme for a water quality model

Residual type *a posteriori* error estimators are introduced in this chapter for an advection-diffusion-reaction problem with a Dirac delta source term. The error is measured in an adequately weighted $\mathrm{W}^{1,p}$-norm. These estimators are proved to yield global upper and local lower bounds for the corresponding norms of the error. They are used to guide adaptive procedures, which are experimentally shown to lead to optimal orders of convergence.

5.1 Introduction

This chapter deals with the advection-diffusion-reaction equation with a Dirac delta source term. This kind of problems arise, for example, when modeling pollutant transport and degradation in an aquatic media if the pollution source is a single point. In particular, our work is motivated by the need of an efficient scheme to be used in a water quality model for the river Bío-Bío in Chile.

It is simple to show that the solution of this problem belongs to L^p for $p < \infty$ and to $W^{1,p}$ for $p < 2$. In spite of the fact that the solution does not belong to H^1, this problem can be numerically approximated by standard finite elements.

Specially interesting is the case when the advective term is dominant, as typically happens in real problems. In this case, the solution of the equation has a strong inner layer arising from the source point aligned with the velocity direction. The standard Galerkin approximation usually fails in this situation because this method introduces non-physical oscillations.

A possible remedy for this situation is to add to the variational formulation some numerical diffusion terms to stabilize the finite element solution. Some examples of this approach are the streamline upwind Petrov-Galerkin method (SUPG) (see [11]), the Galerkin least squares approximation (GLS) (see [18]), the Douglas-Wang method (see [16]), the unusual stabilized finite element method (USFEM) (see [19]) and the residual-free bubbles approximation (RFB) (see [10]). The drawback with most of these methods is that the amount of numerical diffusion added to the discretization tends to be large. This means that the solution layers are not always very well resolved because the layer zone is artificially wide. Furthermore, all this stabilization techniques do not consider non regular right hand sides as, for example, a Dirac delta measure.

Due to the nature of the solution, when a strong inner layer is present, it is convenient to compute the numerical solution in a well adapted mesh, which should be obtained by means of an adaptive scheme.

There are not many references in the literature dealing with *a posteriori* techniques for this equation. The reason of this is that most of the standard error estimators involve equivalence constants depending on negative powers of the diffusion parameter, which leads to very poor results in the advection or reaction dominated cases. An error estimator which is robust in the sense of leading to global upper and local lower bounds depending at most on the local mesh Peclet number has been developed by Verfürth (see [33] and [32]). Using these results, Sangalli has analyzed a residual *a posteriori* error estimate for the residual-free bubbles scheme (see [25]). On the other hand, Knop *et al.* have developed some *a posteriori* error estimates using a stabilized scheme combined with a shock capture technique to control the local oscillations in the crosswind direction (see [22]). Finally, Wang has introduced an error estimate for the advection-diffusion equation based on the solution of local problems on each element of the triangulation (see [35]). In all these works smooth source terms are considered. On the other hand, an a posteriori error analysis has been recently developed in [5] for the Laplace equation with a delta source term. To the best of the authors knowledge, no a posteriori error analysis has been performed for the advection-diffusion-reaction equation with a non regular right hand side.

In this paper we introduce and analyze from theoretical and experimental points of view an adaptive scheme to efficiently solve the advection-reaction-diffusion equation with a Dirac delta source term. This scheme is based on the stabilized finite element method introduced in [19], combined with an error estimator similar to that developed in [32] and [4]. Although the stabilization technique [19] has been analyzed only for regular right hand sides, our experiments show that the numerical scheme is convergent also in our case.

Under appropriate assumptions, we prove global upper and local lower error estimates in a weighted $W^{1,p}$-norm, with constants which depend on the shape-regularity of the mesh, the polynomial degree of the finite element approximating space, and, eventually, on the diffusion parameter. Because of this last dependence, our theoretical results are not optimal. However, we perform several numerical experiments in order to show the effectiveness of our approach to capture the layers very sharply and without significant oscillations.

The paper is organized as follows. In Section 5.2 we recall the advection-diffusion-reaction problem under consideration and the stabilized scheme. In Section 5.3 we define an *a posteriori* error estimator, prove some technical lemmas and show its equivalence with the norm of the finite element approximation error. Finally, in Section 5.4, we introduce the adaptive scheme and report the results of some numerical tests which allow us to asses the performance of our approach.

5.2 A stabilized method for a model problem

Let $\Omega \subset \mathbb{R}^2$ be a bounded polygonal domain with a Lipschitz boundary $\Gamma = \bar{\Gamma}_{\mathrm{D}} \cup \bar{\Gamma}_{\mathrm{N}}$, with $\Gamma_{\mathrm{D}} \cap \Gamma_{\mathrm{N}} = \emptyset$. We denote by $\boldsymbol{n}$ the outer unit normal vector to Γ. Let δ_{x_0} be the Dirac delta measure supported at an inner point $x_0 \in \Omega$.

Our model problem is the advection-reaction-diffusion equation

$$\begin{cases} -\varepsilon\Delta u + \boldsymbol{a}\cdot\nabla u + bu &= \delta_{x_0} \quad \text{in } \Omega, \\ u &= 0 \quad \text{on } \Gamma_{\mathrm{D}}, \\ \varepsilon\dfrac{\partial u}{\partial \boldsymbol{n}} &= g \quad \text{on } \Gamma_{\mathrm{N}}, \end{cases} \tag{5.1}$$

where:

(A1) $\varepsilon \in \mathbb{R} : \ \varepsilon > 0$;

(A2) $\boldsymbol{a} \in \mathrm{W}^{1,\infty}(\Omega)^2, \ \operatorname{div} \boldsymbol{a} = 0$;

(A3) $b \in \mathbb{R}, \ b \geq 0$;

(A4) $\Gamma_{\mathrm{D}} \supset \{\boldsymbol{x} \in \Gamma : \ \boldsymbol{a}(\boldsymbol{x}) \cdot \boldsymbol{n}(\boldsymbol{x}) < 0\}$;

(A5) $g \in \mathrm{L}^2(\Gamma_{\mathrm{N}})$;

(A6) either $b > 0$ or $|\Gamma_{\mathrm{D}}| > 0$.

We are interested in the advection-reaction dominated case in which $\varepsilon \ll \|\boldsymbol{a}\|_{0,\infty,\Omega} + b$.

Here and thereafter we use standard notation for Sobolev and Lebesgue spaces and norms. Moreover, let $W_D^{1,r}(\Omega) := \left\{\varphi \in W^{1,r}(\Omega) : \varphi|_{\Gamma_{\mathrm{D}}} = 0\right\}$, $1 < r < \infty$.

Let us remark that problem (5.1) does not have a solution in $H^1(\Omega)$. However, it has a solution in $W^{1,p}(\Omega)$ $\forall p < 2$. In fact, let $G(x) := \frac{1}{2\pi}\log|x - x_0|$ be such that

$$-\Delta G = \delta_{x_0} \text{ in } \Omega;$$

i.e., $-G$ is a fundamental solution of the Laplace operator. Straightforward calculations show that $G \in W^{1,p}(\Omega)$ $\forall p \in [1,2)$. Hence, substituting $u = w + \varepsilon^{-1}G$ in (5.1), we observe that problem (5.1) has a unique solution if and only if the following problem does it:

$$\left\{\begin{aligned} -\varepsilon\Delta w + \boldsymbol{a}\cdot\nabla w + bw &= -\varepsilon^{-1}\boldsymbol{a}\cdot\nabla G - \varepsilon^{-1}bG && \text{in } \Omega, \\ w &= -\varepsilon^{-1}G && \text{on } \Gamma_{\mathrm{D}}, \\ \varepsilon\frac{\partial w}{\partial \boldsymbol{n}} &= g - \frac{\partial G}{\partial \boldsymbol{n}} && \text{on } \Gamma_{\mathrm{N}}. \end{aligned}\right. \tag{5.2}$$

Since $x_0 \notin \partial\Omega$, G and its normal derivative are smooth on $\partial\Omega$. Hence, standard arguments show that problem (5.2) has a unique solution $w \in H^1(\Omega)$(see for instance [24]). Moreover, according to the results of [20], problem (5.2) has a unique solution $w \in W_D^{1,p}(\Omega)$ for $p \in (p^*, 2)$, where $p^* := \frac{2}{1+\pi/(2\omega)}$, with ω being the largest reentrant corner on the domain Ω.

Consequently, problem (5.1) has a solution $u \in W^{1,p}(\Omega)$ $\quad\forall p < 2$, and this solution is unique if $p^* \le p < 2$. Let us remark that for any polygonal domain Ω, $p^* \le 8/5$. Moreover, if Ω is convex, then $p^* < 4/3$. From now on we restrict our analysis to a fixed $p \in (p^*, 2)$. Moreover, let $q \in (2, \infty)$ be such that $\frac{1}{p} + \frac{1}{q} = 1$.

Let B be the bilinear form defined on $W_D^{1,p}(\Omega) \times W_D^{1,q}(\Omega)$ by

$$B(v, w) := \int_\Omega (\varepsilon\nabla v\cdot\nabla w + \boldsymbol{a}\cdot\nabla v\; w + bvw)\,. \tag{5.3}$$

The following is a variational formulation of problem (5.1): Find $u \in W_D^{1,p}(\Omega)$ such that

$$B(u, v) = \langle\delta_{x_0}, v\rangle + \int_{\Gamma_{\mathrm{N}}} gv \quad \forall v \in W_D^{1,q}(\Omega). \tag{5.4}$$

(In the expression above $\langle\delta_{x_0}, v\rangle = v(x_0)$).

It is clear that a solution of (5.1) in $W_D^{1,p}(\Omega)$ is also solution of (5.4). Straightforward calculations show that the solution of (5.4) satisfies (5.1). Then (5.4) has a unique solution, too.

We consider the following norms on $W_D^{1,p}(\Omega)$ and $W_D^{1,q}(\Omega)$:

$$|||u|||_p := \left(\varepsilon^{\frac{p}{q}} \|\nabla u\|_{0,p,\Omega}^p + b^{\frac{p}{q}} \|u\|_{0,p,\Omega}^p\right)^{\frac{1}{p}}, \; |||v|||_q := \left(\varepsilon^{\frac{q}{p}} \|\nabla v\|_{0,q,\Omega}^q + b^{\frac{q}{p}} \|v\|_{0,q,\Omega}^q\right)^{\frac{1}{q}}.$$

Assumptions (A1)–(A3) imply that

$$B(v,w) \le \left(1 + \varepsilon^{-\frac{1}{q}} \|\boldsymbol{a}\|_{0,\infty,\Omega}\right) |||v|||_p \, |||w|||_q \,. \tag{5.5}$$

On the other hand we also assume an inf-sup condition for B; namely, that there exists $\beta > 0$ such that

$$\sup_{v \in W_D^{1,q}(\Omega)} \frac{B(u,v)}{|||v|||_q} \ge \beta \, |||u|||_p \qquad \forall u \in W_D^{1,p}(\Omega). \tag{5.6}$$

Remark 5.2.1 *The condition above holds true (with β eventually depending on ε) if and only if, for all $f \in [W_D^{1,q}(\Omega)]'$ the problem*

$$\textit{Find } u \in W_D^{1,p}(\Omega): \quad B(u,v) = \langle f, v\rangle \quad \forall v \in W_D^{1,q}(\Omega),$$

has a unique solution (see for instance [17]). In its turn, the latter holds true for all p in a neighborhood of 2. The length of this neighborhood depends on the geometry of Ω and the boundary conditions (see [15]).

Let $\{\mathcal{T}_h\}_{h>0}$, be a family of shape-regular partitions of Ω into triangles. Let $V_h := \left\{\varphi \in \mathcal{C}(\Omega) : \varphi|_T \in \mathcal{P}_k \; \forall T \in \mathcal{T}_h \text{ and } \varphi|_{\Gamma_{\mathrm{D}}} = 0\right\} \subset W_D^{1,q}(\Omega) \subset W_D^{1,p}(\Omega)$, where, for $k \in \mathbb{N}$, $\mathcal{P}_k$ denotes the space of polynomials of degree at most k. It is well known that the standard Galerkin method based on this finite element space yields poor approximation when $\varepsilon \ll \|\boldsymbol{a}\|_{0,\infty,\Omega} + b$. For this reason, we consider the following stabilized formulation introduced in [19]: Find $u_h \in V_h$ such that

$$B_\tau(u_h, v_h) = F_\tau(v_h) \quad \forall v_h \in V_h, \tag{5.7}$$

where, for $v_h, w_h \in V_h$,

$$\begin{aligned} B_\tau(v_h, w_h) &:= B(v_h, w_h) \\ &- \sum_{T \in \mathcal{T}_h} \int_T \tau_T \left(-\varepsilon \Delta v_h + \boldsymbol{a} \cdot \nabla v_h + b v_h\right)\left(-\varepsilon \Delta w_h - \boldsymbol{a} \cdot \nabla w_h + b w_h\right) \end{aligned} \tag{5.8}$$

and

$$F_\tau(v_h) := \langle \delta_{x_0}, v_h\rangle + \int_{\Gamma_{\mathrm{N}}} g v_h - \tau_T \langle \delta_{x_0}, -\varepsilon \Delta v_h - \boldsymbol{a} \cdot \nabla v_h + b v_h\rangle. \tag{5.9}$$

In the expressions above, the stabilization parameter τ_T is defined as follows:

$$\tau_T(\boldsymbol{x}) := \frac{h_T^2}{b h_T^2 \max\{1, \mathrm{Pe}_T^{\mathrm{R}}(\boldsymbol{x})\} + (2\varepsilon/m_k)\max\{1, \mathrm{Pe}_T^{\mathrm{A}}(\boldsymbol{x})\}}, \tag{5.10}$$

with $\mathrm{Pe}_T^{\mathrm{R}}(\boldsymbol{x})$ and $\mathrm{Pe}_T^{\mathrm{A}}(\boldsymbol{x})$ being the Peclet numbers respectively defined by

$$\mathrm{Pe}_T^{\mathrm{R}}(\boldsymbol{x}) := \frac{2\varepsilon}{m_k b h_T^2} \qquad \text{and} \qquad \mathrm{Pe}_T^{\mathrm{A}}(\boldsymbol{x}) := \frac{m_k\,|\boldsymbol{a}(\boldsymbol{x})|\,h_T}{\varepsilon}, \tag{5.11}$$

where

$$m_k := \min\{1/3, C_k\},$$

with C_k being a positive constant satisfying

$$C_k \sum_{T\in\mathcal{T}_h} h_T^2\,\|\Delta v_h\|_{0,T}^2 \le \|\nabla v_h\|_{0,\Omega}^2 \quad \forall v_h \in V_h,$$

which only depends on the polynomial degree k and the shape-regularity of the mesh.

The convergence and stabilization properties of this scheme have been investigated in [19] for a smooth source term. However, for a non regular right hand side, no a priori error estimates are known for this stabilized scheme.

In the following section we introduce a posteriori error estimators which will allow us to create meshes correctly refined to solve the problem. We demonstrate numerically the effectiveness of this approach in the last section.

From now on, C denotes a generic positive constant, not necessarily the same at each occurrence, but always independent of the mesh-size and the small parameter ε.

5.3 A posteriori error estimator.

In this section we define a residual error estimator by combining ideas from [32] and [4] for advection-reaction-diffusion problems with those in [5] for problems with a delta source term.

For simplicity, we assume that the support x_0 of the Dirac delta measure is a vertex of the triangulation and that g is piecewise polynomial.

Let $\mathcal{E}_h$ denote the set of all edges in $\mathcal{T}_h$ and, for $E \in \mathcal{E}_h$, let h_E be the length of E. We define the volumetric and edge residuals by

$$R_T := \varepsilon\Delta u_h - \boldsymbol{a}\cdot\nabla u_h - b u_h, \qquad T \in \mathcal{T}_h, \tag{5.12}$$

$$R_E := \begin{cases} -\left[\!\left[\varepsilon \dfrac{\partial u_h}{\partial \boldsymbol{n}_E}\right]\!\right]_E, & \text{if } E \in \mathcal{E}_h :\ E \not\subseteq \Gamma, \\ g - \varepsilon \dfrac{\partial u_h}{\partial \boldsymbol{n}}, & \text{if } E \in \mathcal{E}_h :\ E \subset \Gamma_{\mathrm{N}}, \\ 0, & \text{if } E \in \mathcal{E}_h :\ E \subset \Gamma_{\mathrm{D}}, \end{cases} \tag{5.13}$$

where $[\![\cdot]\!]_E$ denotes the jump across the edge E.

These residuals are used to define an estimator of the local error as follows:

$$\eta_{T,p} := \begin{cases} \left(\alpha_T^p h_T^{-\frac{2p}{q}} + \alpha_T^p \|R_T\|_{0,p,T}^p + \displaystyle\sum_{E\subset\partial T} \varepsilon^{-\frac{1}{q}} \alpha_E \|R_E\|_{0,p,E}^p\right)^{\frac{1}{p}}, & T \ni x_0, \\ \left(\alpha_T^p \|R_T\|_{0,p,T}^p + \displaystyle\sum_{E\subset\partial T} \varepsilon^{-\frac{1}{q}} \alpha_E \|R_E\|_{0,p,E}^p\right)^{\frac{1}{p}}, & T \not\ni x_0, \end{cases} \tag{5.14}$$

where, for $S = T \in \mathcal{T}_h$ or $S = E \in \mathcal{E}_h$,

$$\alpha_S := \begin{cases} \min\left\{h_S \varepsilon^{-\frac{1}{p}}, b^{-\frac{1}{p}}\right\}, & b > 0; \\ h_S \varepsilon^{-\frac{1}{p}}, & b = 0. \end{cases} \tag{5.15}$$

In what follows we prove some technical lemmas.

Let $\omega_0 := \bigcup\{T \in \mathcal{T}_h : x_0 \in T\}$ and $d := \operatorname{dist}(x_0, \partial\omega_0)$ (see Fig. 5.1). Notice that, because of the regularity of the mesh, $h_T \leq Cd$. Let ψ_{x_0} be a smooth bubble function defined in Ω with support in ω_0 and satisfying:

$$0 \leq \psi_{x_0}(x) \leq 1 \qquad \forall x \in \Omega, \tag{5.16}$$

$$\psi_{x_0}(x) = 1 \qquad \forall x \in \Omega :\ |x - x_0| \leq \frac{d}{4}, \tag{5.17}$$

$$\psi_{x_0}(x) = 0 \qquad \forall x \in \Omega :\ |x - x_0| \geq \frac{3d}{4}, \tag{5.18}$$

$$|\psi_{x_0}|_{m,\infty,\omega_0} \leq Cd^{-m}, \qquad m = 1, 2. \tag{5.19}$$

Such function can be easily obtained by convolution of the characteristic function of the set $\{x \in \Omega :\ |x - x_0| < d/4\}$ with a mollifier.

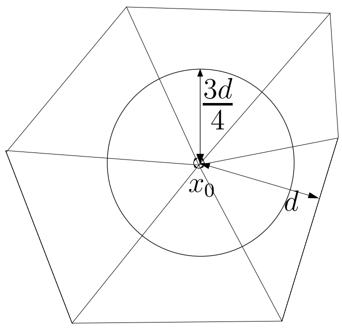

Figure 5.1: Domain ω_0 and support of ψ_{x_0}.

LEMMA 5.3.1 *Let $T \ni x_0$. Let ψ_{x_0} and ω_0 be defined as above. Then*

$$\begin{aligned} \|\psi_{x_0}\|_{0,q,E} &\leq Ch_T^{1/q}, \\ \|\psi_{x_0}\|_{0,q,T} &\leq Ch_T^{2/q}, \\ |||\psi_{x_0}|||_{q,T} &\leq C\alpha_T^{-1}h_T^{2/q}. \end{aligned}$$

PROOF. Using (5.19) and the fact that $h_T \leq Cd$, the definition of $|\cdot|_{m,q}$ yields

$$|\psi_{x_0}|_{m,q,E} = \left[\int_E |D^m\psi_{x_0}(x)|^q\right]^{1/q} \leq Cd^{-m}h_T^{1/q} \leq Ch_T^{-m+1/q}.$$

The same arguments give

$$|\psi_{x_0}|_{m,q,T} = \left[\int_T |D^m\psi_{x_0}(x)|^q\right]^{1/q} \leq Cd^{-m}h_T^{2/q} \leq Ch_T^{-m+2/q}.$$

This inequality and the definition of $|||\cdot|||_q$ allow us to complete the proof. □

LEMMA 5.3.2 *Given $T \in \mathcal{T}_h$, let τ_T be defined by (5.10). Then the following bounds hold $\forall \boldsymbol{x} \in T$:*

$$\varepsilon\tau_T(\boldsymbol{x}) \leq \frac{1}{6}h_T^2, \qquad |\boldsymbol{a}(\boldsymbol{x})|\,\tau_T(\boldsymbol{x}) \leq \frac{1}{2}h_T, \qquad b\tau_T(\boldsymbol{x}) \leq 1.$$

Furthermore,

$$b\tau_T(\boldsymbol{x}) \leq Cb^{\frac{1}{p}}\alpha_T.$$

PROOF.

For the first estimate, we use (5.10) and (5.11) to obtain

$$\varepsilon\tau_T(\boldsymbol{x}) \leq \frac{\varepsilon h_T^2}{bh_T^2\max\{1, \mathrm{Pe}_T^{\mathrm{R}}(\boldsymbol{x})\}} \leq \frac{\varepsilon h_T^2}{bh_T^2\mathrm{Pe}_T^{\mathrm{R}}(\boldsymbol{x})} \leq \frac{m_k}{2}h_T^2 \leq \frac{1}{6}h_T^2.$$

For the second one, if $\boldsymbol{a}(\boldsymbol{x}) = \boldsymbol{0}$ there is nothing to prove; otherwise, by using (5.10) and (5.11) we have

$$|\boldsymbol{a}(\boldsymbol{x})|\,\tau_T(\boldsymbol{x}) \le \frac{|\boldsymbol{a}(\boldsymbol{x})|\,m_k h_T^2}{2\varepsilon \max\{1, \mathrm{Pe}_T^{\mathrm{A}}(\boldsymbol{x})\}} \le \frac{|\boldsymbol{a}(\boldsymbol{x})|\,m_k h_T^2}{2\varepsilon \mathrm{Pe}_T^{\mathrm{A}}(\boldsymbol{x})} \le \frac{1}{2} h_T.$$

For the third bound, (5.10) yields

$$b\tau_T(\boldsymbol{x}) \le \frac{1}{\max\{1, \mathrm{Pe}_T^{\mathrm{R}}(\boldsymbol{x})\}} \le 1.$$

Moreover, from the first estimate of this lemma, $b\tau_T(\boldsymbol{x}) \le Cbh_T^2\varepsilon^{-1}$, too. Hence, taking a weighted geometric mean of this and the third estimate, we have

$$b\tau_T(\boldsymbol{x}) \le Cb^{\frac{1}{p}} h_T^{\frac{2}{p}} \varepsilon^{-\frac{1}{p}} \le C\,|\Omega|^{\frac{2}{p}}\, b^{\frac{1}{p}} \left(\frac{h_T}{|\Omega|}\right)^{\frac{2}{p}} \varepsilon^{-\frac{1}{p}} \le Cb^{\frac{1}{p}} h_T \varepsilon^{-\frac{1}{p}}.$$

$\square$

Lemma 5.3.3 *The following estimates hold for all $w_h \in V_h$:*

$$|w_h|_{m,q,T} \le Ch_T^{-m}\alpha_T\, |||w_h|||_T\,, \qquad m = 1, 2.$$

Proof. The definition of the norm $|||\cdot|||_{q,T}$ implies that

$$|w_h|_{1,q,T} \le \varepsilon^{-\frac{1}{p}}\, |||w_h|||_{q,T}\,, \tag{5.20}$$

whereas, because of a standard scaling argument,

$$|w_h|_{1,q,T} \le Ch_T^{-1}\, \|w_h\|_{0,q,T} \le Ch_T^{-1} b^{-\frac{1}{p}}\, |||w_h|||_{q,T}\,.$$

From these two inequalities we obtain

$$|w_h|_{1,q,T} \le Ch_T^{-1}\alpha_T\, |||w_h|||_{q,T}\,. \tag{5.21}$$

On the other hand, another scaling argument and (5.21) yield

$$|w_h|_{2,q,T} \le Ch_T^{-1} |w_h|_{1,q,T} \le Ch_T^{-2}\alpha_T\, |||w_h|||_{q,T}\,,$$

which completes the proof. $\square$

Lemma 5.3.4 *The following estimates hold for all $w_h \in V_h$:*

$$|w_h|_{m,\infty,T} \le Ch_T^{-m-\frac{2}{q}}\alpha_T\, |||w_h|||_T\,, \qquad m = 1, 2.$$

Proof. Standard scaling arguments yield

$$|w_h|_{m,\infty,T} \leq Ch_T^{-\frac{2}{q}} |w_h|_{m,q,T}, \qquad m = 0, 1, 2.$$

Finally, this estimate in addition to Lemma 5.3.3 complete the proof. □

Denote by $I_C : L^2(\Omega) \longrightarrow V_h$ the Clément-like interpolation operator introduced in [8]. Given $T \in \mathcal{T}_h$, let

$$\widetilde{\omega}_T := \bigcup \{T' \in \mathcal{T}_h : T' \cap T \neq \emptyset\}. \tag{5.22}$$

We prove several error estimates analogous to those in Lemma 3.2 of [32] .

Lemma 5.3.5 *For all $T \in \mathcal{T}_h$, $E \in \partial T$ and $v \in \mathrm{W}^{1,q}(\widetilde{\omega}_T)$, the following error estimates hold:*

$$\begin{aligned} \|v - I_C v\|_{0,q,T} &\leq C\alpha_T \, |||v|||_{q,\widetilde{\omega}_T}, \\ \|v - I_C v\|_{0,q,E} &\leq C\varepsilon^{-1/(pq)} \alpha_E^{1/p} \, |||v|||_{q,\widetilde{\omega}_T}, \\ |||I_C v|||_{q,T} &\leq C \, |||v|||_{q,\widetilde{\omega}_T}. \end{aligned}$$

Proof. The following error estimate for I_C has been proved in [8]:

$$|v - I_C v|_{l,q,T} \leq Ch_T^{k-l} \, |v|_{k,q,\widetilde{\omega}_T}, \quad \forall k, l : 0 \leq l \leq k \leq 1. \tag{5.23}$$

The first inequality of this lemma follows from this estimate with $l = 0$ and $k = 0, 1$.

The following trace inequality can be proved by standard scaling arguments:

$$\|v - I_C v\|_{0,q,E} \leq C \left(h_E^{-1/q} \|v - I_C v\|_{0,q,T} + \|v - I_C v\|_{0,q,T}^{1/p} \, |v - I_C v|_{1,q,T}^{1/q} \right).$$

Therefore, this inequality and the first inequality of this lemma yields

$$\begin{aligned} \|v - I_C v\|_{0,q,E} &\leq C \left(h_E^{-1/q} \alpha_T \, |||v|||_{q,\widetilde{\omega}_T} + \alpha_T^{1/p} \, |||v|||_{q,\widetilde{\omega}_T}^{1/p} \, |v|_{1,q,\widetilde{\omega}_T}^{1/q} \right) \\ &\leq C \left(h_E^{-1/q} \alpha_T^{1/p} \alpha_T^{1/q} \, |||v|||_{q,\widetilde{\omega}_T} + \alpha_T^{1/p} \varepsilon^{-1/(pq)} \, |||v|||_{q,\widetilde{\omega}_T} \right) \\ &\leq C\varepsilon^{-1/(pq)} \alpha_E^{1/p} \, |||v|||_{q,\widetilde{\omega}_T}. \end{aligned}$$

Finally the third estimate of the lemma is also a consequence of (5.23) and the definition of $\|\cdot\|_{0,q,E}$. □

Lemma 5.3.6 *For all $v \in W^{1,q}(\widetilde{\omega}_T)$, there holds*

$$\|v - I_C v\|_{0,\infty,T} \leq Ch_T^{1-\frac{2}{q}} \varepsilon^{-\frac{1}{p}} \, |||v|||_{q,\widetilde{\omega}_T}.$$

Proof. Let $I_L v$ denote the Lagrange interpolant of v, which is well defined since $v \in W^{1,q}(\widetilde{\omega}_T) \subset \mathcal{C}(\widetilde{\omega}_T)$. The lemma follows from interpolation error estimates and standard scaling arguments:

$$
\begin{aligned}
\|v - I_C v\|_{0,\infty,T} &\leq \|v - I_L v\|_{0,\infty,T} + \|I_L v - I_C v\|_{0,\infty,T}\,, \\
&\leq C\left[h_T^{1-\frac{2}{q}}\,|v|_{1,q,\widetilde{\omega}_T} + h_T^{-\frac{2}{q}}\,\|I_L v - I_C v\|_{0,q,T}\right], \\
&\leq C\left[h_T^{1-\frac{2}{q}}\,|v|_{1,q,\widetilde{\omega}_T} + h_T^{-\frac{2}{q}}\left(\|v - I_L v\|_{0,q,\widetilde{\omega}_T} + \|v - I_C v\|_{0,q,\widetilde{\omega}_T}\right)\right], \\
&\leq C h_T^{1-\frac{2}{q}} \varepsilon^{-\frac{1}{p}}\,|||v|||_{q,\widetilde{\omega}_T}\,.
\end{aligned}
$$

□

For each element $T \in \mathcal{T}_h$ we define the *element bubble function* ψ_T by

$$\psi_T := 27 \prod_{x \in \mathcal{N}(T)} \lambda_x,$$

where $\mathcal{N}(T)$ is the set of vertices of the element T and λ_x denote the corresponding barycentric coordinates.

In the sequel we will also use certain special bubble functions associated to edges $E \in \mathcal{E}_h$ and lifting operators, introduced by Verfürth in [32]. In what follows we remind their definitions. Let $\widehat{T}$ be the standard reference element, of vertices $(1,0), (0,1)$ and (0,0). Given any number $\theta \in (0,1]$, denote by $\Phi_\theta : \mathbb{R}^2 \to \mathbb{R}^2$ the transformation which maps (x,y) onto $(x, \theta y)$. Let

$$\widehat{T}_\theta := \Phi_\theta(\widehat{T}),$$

and denote by $\hat{\lambda}_{1,\theta}$, $\hat{\lambda}_{2,\theta}$, and $\hat{\lambda}_{3,\theta}$ the barycentric coordinates corresponding to the points P_1, P_2, and P_3, as shown in Figure 5.2.

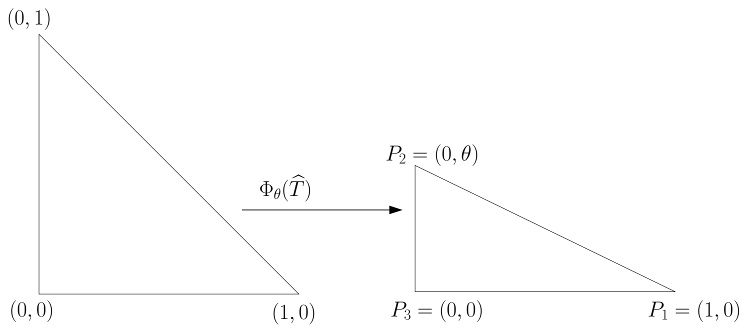

Figure 5.2: Triangles $\widehat{T}$ and $\widehat{T}_\theta$.

Let

$$\psi_{\widehat{E},\theta} := \begin{cases} 4\,\hat{\lambda}_{3,\theta}\hat{\lambda}_{1,\theta} & \text{on } \widehat{T}_\theta, \\ 0 & \text{on } \widehat{T} \setminus \widehat{T}_\theta, \end{cases}$$

where $\widehat{E} := \{(t,0) \in \mathbb{R}^2 : 0 \le t \le 1\}$.

Let $E \in \mathcal{E}_h$ be an inner edge and denote by T_1, T_2 the two triangles sharing E. Let

$$\omega_E := T_1 \cup T_2.$$

Denote by $G_{E,i}$, $i = 1, 2$, the orientation preserving affine transformation which maps $\widehat{T}$ onto T_i and $\widehat{E}$ onto E (see Figure 5.3).

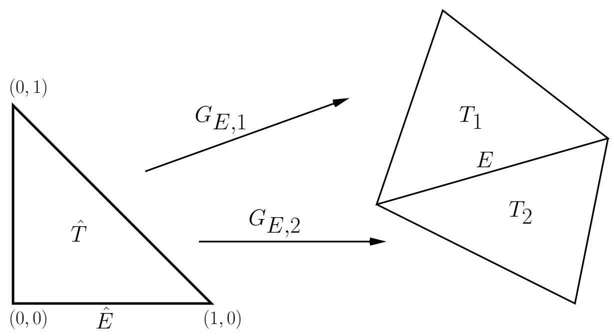

Figure 5.3: Domain ω_E and affine transformations $G_{E,i}$, $i = 1, 2$.

For $E \in \mathcal{E}_h$, let

$$\theta_E := \begin{cases} \min\{\varepsilon^{1/p} b^{-1/p} h_E^{-1}, 1\}, & b > 0, \\ 1, & b = 0, \end{cases}$$

and

$$\psi_{E} := \begin{cases} \psi_{\widehat{E},\theta_E} \circ G_{E,i}^{-1} & \text{in } T_i,\ i = 1, 2, \\ 0 & \text{in } \Omega \setminus \omega_E. \end{cases}$$

Let $\hat{\Pi} := \{(x, 0) : x \in \mathbb{R}\}$ and $\hat{Q} : \mathbb{R}^2 \to \hat{\Pi}$ be the orthogonal projection from $\mathbb{R}^2$ onto $\hat{\Pi}$. We introduce the lifting operator $\hat{P}_{\hat{E}} : \mathcal{P}_k(\hat{E}) \to \mathcal{P}_k(\hat{T})$ by

$$\hat{P}_{\hat{E}}(\hat{\sigma}) = \hat{\sigma} \circ \hat{Q}.$$

Let $P_{E,T_i} : \mathcal{P}_k(E) \to \mathcal{P}_k(T_i)$ defined by

$$P_{E,T_i}(\sigma) = \hat{P}_{\hat{E}}(\sigma \circ G_{E,i}) \circ G_{E,i}^{-1}, \quad i = 1, 2.$$

Finally, we define a lifting operator for $\sigma \in \mathcal{P}_k(E)$ by

$$P_E(\sigma) := \begin{cases} P_{E,T_1}(\sigma) & \text{in } T_1, \\ P_{E,T_2}(\sigma) & \text{in } T_2. \end{cases}$$

For $E \in \mathcal{E}_h$ such that $E \subset \Gamma_N$, the function ψ_E and the lifting operator P_E are similarly defined with the obvious modifications.

Lemma 5.3.7 *The following estimates hold for all $v \in \mathcal{P}_k$ and $T \in \mathcal{T}_h$:*

$$\begin{aligned} \|v\|_{0,p,T} \|v\|_{0,q,T} &\leq C(v, \psi_T v)_T, \\ |||\psi_T v|||_{q,T} &\leq C\alpha_T^{-1} \|v\|_{0,q,T}. \end{aligned}$$

Furthermore, for all $E \in \mathcal{E}_h$ and $\sigma \in \mathcal{P}_k(E)$, the following estimates hold:

$$\begin{aligned} \|\sigma\|_{0,p,E} \|\sigma\|_{0,q,E} &\leq C(\sigma, \psi_E \sigma)_E, \\ \|\psi_E P_E(\sigma)\|_{0,q,\omega_E} &\leq C\varepsilon^{1/(pq)} \alpha_E^{1/q} \|\sigma\|_{0,q,E}, \\ |||\psi_E P_E(\sigma)|||_{q,\omega_E} &\leq C\varepsilon^{1/(pq)} \alpha_E^{-1/p} \|\sigma\|_{0,q,E}. \end{aligned}$$

Proof. Scaling arguments show that

$$\|v\|_{0,r,T} \leq Ch^{\frac{2}{r}-1}(v, \psi_T v)_T^{1/2} \qquad \text{with} \quad r = p, q,$$

which yield the first inequality. The third inequality follows from a similar argument.

For the second one, using the fact that $|\nabla \psi_T| \leq Ch_T^{-1}$ and standard scaling arguments, we have

$$\begin{aligned} |||v\psi_T|||_{q,T} &\leq C\left[\varepsilon^{\frac{1}{p}} \|\nabla(v\psi_T)\|_{0,q,T} + b^{\frac{1}{p}} \|v\psi_T\|_{0,q,T}\right] \\ &\leq C\left[\varepsilon^{\frac{1}{p}} \left(\|v\nabla\psi_T\|_{0,q,T} + \|\psi_T \nabla v\|_{0,q,T}\right) + b^{\frac{1}{p}} \|v\psi_T\|_{0,q,T}\right] \\ &\leq C\left[\varepsilon^{\frac{1}{p}} h_T^{-1} \|v\|_{0,q,T} + b^{\frac{1}{p}} \|v\|_{0,q,T}\right] \\ &\leq C \max\{\varepsilon^{\frac{1}{p}} h_T^{-1}, b^{\frac{1}{p}}\} \|v\|_{0,q,T} \\ &= C\alpha_T^{-1} \|v\|_{0,q,T}. \end{aligned}$$

The fourth inequality of the lemma follows from the definition of $\|\cdot\|_{0,q,\omega_E}$ and the fact that the size of the support of ψ_E in the orthogonal direction to E is bounded by $C\theta_E h_E$, with C only depending on the shape ratio of T. (see Fig. 5.4):

$$\|\psi_E P_E(\sigma)\|_{0,q,\omega_E} = \left[\int_{\omega_E} \psi_E P_E(\sigma)\right]^{1/q} \leq C\left[\theta_E h_E \int_E \psi_E \sigma\right]^{1/q} \leq C\varepsilon^{\frac{1}{pq}} \alpha_E^{\frac{1}{q}} \|\sigma\|_{0,q,E}.$$

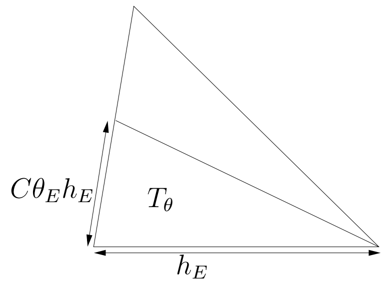

Figure 5.4: Domain T_θ

The last inequality of the lemma follows from the fact that $|\nabla\psi_E| \le C(\theta_E h_E)^{-1}$ and standard scaling arguments:

$$\begin{aligned}
|||\psi_E P_E(\sigma)|||_{q,\omega_E} &\le C\left[\varepsilon^{\frac{1}{p}}\left\|\nabla(\psi_E P_E(\sigma))\right\|_{0,q,\omega_E} + b^{\frac{1}{p}}\left\|\psi_E P_E(\sigma)\right\|_{0,q,\omega_E}\right] \\
&\le C\left[\varepsilon^{\frac{1}{p}}\left(\left\|\nabla\psi_E P_E(\sigma)\right\|_{0,q,\omega_E} + \left\|\psi_E \nabla P_E(\sigma)\right\|_{0,q,\omega_E}\right)\right. \\
&\quad \left. + b^{\frac{1}{p}}\left\|\psi_E P_E(\sigma)\right\|_{0,q,\omega_E}\right] \\
&\le C\left[\varepsilon^{\frac{1}{p}}(\theta_E h_T)^{-1}\left\|P_E(\sigma)\right\|_{0,q,\omega_E} + b^{\frac{1}{p}}\left\|P_E(\sigma)\right\|_{0,q,\omega_E}\right] \\
&\le C\max\{\varepsilon^{\frac{1}{p}}h_T^{-1}, b^{\frac{1}{p}}\}\left\|P_E(\sigma)\right\|_{0,q,\omega_E} \\
&\le C\varepsilon^{\frac{1}{pq}}\alpha_E^{-\frac{1}{p}}\left\|\sigma\right\|_{0,q,E},
\end{aligned}$$

where we have also used the fourth inequality of this lemma. □

Now we are in position to state the main theoretical result of the paper.

THEOREM 5.3.1 *Let B be defined by (5.3). Let $p < 2$ be such that B satisfies (5.6) with a constant $\beta > 0$. Let u and u_h be the solutions of problems (5.4) and (5.7), respectively. Let $\eta_{T,p}$ be defined by (5.12)–(5.15) and, $\forall T \ni x_0$, let $\eta_{0,T}$ be defined by*

$$\eta_{0,T} := \begin{cases} h_T^{\frac{2-p}{p}}\varepsilon^{-\frac{1}{p}}, & \textit{if} \quad bh_T^p > \varepsilon, \\ 0, & \textit{if} \quad bh_T^p \le \varepsilon. \end{cases} \tag{5.24}$$

Then, there exist constants C and C', only depending on the regularity of the mesh and the polynomial degree of the finite elements, such that

$$|||u - u_h|||_p \le \frac{C}{\beta}\left(\sum_{T\in\mathcal{T}_h}\eta_{T,p}^p + \sum_{T\ni x_0}\eta_{0,T}^p\right)^{\frac{1}{p}}$$

and

$$\eta_{T,p} \le C'\left(1 + \varepsilon^{-\frac{1}{q}}\left\|\boldsymbol{a}\right\|_{0,\infty,\widetilde{\omega}_T}\right)|||u - u_h|||_{p,\widetilde{\omega}_T} \quad \forall T \in \mathcal{T}_h,$$

where $\widetilde{\omega}_T$ is defined by (5.22).

Proof. First, we write from (5.6),

$$\beta \left|\!\left|\!\left| u - u_h \right|\!\right|\!\right|_p \leq \sup_{v \in W_D^{1,q}(\Omega)} \frac{B(u-u_h, v)}{\left|\!\left|\!\left| v \right|\!\right|\!\right|_q}. \tag{5.25}$$

Now, consider an arbitrary $v \in W_D^{1,q}(\Omega)$ with $\left|\!\left|\!\left| v \right|\!\right|\!\right|_q = 1$. Obviously, we have

$$B(u-u_h, v) = B(u-u_h, v - I_C v) + B(u-u_h, I_C v). \tag{5.26}$$

Element-wise integration by parts yields

$$B(u-u_h, w) \;=\; \langle \delta_{x_0}, w\rangle + \sum_{T\in\mathcal{T}_h} (R_T, w)_T + \sum_{E\in\mathcal{E}_h} (R_E, w)_E \quad \forall w \in W_D^{1,q}(\Omega). \tag{5.27}$$

Taking $w = v - I_C v$, invoking Hölder's inequality and Lemmas 5.3.5 and 5.3.6, we have

$$\begin{aligned} B(u-u_h, v - I_C v) \;&\leq\; C \Bigg[\sum_{T\ni x_0} \eta_{0,T}^p + \sum_{T\in\mathcal{T}_h} \alpha_T^p \left\| R_T \right\|_{0,p,T}^p \\ &\qquad + \sum_{E\in\mathcal{E}_h} \varepsilon^{-1/q} \alpha_E \left\| R_E \right\|_{0,p,E}^p \Bigg]^{\frac{1}{p}} \\ &\leq\; C \Bigg[\sum_{T\ni x_0} \eta_{0,T}^p + \sum_{T\in\mathcal{T}_h} \eta_{T,p}^p \Bigg]^{\frac{1}{p}}. \end{aligned} \tag{5.28}$$

For the second term in the right hand side of (5.26), from (5.3), (5.4), (5.7), (5.8), and (5.9), we have

$$\begin{aligned} B(u-u_h, w_h) = \;& \tau_{T_0} \langle \delta_{x_0}, -\varepsilon\Delta w_h - \boldsymbol{a}\cdot\nabla w_h + b w_h \rangle \\ & - \sum_{T\in\mathcal{T}_h} \int_T \tau_T (R_T, -\varepsilon\Delta w_h - \boldsymbol{a}\cdot\nabla w_h + b w_h). \end{aligned}$$

Next, from Lemmas 5.3.2 and 5.3.3, straightforward computations lead to

$$\int_T \tau_T (R_T, -\varepsilon\Delta w_h - \boldsymbol{a}\cdot\nabla w_h + b w_h) \leq C \alpha_T \left\| R_T \right\|_{0,p,T} \left|\!\left|\!\left| w_h \right|\!\right|\!\right|_{q,T},$$

whereas from Lemmas 5.3.2 and 5.3.4 we have

$$\tau_{T_0} \langle \delta_{x_0}, -\varepsilon\Delta w_h - \boldsymbol{a}\cdot\nabla w_h + b w_h \rangle \leq C \alpha_{T_0} h_{T_0}^{-\frac{2}{q}} \left|\!\left|\!\left| w_h \right|\!\right|\!\right|_{q,T_0}.$$

Finally, we replace w_h by $I_C v$ and use Lemma 5.3.5 to obtain

$$B(u-u_h, I_C v) \leq C\left(\alpha_{T_0} h_{T_0}^{-\frac{2}{q}} |||v|||_{q,\widetilde{\omega}_{T_0}} + \sum_{T\in\mathcal{T}_h} \alpha_T \|R_T\|_{0,p,T} |||v|||_{q,\widetilde{\omega}_T}\right).$$

From the regularity of the mesh and the fact that $|||v|||_q = 1$, hold

$$B(u-u_h, I_C v) \leq C\left[\sum_{T\ni x_0} \alpha_T^p h_T^{-\frac{2p}{q}} + \sum_{T\in\mathcal{T}_h} \alpha_T^p \|R_T\|_{0,T}^p\right]^{\frac{1}{p}} \leq C\left[\sum_{T\in\mathcal{T}_h} \eta_{T,p}^p\right]^{\frac{1}{p}}. \tag{5.29}$$

Thus, the first estimate of the theorem is a consequence of (5.25), (5.26), (5.28), and (5.29).

To derive the other estimate of the theorem, we consider an arbitrary $T \in \mathcal{T}_h$. First, we take $w = \psi_T R_T$ in (5.27), and we have

$$B(u-u_h, \psi_T R_T) = (R_T, \psi_T R_T)_T. \tag{5.30}$$

Using Lemma 5.3.7, (5.30), and Lemma 5.3.7 again, we have

$$\begin{aligned}
\|R_T\|_{0,p,T} \|R_T\|_{0,q,T} &\leq C(R_T, \psi_T R_T)_T \\
&= CB(u-u_h, \psi_T R_T) \\
&\leq C\left(1+\varepsilon^{-\frac{1}{q}} \|\boldsymbol{a}\|_{0,\infty,T}\right) |||u-u_h|||_{p,T} |||\psi_T R_T|||_{q,T} \\
&\leq C\left(1+\varepsilon^{-\frac{1}{q}} \|\boldsymbol{a}\|_{0,\infty,T}\right) |||u-u_h|||_{p,T} \alpha_T^{-1} \|R_T\|_{0,q,T}.
\end{aligned}$$

Hence,

$$\alpha_T \|R_T\|_{0,p,T} \leq C\left(1+\varepsilon^{-\frac{1}{q}} \|\boldsymbol{a}\|_{0,\infty,T}\right) |||u-u_h|||_{p,T}. \tag{5.31}$$

On the other hand, taking $w = \psi_E P_E(R_E)$ in (5.27) we obtain

$$\begin{aligned}
(R_E, w)_E &= B(u-u_h, w) - \sum_{T\in\omega_E} (R_T, w)_T \\
&\leq \left(1+\varepsilon^{-\frac{1}{q}} \|\boldsymbol{a}\|_{0,\infty,\omega_E}\right) |||u-u_h|||_{p,\omega_E} |||w|||_{q,\omega_E} \\
&\quad + \sum_{T\in\omega_E} \|R_T\|_{0,p,T} \|w\|_{0,q,T}.
\end{aligned}$$

Now, from Lemma 5.3.7,

$$\begin{aligned}
\|R_E\|_{0,p,E} \|R_E\|_{0,q,E} \leq C\Bigg[&\left(1+\varepsilon^{\frac{1}{q}} \|\boldsymbol{a}\|_{0,\infty,\omega_E}\right) |||u-u_h|||_{p,\omega_E} \varepsilon^{\frac{1}{pq}} \alpha_E^{-\frac{1}{p}} \|R_E\|_{0,q,E} \\
&+ \sum_{T\in\omega_E} \|R_T\|_{0,p,T} \varepsilon^{1/(pq)} \alpha_E^{1/q} \|R_E\|_{0,q,E}\Bigg],
\end{aligned}$$

and, multiplying by $\varepsilon^{-1/(pq)}\alpha_E^{1/p}$, we obtain

$$\begin{aligned}\varepsilon^{-1/(pq)}\alpha_E^{1/p}\left\|R_E\right\|_{0,p,E} &\le C\left[\left(1+\varepsilon^{\frac{1}{q}}\left\|\boldsymbol{a}\right\|_{0,\infty,\omega_E}\right)|||u-u_h|||_{p,T}\right.\\ &\left.+\sum_{T\in\omega_E}\alpha_T\left\|R_T\right\|_{0,p,T}\right]. \end{aligned}\tag{5.32}$$

Finally, taking $w=\psi_{x_0}$ in (5.27), we have

$$\langle\delta_{x_0},\psi_{x_0}\rangle = B(u-u_h,\psi_{x_0})-\sum_{T\in\mathcal{T}_h}(R_T,\psi_{x_0})_T-\sum_{E\in\mathcal{E}_h}(R_E,\psi_{x_0})_E.$$

Using the properties of ψ_{x_0} from Lemma 5.3.1, (5.5), and Hölder's inequality, we obtain

$$\begin{aligned} 1 &\le \left(1+\varepsilon^{-\frac{1}{q}}\left\|\boldsymbol{a}\right\|_{0,\infty,T}\right)|||u-u_h|||_{p,T}\,|||\psi_{x_0}|||_{0,q,T}\\ &\quad+\sum_{T\in w_T}\left\|R_T\right\|_{0,p,T}\left\|\psi_{x_0}\right\|_{0,q,T}+\sum_{E\in\mathcal{E}_h}\left\|R_E\right\|_{0,p,E}\left\|\psi_{x_0}\right\|_{0,q,E}\\ &\le C\left[\left(1+\varepsilon^{-\frac{1}{q}}\left\|\boldsymbol{a}\right\|_{0,\infty,T}\right)|||u-u_h|||_{p,T}\,h_T^{2/q}\alpha_T^{-1}\right.\\ &\quad\left.+\sum_{T\in w_T}\left\|R_T\right\|_{0,p,T}h_T^{2/q}+\sum_{E\in\mathcal{E}_h}\left\|R_E\right\|_{0,p,E}h_T^{1/q}\right]. \end{aligned}$$

Thus,

$$\begin{aligned} h_{T_0}^{-2/q}\alpha_{T_0} &\le C\left[\left(1+\varepsilon^{-\frac{1}{q}}\left\|\boldsymbol{a}\right\|_{0,\infty,T}\right)|||u-u_h|||_{0,p,T}\right.\\ &\quad\left.+\sum_{T\in w_T}\alpha_T\left\|R_T\right\|_{0,p,T}+\sum_{E\in\mathcal{E}_h}\varepsilon^{-\frac{1}{pq}}\alpha_E^{\frac{1}{p}}\left\|R_E\right\|_{0,p,E}\right], \end{aligned}\tag{5.33}$$

where we have used the fact that $h_T^{-\frac{1}{q}}\alpha_E \le \varepsilon^{-\frac{1}{pq}}\alpha_E^{\frac{1}{p}}$ and the regularity of the mesh.

Thus, the second estimate of the theorem follows from (5.31), (5.32), (5.33), and the definition of the estimator $\eta_{T,p}$, and we conclude the proof . □

REMARK 5.3.1 *In absence of reaction, $b=0$ and, according to (5.24), $\eta_{0,T}=0$, too. Consequently, the estimator $\left(\sum_{T\in\mathcal{T}_h}\eta_{T,p}^p\right)^{\frac{1}{p}}$ is actually equivalent to the error for the advection-diffusion problem.*

5.4 Numerical experiments

In this section we report several numerical experiments which allow us to assess the performance of an h-adaptive mesh-refinement strategy based on the error estimator $\eta_{T,p}$.

The adaptive procedure consists in solving problem (5.7) on a sequence of meshes up to finally attain a solution with an estimated error within a prescribed tolerance. With this purpose, we initiate the process with a quasi-uniform mesh and, at each step, a new mesh better adapted to the solution of problem (5.4) must be created. This is done by computing the local error estimators $\eta_{T,p}$ for all T in the 'old' mesh $\mathcal{T}_h$, and refining those elements T with $\eta_{T,p} \geq \mu \max\{\eta_{T,p} : \ T \in \mathcal{T}_h\}$, where $\mu \in (0,1)$ is a prescribed parameter. In all our experiments we have chosen $\mu = \frac{1}{2}$ and $p = 1.5$. The last choice guarantees that (5.6) holds true. Indeed, according to [15], (5.6) is valid for $p \in (1,\infty)$ in the first two cases and for $p \in \left(\frac{4}{3}, 4\right)$ in the third one. To refine the meshes we have used the red-green-blue strategy described in [31].

5.4.1 Test 1: A diffusion-reaction problem

For the first test we consider the problem

$$-\varepsilon\Delta u + bu = \delta_{x_0}. \tag{5.34}$$

A fundamental solution of (5.34) is given by

$$u(x) := \frac{1}{4i\varepsilon} H_0^{(1)}\left(\sqrt{\frac{b}{\varepsilon}}\, i\,|x - x_0|\right), \tag{5.35}$$

where $H_0^{(1)}$ denotes the Hankel function of order zero (see [1]). The test consists of solving problem (5.34) with $x_0 = (0,0)$ on the square $\Omega := (-1,1)\times(-1,1)$, $\varepsilon = 10^{-4}$ and $b = 1$. We choose a Dirichlet boundary condition such that the exact solution is given by the real part of (5.35).

We report the results obtained for the adaptive process with $\eta_{T,p}$ as estimator of the error. Fig. 5.5 shows some of the successively refined meshes created in the adaptive process and the corresponding computed solutions. The iteration number and the number of degrees of freedom (d.o.f.) of each mesh are also reported in this figure.

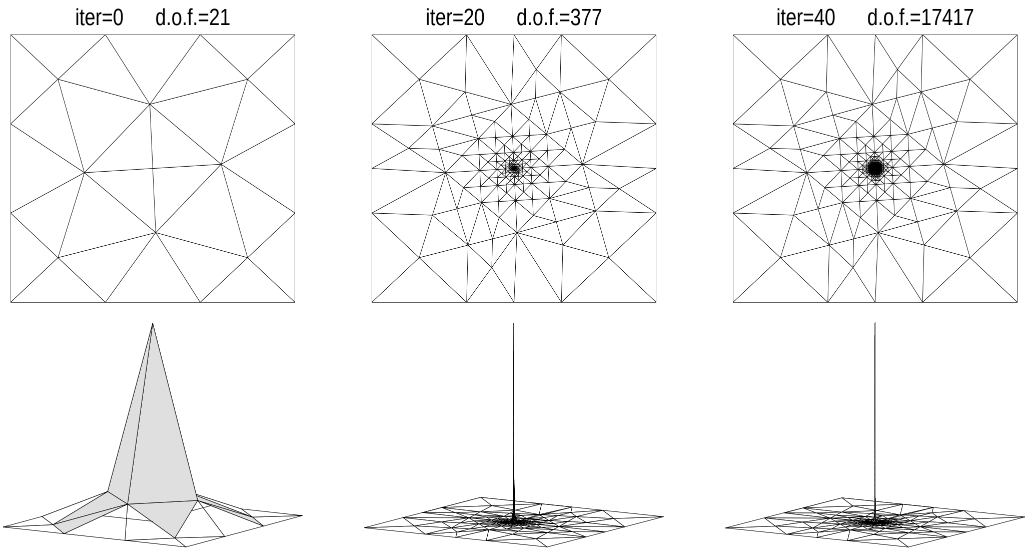

Figure 5.5: Test 1. Meshes and computed solutions.

Fig. 5.6 shows successive zooms of the final adapted mesh around x_0. The second square corresponds to the white inner square in the first one amplified 10 times around x_0, and so on.

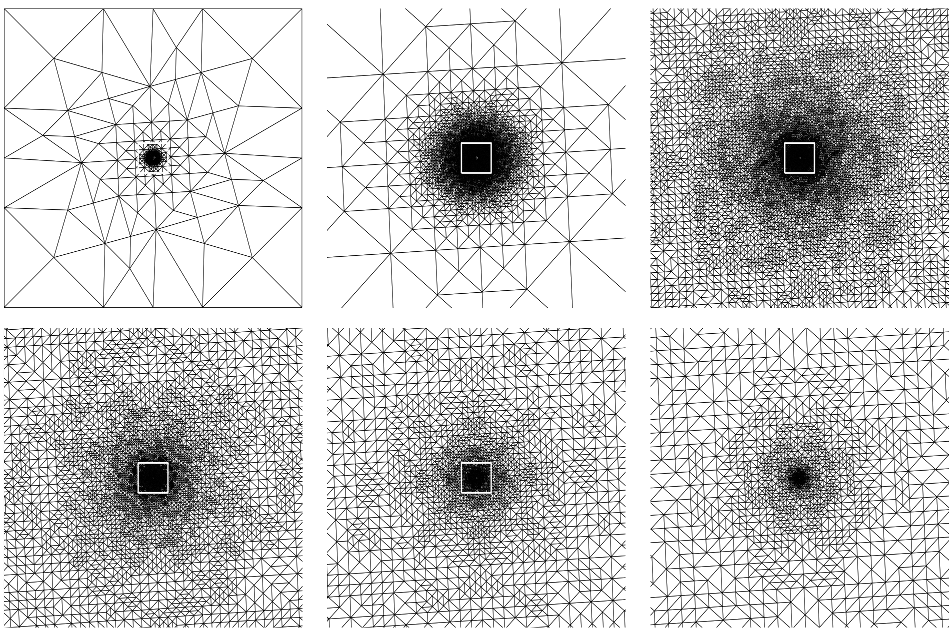

Figure 5.6: Test 1. Successive zooms of the final adapted mesh.

It can be seen from Fig. 5.5 and 5.6 that the adaptive process leads to meshes densely refined around x_0.

Fig. 5.7 shows the error curves of the whole process for the exact error and for the error estimators $\eta := \left(\sum_{T\in\mathcal{T}_h} \eta_{T,p}^p\right)^{\frac{1}{p}}$ and $\eta_* := \left(\sum_{T\in\mathcal{T}_h} \eta_{T,p}^p + \sum_{T\ni x_0} \eta_{0,T}^p\right)^{\frac{1}{p}}$, which, according to Theorem 5.3.1, are lower and upper error estimators, respectively. This figure also includes a line with slope $-1/2$, which corresponds to the theoretically optimal order of convergence for piecewise linear elements.

Both estimators η and η_* are significantly different during the first steps of the adaptive process. In fact, although they only differ in the triangles $T \ni x_0$, the error concentrates on these elements. This is the reason why the difference between η and η_* is so pronounced.

However both estimators are equally good to guide the adaptive process. Indeed, exactly the same meshes appear if η_* is used instead of η in this test. Once the elements T around x_0 are sufficiently refined so that $bh_T^p \leq \varepsilon$, according to the definition of $\eta_{0,T}$, both estimators coincide. It can be seen from Fig. 5.7 that this happens in this test after around 10 steps.

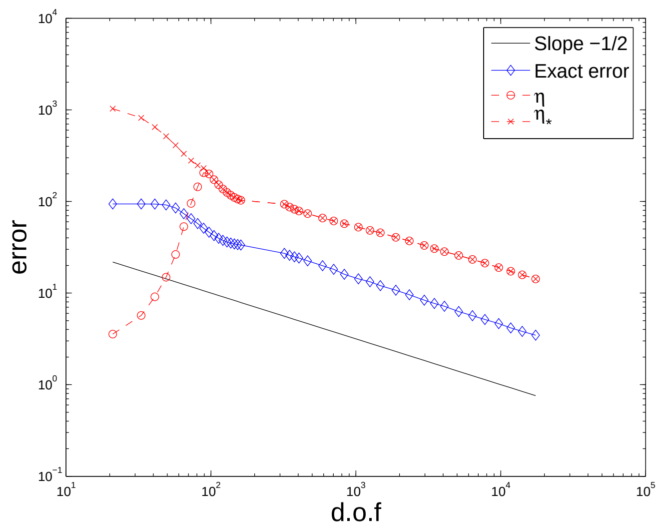

Figure 5.7: Test 1. Estimators η and η_*, and exact $W_D^{1,p}(\Omega)$-norm error curves.

The error curves show that, at the final stage, the adaptive process yields an optimal order of convergence: the exact and estimated error curves have both approximately the same optimal slope $-1/2$.

5.4.2 Test 2: An advection-diffusion problem

The second test consists of solving the problem

$$-\varepsilon\Delta u + \boldsymbol{a}\cdot\nabla u = \delta_{x_0},$$

with $x_0 = (0.5, 0.5)$, $\Omega := (0,3)\times(0,1)$, $\varepsilon = 10^{-4}$, and $\boldsymbol{a} = (1,0)$. We choose boundary conditions as shown in Fig. 5.8.

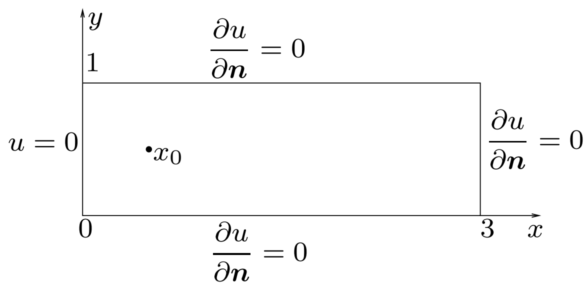

Figure 5.8: Test 2. Boundary conditions.

Let us recall that in this case ($b = 0$), both estimators η and η^*, coincide.

Fig. 5.9 shows some of the successively refined meshes created in the adaptive process for $\eta_{T,p}$, with $p = 1.5$.

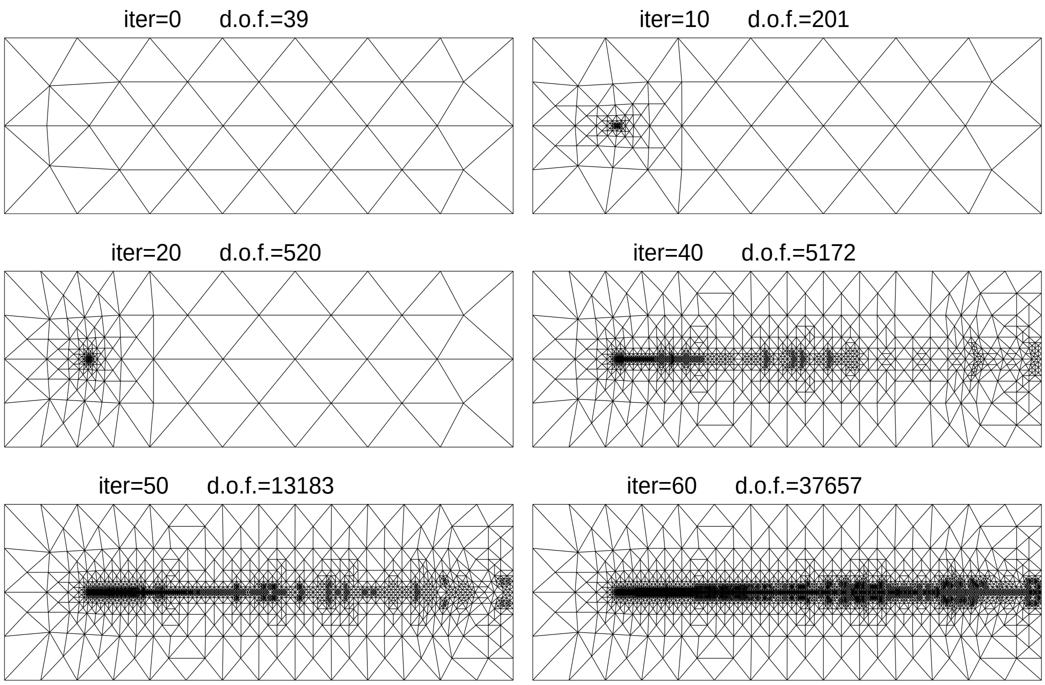

Figure 5.9: Test 2. Meshes obtained by the adaptive process.

Fig. 5.10 shows successive zooms around x_0 of the final adapted mesh. It can be seen from Fig. 5.9 and Fig. 5.10 that the adaptive process leads to meshes refined around both, x_0 and the inner layer.

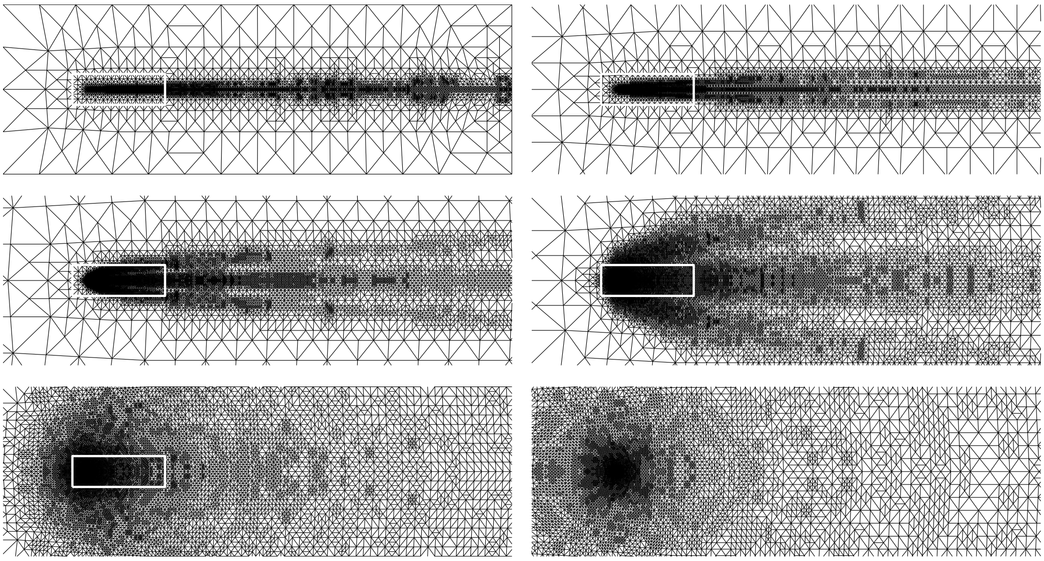

Figure 5.10: Test 2. Successive zooms of the final adapted mesh.

Fig. 5.11 shows the error curves of the whole process for the estimated errors. A computed order of convergence of approximately -0.4 was obtained by means of a least squares fitting.

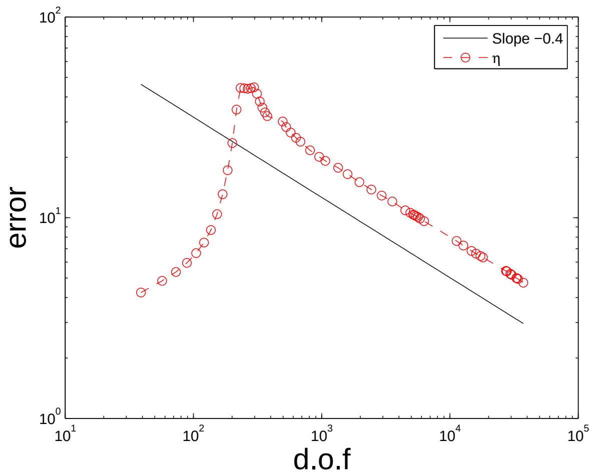

Figure 5.11: Test 2. Error curves for the estimator η.

Fig. 5.12 shows several cross sections with vertical planes $x =$ constant. It can be seen that the numerical results present no spurious oscillations in the layer zone.

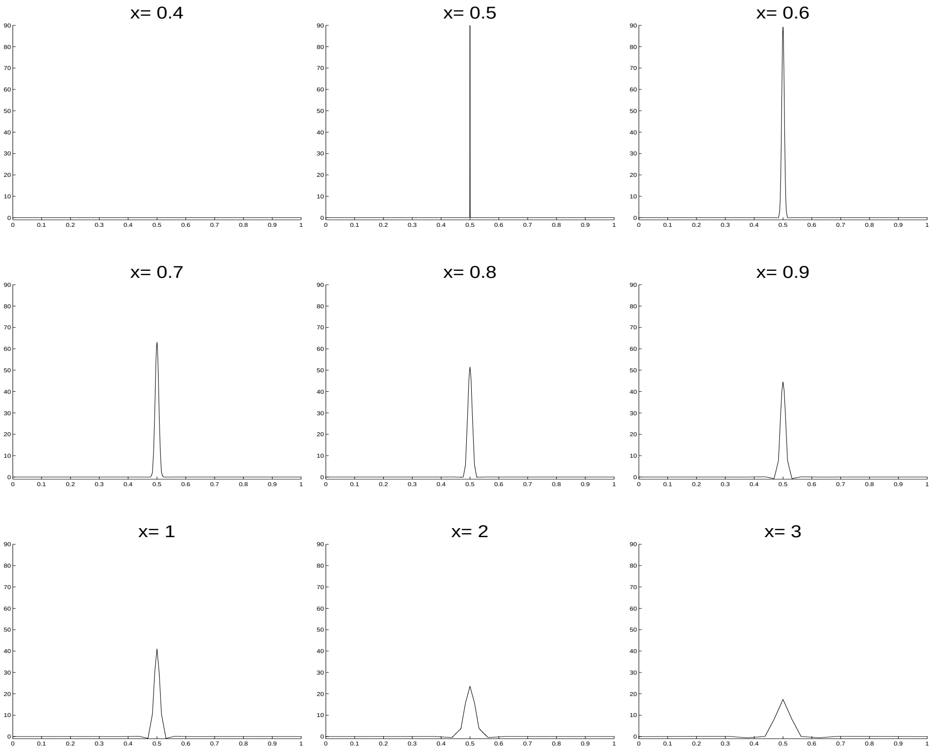

Figure 5.12: Test 2. Cross sections of the computed solution.

5.4.3 Test 3: Application to the Bío-Bío river

Our last test consists of an application of the described methodology to a realistic scenario: a water quality model for Bío-Bío river in Chile. With this purpose we have solved the advection-diffusion-reaction equation (5.1) which describes transport and degradation of pollutants arising from a point source. Fig. 5.13 shows the geometry of the domain, which correspond to a section of Bío-Bío river and two tributaries. It also shows the initial used mesh (773 nodes) and the source point at one of the tributaries.

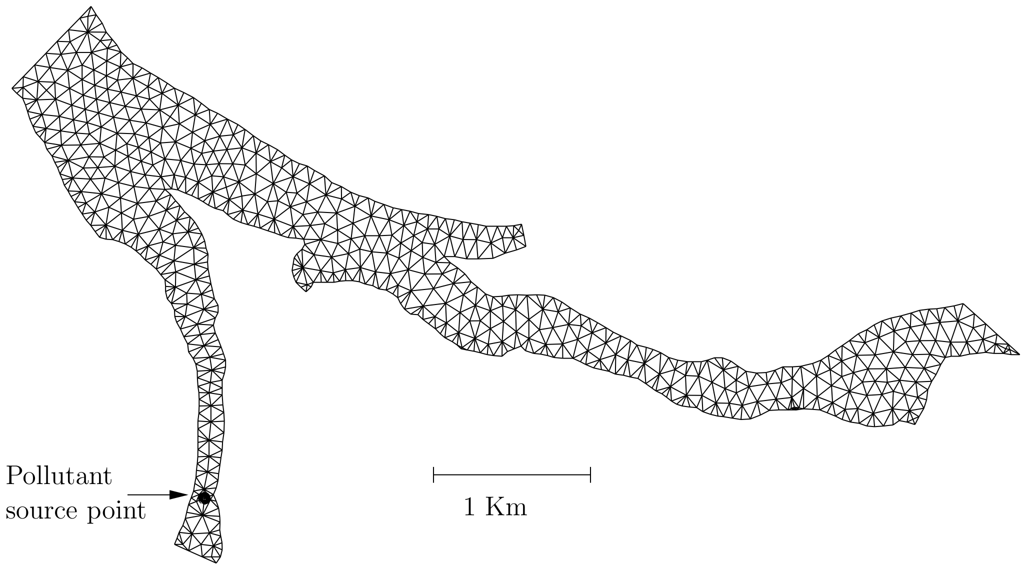

Figure 5.13: Test 3. Initial mesh and location of the source point.

Fig. 5.14 shows the velocity field $\boldsymbol{a}$; the average speed is 0.02 Km/s. We have used $\varepsilon = 10^{-6}$ Km^2/s and $b = 10^{-3}$ s^{-1}. We have taken the following boundary conditions: $u = 0$ on the three inflow parts of the boundary and $\partial u/\partial \boldsymbol{n} = 0$ on the banks and the outflow boundary.

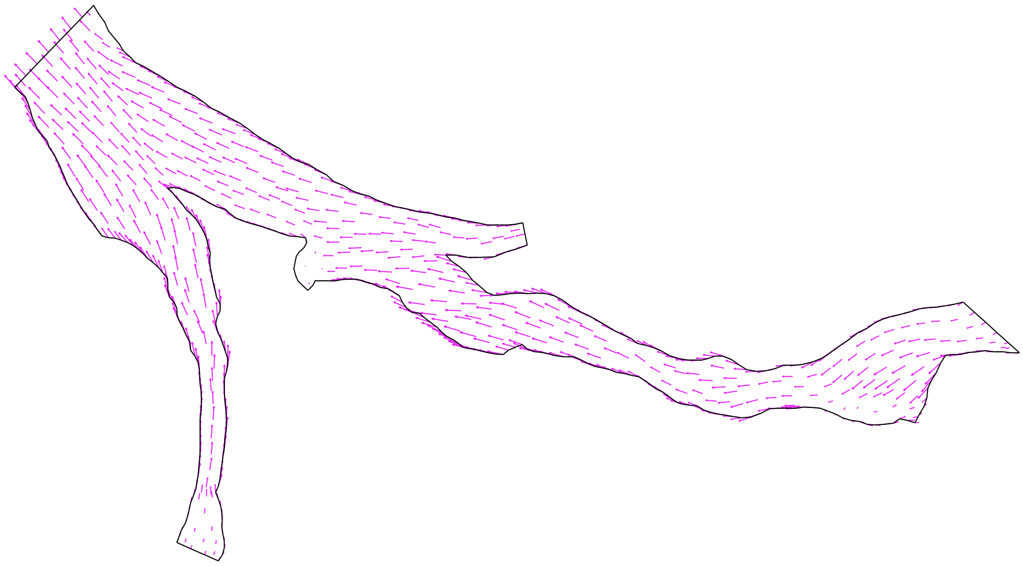

Figure 5.14: Test 3. Velocity field $\boldsymbol{a}$.

Fig. 5.15 shows the final mesh (19884 nodes) after 60 steps of the adaptive process. It can be seen that the mesh is well aligned with the inner layer.

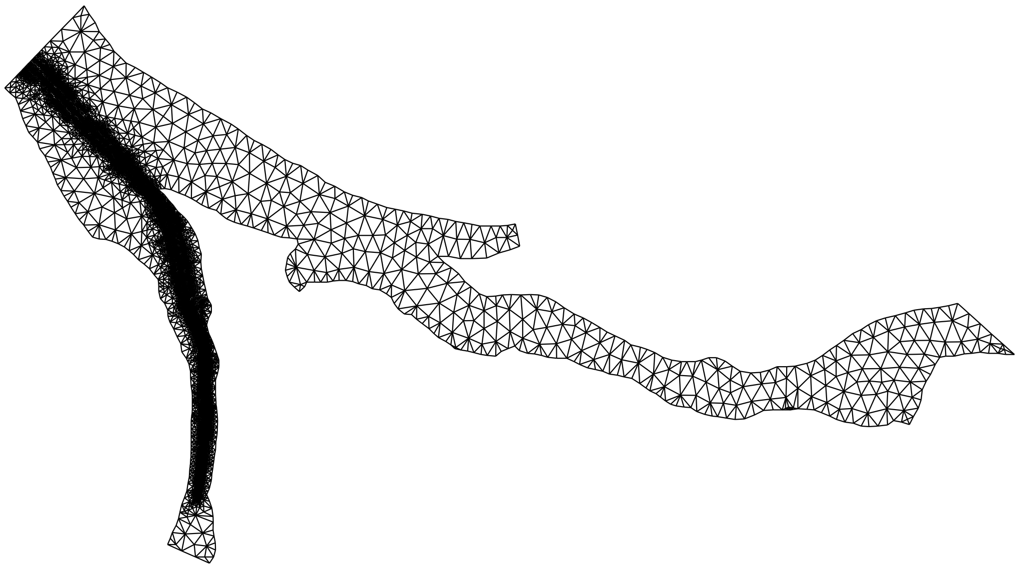

Figure 5.15: Test 3. Final mesh.

Fig. 5.16 shows the isovalues of the computed solution in the range 10^{-1}–10^{3} on the final adapted mesh. It can be clearly seen that the combined effect of the stabilization and the adaptive process allow us to identify the inner layer and get rid of any spurious oscillation.

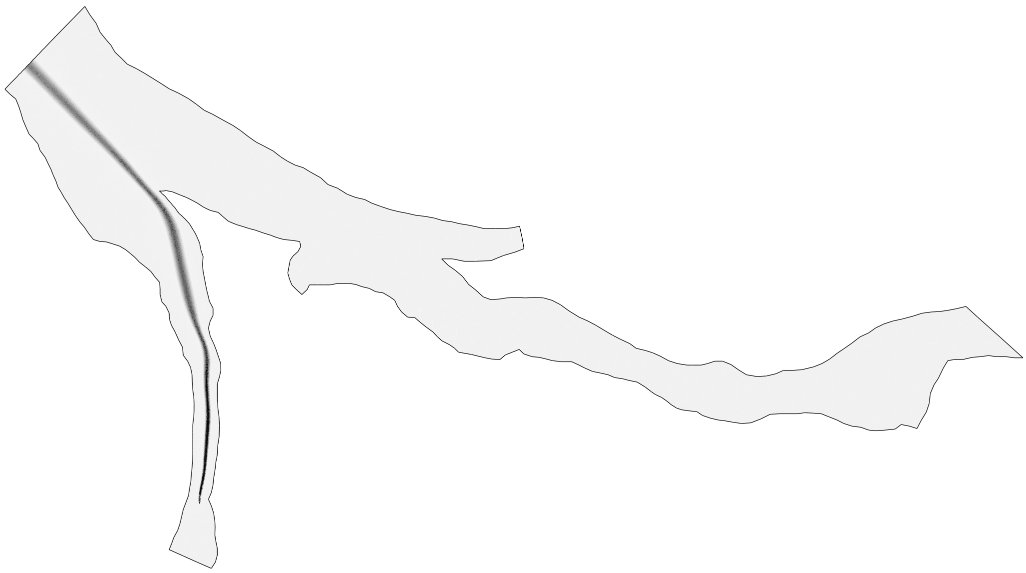

Figure 5.16: Test 3. Isovalues of the computed solution.

5.5 Conclusions

An adaptive finite element scheme for the advection-reaction-diffusion equation with a Dirac delta source term has been introduced. This scheme is based on a stabilized finite element method combined with a residual error estimator. In spite of the fact that the used stabilization technique was originally introduced only for regular right hand sides, our numerical experiments show that the scheme is convergent in our case, too. On the other hand, the estimator is shown to be reliable and efficient in that global upper and local lower error estimates are proved, although with constants eventually depending on the diffusion parameter.

Several numerical experiments are reported. All of them show the effectiveness of this scheme to capture the layers very sharply and without significant oscillations.

Bibliography

[1] M. Abramowitz and I.A. Stegun. *Handbook of mathematical functions with formulas, graphs, and mathematical tables*, volume 55 of *National Bureau of Standards Applied Mathematics Series*. U.S. Government Printing Office, Washington, D.C., 1964.

[2] J. Alberty, C. Carstensen, and S.A. Funken. Remarks around 50 lines of Matlab: short finite element implementation. *Numer. Algorithms*, 20(2-3):117–137, 1999.

[3] R. Araya, E. Behrens, and R. Rodríguez. An adaptive stabilized finite element scheme for a water quality model. Technical Report 2005-21, Universidad de Concepción, Concepción, 2005.

[4] R. Araya, E. Behrens, and R. Rodríguez. An adaptive stabilized finite element scheme for the advection-reaction-diffusion equation. *Appl. Numer. Math.*, 54(3-4):491–503, 2005.

[5] R. Araya, E. Behrens, and R. Rodríguez. A posteriori error estimates for elliptic problems with dirac delta source terms. Technical Report 2005-15, Universidad de Concepción, Concepción, 2005.

[6] R. Araya, E. Behrens, and R. Rodríguez. Error estimators for advection-reaction-diffusion equations based on the solution of local problems. Technical Report 2006-03, Universidad de Concepción, Concepción, 2006.

[7] I. Babuvska, J. Osborn, and J. Pitkäranta. Analysis of mixed methods using mesh dependent norms. *Math. Comp.*, 35(152):1039–1062, 1980.

[8] C. Bernardi and V. Girault. A local regularization operator for triangular and quadrilateral finite elements. *SIAM J. Numer. Anal.*, 35(5):1893–1916, 1998.

[9] S.C. Brenner and L.R. Scott. *The mathematical theory of finite element methods*, volume 15 of *Texts in Applied Mathematics*. Springer-Verlag, New York, 1994.

[10] F. Brezzi, D. Marini, and A. Russo. Applications of the pseudo residual-free bubbles to the stabilization of convection-diffusion problems. *Comput. Methods Appl. Mech. Engrg.*, 166(1-2):51–63, 1998.

[11] A.N. Brooks and T.J.R. Hughes. Streamline upwind/Petrov-Galerkin formulations for convection dominated flows with particular emphasis on the incompressible Navier-Stokes equations. *Comput. Methods Appl. Mech. Engrg.*, 32(1-3):199–259, 1982.

[12] E. Casas. L^2 estimates for the finite element method for the Dirichlet problem with singular data. *Numer. Math.*, 47(4):627–632, 1985.

[13] P.G. Ciarlet. *The finite element method for elliptic problems*, volume 40 of *Classics in Applied Mathematics*. Society for Industrial and Applied Mathematics (SIAM), Philadelphia, PA, 2002.

[14] Ph. Clément. Approximation by finite element functions using local regularization. *Rev. Française Automat. Informat. Recherche Opérationnelle Sér. RAIRO Analyse Numérique*, 9(R-2):77–84, 1975.

[15] M. Dauge. *Elliptic boundary value problems on corner domains*, volume 1341 of *Lecture Notes in Mathematics*. Springer-Verlag, Berlin, 1988.

[16] J. Douglas, Jr. and J.P. Wang. An absolutely stabilized finite element method for the Stokes problem. *Math. Comp.*, 52(186):495–508, 1989.

[17] A. Ern and J.L. Guermond. *Theory and practice of finite elements*, volume 159 of *Applied Mathematical Sciences*. Springer-Verlag, New York, 2004.

[18] L.P. Franca, S.L. Frey, and T. J. R. Hughes. Stabilized finite element methods. I. Application to the advective-diffusive model. *Comput. Methods Appl. Mech. Engrg.*, 95(2):253–276, 1992.

[19] L.P. Franca and F. Valentin. On an improved unusual stabilized finite element method for the advective-reactive-diffusive equation. *Comput. Methods Appl. Mech. Engrg.*, 190(13-14):1785–1800, 2000.

[20] P. Grisvard. *Elliptic problems in nonsmooth domains*, volume 24 of *Monographs and Studies in Mathematics*. Pitman (Advanced Publishing Program), Boston, MA, 1985.

[21] V. John. A numerical study of a posteriori error estimators for convection-diffusion equations. *Comput. Methods Appl. Mech. Engrg.*, 190(5-7):757–781, 2000.

[22] T. Knopp, G. Lube, and G. Rapin. Stabilized finite element methods with shock capturing for advection-diffusion problems. *Comput. Methods Appl. Mech. Engrg.*, 191(27-28):2997–3013, 2002.

[23] X. Liao and R. Nochetto. Local a posteriori error estimates and adaptive control of pollution effects. *Numer. Methods Partial Differential Equations*, 19(4):421–442, 2003.

[24] H.G. Roos, M. Stynes, and L. Tobiska. *Numerical methods for singularly perturbed differential equations*, volume 24 of *Springer Series in Computational Mathematics*. Springer-Verlag, Berlin, 1996.

[25] G. Sangalli. A robust a posteriori estimator for the residual-free bubbles method applied to advection-diffusion problems. *Numer. Math.*, 89(2):379–399, 2001.

[26] G. Sangalli. On robust a posteriori estimators for the advection-diffusion-reaction problem. Technical Report 55, Institute for Computational Engineering and Sciences, Austin, Texas, USA, 2004.

[27] G. Sangalli. A uniform analysis of nonsymmetric and coercive linear operators. *SIAM J. Math. Anal.*, 36(6):2033–2048, 2005.

[28] A. H. Schatz and L. B. Wahlbin. Interior maximum norm estimates for finite element methods. *Math. Comp.*, 31(138):414–442, 1977.

[29] R. Scott. Finite element convergence for singular data. *Numer. Math.*, 21:317–327, 1973/74.

[30] J.R. Shewchuk. Delaunay refinement algorithms for triangular mesh generation. *Comput. Geom.*, 22(1-3):21–74, 2002.

[31] R. Verfürth. *A Review of a posteriori error estimation and adaptive mesh-refinement techniques*. John Wiley, 1996.

[32] R. Verfürth. A posteriori error estimators for convection-diffusion equations. *Numer. Math.*, 80(4):641–663, 1998.

[33] R. Verfürth. Robust a posteriori error estimators for a singularly perturbed reaction-diffusion equation. *Numer. Math.*, 78(3):479–493, 1998.

[34] R. Verfürth. Robust a posteriori error estimates for stationary convection-diffusion equations. *SIAM J. Numer. Anal.*, 43(4):1766–1782, 2005.

[35] S. Wang. An a posteriori error estimate for finite element approximations of a singularly perturbed advection-diffusion problem. *J. Comput. Appl. Math.*, 87(2):227–242, 1997.